The Nitrogen Cycle and Ecohydrology of Seasonally Dry Grasslands

by

Anthony Joseph Parolari

B.S., University of Michigan (2004)
M.S., University of Michigan (2005)

Submitted to the Department of Civil and Environmental Engineering
in partial fulfillment of the requirements for the degree of

Doctor of Philosophy in the Field of Hydrology

at the

MASSACHUSETTS INSTITUTE OF TECHNOLOGY

February 2013

Author .....
Department of Civil and Environmental Engineering
September 26, 2012

Certified by .....
Rafael L. Bras
Professor Emeritus of Civil and Environmental Engineering,
Provost and Executive Vice President for Academic Affairs,
Georgia Institute of Technology
Thesis Supervisor

Accepted by .....
Heidi M. Nepf
Chair, Departmental Committee for Graduate Students

The Nitrogen Cycle and Ecohydrology of Seasonally Dry Grasslands

by

Anthony Joseph Parolari

Submitted to the Department of Civil and Environmental Engineering
on September 26, 2012, in partial fulfillment of the
requirements for the degree of
Doctor of Philosophy in the Field of Hydrology

Abstract

This thesis addresses the coupling of hydrologic and biogeochemical processes and, specifically, the organization of ecosystem traits with the water, carbon, and nitrogen cycles. Observations from a factorial irrigation-fertilization experiment in a seasonally dry annual grassland are combined with a simple ecosystem model to identify relationships between vegetation, nitrogen availability, and hydrology. Assuming primary productivity is water-limited, data analysis indicates that soil moisture and canopy conductance are insensitive to nitrogen supply, owing to a trade-off between canopy density and leaf conductance that maximizes efficient use of available water. That is, fertilization-induced increases in leaf area index are offset by reduced leaf area-based stomatal conductance. When primary productivity is assumed to be co-limited by water and nitrogen availability, total surface conductance is estimated to be insensitive to nitrogen supply, but added nitrogen increases the ratio of transpiration to evaporation. This coupled water-carbon-nitrogen model is then extended to predict ecosystem sensitivity across independently varied gradients of water and nitrogen supply rates. This analysis reveals two distinct regimes of plant-resource organization. In arid climates, rooting depths decrease with increasing aridity, while in humid climates, rooting depths increase with aridity. In all climates, rooting depths increase with increased nitrogen supply. Further, relative root-carbon allocation always increases with aridity and decreases with nitrogen supply. These resource use strategies result in an efficient use of available water in arid climates and efficient use of available nitrogen in humid climates. The associated ecosystem process rates indicate that nitrogen supply is an important determinant of surface water and carbon fluxes in humid climates, but only of carbon fluxes in arid climates.

Thesis Supervisor: Rafael L. Bras
Title: Professor Emeritus of Civil and Environmental Engineering,
Provost and Executive Vice President for Academic Affairs,
Georgia Institute of Technology

Acknowledgments

First and foremost, my thesis is dedicated to my family. Thank you to Mom, Dad, Jessica, and Nick for paving the way toward making this possible. I owe all of my accomplishments to your love, hard work, and sacrifice.

Secondly, I am grateful for the financial support that allowed me to complete this research. I was supported by a graduate fellowship from the Department of Defense as well as by a National Science Foundation grant [EAR 0962253]. Also, the Department of Energy [FG02-05ER64021] has supported the Michael Goulden Lab at UC Irvine, who graciously provided the necessary data.

Thank you to my advisor, Rafael Bras, for your consistent guidance and patience. You've set a remarkable example through your dedication to both the field of hydrology and the education of the next generation of young engineers and scientists – an example I am eager to emulate. I am always amazed at the level of energy you continue to bring to your students' research, while balancing commitments as an administrator and family. I am grateful for the freedom to pursue research on my own terms and for all of the "aha" moments during group meeting.

I am also very much indebted to the support of my committee – Professors Elfatih Eltahir (MIT), Michael Goulden (UC Irvine), and Ignacio Rodriguez-Iturbe (Princeton) – who have all contributed in their own way. Fatih, thank you for the many times you helped me organize my work and see the big picture. You always had a fresh perspective. Mike, thank you for digging into the details with me, sharing your hands-on knowledge, and providing momentum for my ideas. And, Ignacio, there is no way I could ever match your enthusiasm, which guided me through times of uncertainty and frustration.

To past and present Bras Group members (in Cambridge, Irvine, and Atlanta), we sure had some great times. Thank you for all the chalkboard and Muddy sessions, where all the real work got done, and for help navigating the research process. This thesis would not have been possible without it.

And, finally, thank you for the many friendships that have grown throughout this journey, within and outside of Parsons Lab – you know who you are.

Contents

List of Figures

List of Tables

Chapter 1

Introduction

> "In terms of conventional physics, the grouse represents only a millionth of either the mass or the energy of an acre. Yet, subtract the grouse and the whole thing is dead."
>
> ~ Aldo Leopold, from *A Sand County Almanac*

This thesis addresses the coupling of hydrologic and biogeochemical processes. The introductory chapter is intended to familiarize the reader with the role of ecosystem processes in the earth system and to motivate the study of coupled water, carbon, and nitrogen cycles in semi-arid grasslands. First, the concept of mass and energy cycling is introduced at the global scale. This general view is then expanded by a review of the mechanisms that contribute to the co-variability of these cycles at ecosystem scales, leading to a conceptual framework to guide the remainder of the thesis. Within the context of this framework, several outstanding research questions and the objectives for this work are outlined.

1.1 The earth system, humans, and global change

The earth system is a delicate and complex web of interacting cycles of matter and energy. Energy processed in the earth system is ultimately derived from the sun and from tectonic activity originating deep in the core of the earth. This energy is stored and released while altering the thermodynamic states of the earth system – most importantly, the surface and atmosphere are heated and cooled; water is cycled between solid, liquid, and gaseous states; and chemical reactions convert inorganic matter to organic and back. These cycles, operating on land, in the oceans, and in the atmosphere, underlie many common sights –

from a subtle change in wind direction, to the leaves turning color in fall, to the awesome, but often tragic, earthquakes and hurricanes.

At human time-scales, the primary source of energy driving the earth system is the sun. The sun delivers energy at an approximate rate of 340 [W m^{-2}] at the top of the atmosphere[1] [*Trenberth et al.*, 2009]. Globally, the earth is in approximate thermodynamic equilibrium (i.e. no net heating or cooling), thus the system radiates this same energy flux back to space. On average, 30% of incoming solar energy is directly reflected by aerosols and bright surfaces such as snow, ice, sand, and cloud-tops. The fraction of reflected solar energy is known as the planetary albedo. The remainder is absorbed by the surface, atmosphere, and clouds, then re-emitted away from the earth. Because of this constant outgoing radiation, maintenance of the earth's temperature requires constant solar energy input.

While an observer from space might conclude the earth's temperature to be -19°C in thermodynamic equilibrium, by experience we know it is indeed much warmer at the surface. Local warming of the surface and lower atmosphere is due to the storage of energy near the surface, known as the "greenhouse effect." The greenhouse effect maintains a habitable temperature near the surface favorable to the thermodynamic processes observed to occur there, including those of a dynamic hydrologic cycle. One-third of the energy absorbed by the surface is direct solar energy, whereas the remaining two-thirds is that which has been absorbed by clouds and molecules in the atmosphere and re-radiated downward toward the surface [*Trenberth et al.*, 2009]. These are the greenhouse gases – the most active of which is water vapor, and also known to include carbon dioxide, methane, nitrous oxide, ozone, aerosols, and various halocarbons [*Forster et al.*, 2007]. The total energy absorbed by the surface is thus the sum of the net solar input and the downward radiation from the greenhouse gases.

Energy absorbed by the surface is dissipated through a variety of mechanisms. The earth itself has a temperature and radiates energy upward, some of which is absorbed in the atmosphere and contributes to the greenhouse effect. The remaining energy, called net

[1]The sun illuminates half of the earth surface at any given time and solar energy enters the earth system normal to the projection of this illuminated area. Therefore, the global average energy input is 340 [W m^{-2}], or one quarter of the solar energy flux density, or solar constant. The solar constant is approximately 1361 [W m^{-2}], as estimated from recent Total Irradiance Monitor observations (under NASA's Solar Radiation and Climate Experiment) [*Kopp and Lean*, 2011].

radiation, R_n, is dissipated by heating or cooling of the ground, heating or cooling of the air, or the evaporation of water – or ground, G, sensible, H, and latent heat, λE, fluxes, respectively. Thus, the surface energy balance (SEB) is,

$$R_n = R_s^{\uparrow} - R_s^{\downarrow} + R_l^{\uparrow} - R_l^{\downarrow} = G + H + \lambda E \tag{1.1}$$

where the sign convention is taken as positive away from the surface and R_s and R_l are the shortwave and longwave energy fluxes (i.e. solar and terrestrial, denoted as such due to the respective temperatures of the radiating bodies and associated regions of the electromagnetic spectrum).

The partitioning of R_n into these three fluxes at the earth surface is a primary driver of the hydrologic cycle. It determines the rates at which (1) water stored in the land surface is returned to the atmosphere, λE, and (2) the lower atmosphere is heated, H, which initiates the processes required to produce rainfall. Globally, λE accounts for 82% and H accounts for 17% of R_n [*Trenberth et al.*, 2009], however, this distribution varies substantially at smaller scales.

Latent heat couples the SEB with the surface water balance. Neglecting changes in water storage on land, precipitation, P, is balanced by evaporation, E,[2] surface runoff, R_o, and deep groundwater recharge, R_g,

$$P = E + R_o + R_g \tag{1.2}$$

Taken together, the coupled surface water-energy balance determines the surface climatic states, temperature and humidity, given the energy and water inputs, R_n and P. The significance of these climatic inputs and states for earth system dynamics will be clarified in the next section.

In addition to driving the water cycle, the sun's energy flows through biogeochemical cycles operating within the earth system. First and foremost, solar energy is absorbed in the process of photosynthesis, whereby it is converted to chemical energy by reducing carbon from its inorganic state in the atmosphere, CO_2, to organic matter. The energy utilized

[2] λ=2.25e6 [J kg^{-1}] is the latent heat of vaporization, or the energy required to evaporate 1 kg of water at 25°C. It converts the latent heat flux from units of energy to units of mass.

in photosynthesis is negligible compared to the other surface energy fluxes in equation 1.1 (see Table 1.1 and references), but it is the originating energy source that supports most life-forms on earth and it represents a major component of the land-atmosphere carbon flux. The chemical energy stored by photosynthesis is later released through metabolism (also returning CO_2 to the atmosphere) to support the building and maintenance of plant and microbial organic matter of the primary producers. Energy contained in this organic matter cascades up the food chain from plants to animals and, ultimately, to us.

Enzymes used to carryout photosynthesis and metabolism are not constructed of carbon alone, but require several additional elements in varying quantities. Macronutrients are those required in the largest supply (nitrogen, calcium, potassium, magnesium, phosphorus, etc.) as compared to the micronutrients (iron, manganese, zinc, copper, molybdenum, etc.) required in much lesser amounts. Following hydrogen, carbon, and oxygen, nitrogen (N) is by far the element required in the greatest amount, as evidenced by the typical elemental ratios of organic matter C:N:P=106:16:1 [*Redfield*, 1958; *Vitousek*, 1982; *Falkowski and Davis*, 2004; *Hedin*, 2004]. The availability of N also limits primary productivity in most of the world's ecosystems [*Vitousek and Howarth*, 1991]. On Earth, N is primarily found in the atmosphere as the non-reactive gas, N_2. The strength of the triple bond between N atoms in this state necessitates a large amount of energy to assimilate N_2 into organic matter. In nature, this process is executed by biological nitrogen fixation (BNF), whereby primary producers utilize energy derived from photosynthesis to facilitate N reduction. While BNF is the ultimate source of organic N, most of the inorganic N utilized in primary production is continuously cycled between plants and soil organic matter. This cycling is accompanied by requisite energy fluxes. Heterotrophic decomposers derive their metabolic energy from deceased plant material, a process that releases inorganic N into the soil. Plants subsequently expend energy to collect inorganic N from the soil and reduce it for assimilation into organic matter.

Another element that plants and animals require in high supply, but is often found in limiting supply, is phosphorus (P). P is a component of the cellular energy "shuttle," adenosine triphosphate (ATP), and is the backbone of deoxyribonucleic acid (DNA), the molecule responsible for storing the world's genetic information. P is largely found bound

Table 1.1: Major earth system cycles expressed in terms of power [TW].

	Energy flux	Total power	Sources
Net solar input[1]		121,000	
Surface heating[2]	Net greenhouse effect	11,700	*Forster et al.* [2007];
	Convection	8,700	*Trenberth et al.* [2009]
	Human activity	770	
Water	Total ET	36,000	*Postel et al.* [1996]
	ET on land	5,000	
	Agricultural ET	1,300	
	Diverted runoff	500	
Carbon	Total photosynthesis	107	*Vitousek et al.* [1986];
	Photosynthesis on land	58	*Field et al.* [1998];
	Agriculture	27	*Nealson and Conrad* [1999];
	Fossil fuels[a]	17	*Kleidon* [2012]
Nitrogen[3]	Total N fixation	1.24	*Ramirez and Worrell* [2006];
	N fixation on land	0.83	*Gruber and Galloway* [2008]
	BNF on land	0.24	
	Fertilizer production[a]	0.21	
Phosphorus	Fertilizer production[a]	0.012	*Carpenter et al.* [1998];
	Natural weathering	0.0010	*Gardner* [1990];
			Guidry and Mackenzie [2000];
			Ramirez and Worrell [2006]

[1]Net solar input is calculated as the total solar energy flux less that reflected directly back to space.
[2]Surface heating includes the net greenhouse effect plus sensible heat, the energy that does not evaporate water or immediately escape through the atmosphere.
[3]Calculated assuming 946 [kJ mol^{-1}] energy input required to break N_2 triple bond. These values are likely conservative estimates, as some of this energy may be recaptured in other usable products of the N-fixing process (e.g. see *Ramirez and Worrell* [2006]).
[a]Energy derived from fossil fuels and fertilizer production effectively represent anthropogenic inputs into the system, as these processes release energy from reservoirs with long residence times. Other energy fluxes are included in their respective "total" values.

in rock and initially becomes biologically available via a combination of physical, chemical, and biological processes. The primary mechanism that releases new P into ecosystems is the dissolution of rocks containing P, such as Apatite [*Walker and Syers*, 1976]. Since dissolution rates are surface area-dependent, they may be limited by physical weathering of parent material – from large cohesive rock fragments to tiny soil particles. Physical weathering mechanisms include expansion and contraction (i.e. temperature- and water-driven freeze-thaw or thermal stresses) and bioturbation by roots and burrowing animals. Once dissolved and assimilated into organic matter, P is tightly cycled in the plant-soil system. Similar to those propelling the N cycle, these weathering and recycling processes all depend on energy ultimately derived from the sun.

The water, carbon, nitrogen, and phosphorus cycles exemplify the movement of matter and energy in the earth system. Through latent heat, the energy-demanding processes of photosynthesis, and the propagation of this energy to nutrient acquisition and to higher trophic levels, the sun powers the dynamics of these cycles. The water cycle entrains a substantial amount of energy when compared to the elemental cycles (Table 1.1). Indeed, precipitation is often considered, with temperature, to be the first order control on ecosystem structure and productivity [*Whittaker*, 1975]. Of those elements required in the highest supply (C, N, and P) and those most likely to limit primary productivity (N and P), the C and N cycles utilize the most energy. That energy decreases precipitously with the relative needs for organic matter production, such that N fixation requires several orders of magnitude less energy than photosynthesis and P weathering even less. However, each of these elements is necessary to life found on Earth.

* * *

Human intervention in the earth system is striking. Human societies rely on the water, carbon, nitrogen, and phosphorus cycles to support their livelihood – socio-ecological processes such as food production, drinking and wastewater treatment, transport, and recreation are derived directly from these cycles. As shown in Table 1.1, anthropogenic activities account for a substantial proportion of the energy flow through these cycles.

Water has always played a central role in society. The rivers and oceans serve not only

as a source of drinking water and food, but also as a means of travel and trade. Efforts to store and divert water for agriculture and flood control were practiced as early as 3000 BC [*Biswas*, 1970]. While fishing contributed to human sustenance thousands of years earlier [*Richards and Trinkaus*, 2009], the practice escalated to the global scale around the 13^{th} century, when freshwater fisheries collapsed and English fisherman ventured across the Atlantic to fish off the coast of present-day Newfoundland and Maine [*Bolster*, 2008]. As world population has grown since, these activities have only intensified. Humans now utilize 26% of global land evapotranspiration (ET) and 54% of accessible runoff, of which 42% is used to irrigate cropland [*Postel et al.*, 1996]. In many areas of the world, irrigation water is acquired from groundwater aquifers [*Vorosmarty and Sahagian*, 2000; *Konikow*, 2011]. Globally, groundwater withdrawals only account for approximately 10 TW of latent heat (using the estimates of *Konikow* [2011]), but instantaneously (in geologic time) release water from reservoirs with natural residence times on the order of 10^2-10^4 years. Major rivers have been dammed for hydropower and drinking water, increasing water and sediment storage on land [*Vorosmarty and Sahagian*, 2000], or have been channelized to ease inland transport of goods [*Brookes*, 1985]. This activity increases land-ocean exchange of water and the nutrients and sediment it carries, which is further increased by agricultural land development [*Gottschalk*, 1945; *Brookes*, 1985]. These changes in water fluxes and storage are already manifest at very large scales, such as the almost entirely diverted Colorado River [*Cohen et al.*, 2001], the disappearing Aral Sea [*Micklin*, 2007], and the Gulf of Mexico "dead zone" [*Osterman et al.*, 2009]. The dynamics of this coupled human-water system are accelerated and seldom similar to the natural water cycle.

The C cycle is also central to the human endeavor. As alluded to earlier, agricultural production and animal husbandry depend on photosynthesis and metabolism to generate organic matter, which then becomes our food. Toward this end, the C cycle has been artificially stimulated through irrigation and fertilization, interventions that simultaneously impact the water, C, and N cycles. It is estimated that 31% of terrestrial net primary productivity (NPP) has been appropriated for human use [*Vitousek et al.*, 1986] and the area of irrigated land is projected to double between 2000 and 2050 [*Tilman et al.*, 2001]. Since the industrial revolution (approx. 1750-1850), energy production – for agriculture, transport,

and heating/cooling/lighting our homes – has largely been generated via the burning of fossil fuels. This burning quickly depletes stores of C that have existed for millions of years and contributes to the observed rise in atmospheric CO_2 [*Forster et al.*, 2007]. The interaction between atmospheric CO_2 and energy radiated from the earth surface is implicated in global climate change. In terms of energy, humans appropriate 47% of the C cycle on land and release an amount equivalent to 16% of the global cycle from fossil reservoirs.

It is impossible to discuss either agriculture or energy production without also addressing their impacts on the N cycle. At present, humans account for over half (~59%) of the reactive N entering the cycle, much of which is from N fertilizers [*Gruber and Galloway*, 2008], and this amount is expected to increase 2-3 fold by 2050 [*Tilman et al.*, 2001]. Modern agricultural productivity relies on industrial N fixation via the Haber-Bosch process, which itself consumes fossil fuels. It is estimated that approximately 1-2% of the global energy demand is harnessed to fix N fertilizer [*Gutschick*, 1978; *Ramirez and Worrell*, 2006; *EIA*, 2006] however, humans consume only about 10% of this [*Galloway and Cowling*, 2002]. Fossil fuel combustion releases fixed N as the gases NO and NO_2 that are subsequently re-deposited on the surface. This process accounts for 20% of human reactive N inputs [*Gruber and Galloway*, 2008]. Thus, through the coupled C and N requirements of plants and animals, the fossil energy required to produce N fertilizer, and the byproducts of fossil fuel combustion, the N cycle is strongly regulated by humans and intertwined with the C cycle.

Irreversible changes (at least over human time-scales) to these coupled earth system processes resulting from human activity are evident. Many landscapes have been altered with unintended, long-lasting consequences. Soil erosion under the plow is all too common a story across the United States [*Gottschalk*, 1945; *Costa*, 1975; *Hooke*, 2000], losing soils rich in organic matter that can take hundreds of years to develop. Intense fertilization has saturated soil nutrient storage, such that stream-water nutrient concentrations are elevated and will continue to be so until these stores are depleted [*Basu et al.*, 2010]. Nutrients in agricultural runoff have been observed to decimate receiving water ecosystems beyond recoverable thresholds [*Scheffer et al.*, 1993]. Similarly, vegetation loss from rangeland over-grazing may increase vulnerability to drought and the ability of these ecosystems to regain

productivity in the future [*Schlesinger et al.*, 1990; *Rietkerk et al.*, 1997]. While these studies have focused on local impacts, global scale reactions to increasing human activity are possible [*Wackernagel et al.*, 2002; *Barnosky et al.*, 2012]. Whether or not these harbingers ring true, the current scale of human activity and its consequences are unprecedented, necessitating a careful approach to land development, management, and restoration.

From this global perspective, it is clear that the water, C, and N cycles are (1) necessary to support life on earth, (2) significantly altered by human activity, and (3) closely linked. The first two points indicate the importance of fundamental understanding of these cycles and the third indicates the difficulty in doing so. In the next section, these difficulties are illustrated as we reduce our scale of inquiry to the ecosystem level and consider some of the physical, chemical, and biological mechanisms through which terrestrial ecosystems link energy and elemental cycles.

1.2 Ecosystems: linking the water, carbon, and nitrogen cycles

The short time-scale (i.e. sub-daily to decadal) dynamics of the earth system are driven by strong interactions between the atmosphere and the land and ocean surfaces. In particular, the thin skin of biological material covering the land surface (i.e. soil and vegetation) acts as a reactor for energy and matter. Inputs to this reactor include, from the atmosphere, solar energy, rainfall, and elements such as C and N, and, from the earth, mineral inputs via uplift and rock weathering. The products are subsequently returned to the atmosphere by turbulence in the planetary boundary layer, exported to the ocean by river-flow, or buried beneath the surface. Boundary layer energy, moisture, and carbon fluxes are particularly relevant to both short- and long-term climate dynamics.

The land surface reactor is best described as a mosaic of ecosystems, with both undisturbed and developed lands, whose characteristics govern the rates of energy and matter processing. Aggregate ecosystem behavior depends on interactions among their abiotic (e.g. mineral soil and rock, water, radiant energy) and biotic (e.g. plants, soil and its microbes, animals, humans) components over a wide range of spatial (molecular to landscape, $\sim 10^{-9}$–

10^3 m) and temporal (diurnal to millennial, $\sim 10^3$–10^{10} s) scales.[3] Indeed, *Redfield* [1958] noted,

> "The environment not only determines the conditions under which life exists, but the organisms influence the conditions prevailing in the environment."

From the perspective of terrestrial ecosystems, these biotic-abiotic interactions imply that plants both influence and respond to their resource environments, defined as the prevailing soil and atmospheric conditions. In fact, soil development requires the mere presence of vegetation. Plants "engineer" their soil environments – they fix N, stimulate weathering of inorganic substrate, and generate the organic matrix that serves as nutrient supply and a reservoir for soil moisture. In the atmosphere, plant canopies affect the generation of turbulent eddies, which sets the air temperature and humidity conditions, and may collect moisture directly from the air [*Bonan*, 2002; *Hildebrandt et al.*, 2007]. Once established, these soil-plant-atmosphere systems (the foundation of the ecosystem) are self-sustaining cycles, whose dynamics are regulated by, and regulate, the surface water-energy balance. As such, we can ascertain a strong coupling between the water-energy, C, and N cycles in terrestrial ecosystems (Figure 1-1).

Volumetric soil moisture, θ [m^2 m^{-2}], is often assumed to be the most descriptive state of the ecosystem, or the life-blood that facilitates ecosystem processes, for good reason. From a purely physical perspective, θ acts as a dynamic interface between the subsurface, surface, and atmosphere. Because soil water potential decreases rapidly with soil moisture and soil water storage capacity is finite, infiltration and runoff generation depend strongly on θ [*Horton*, 1933; *Dunne and Black*, 1970]. Likewise, soil conductivity sets a physical limit to evaporation from bare soil. In certain contexts, soil moisture may also interact directly with climate and promote the likelihood of rainfall or drought [*Rodriguez-Iturbe et al.*, 1991; *Eltahir*, 1998; *Zheng and Eltahir*, 1998]. Therefore, the wetting and drying of the landscape depends in large part on its "wetness," or saturation. This interplay between rainfall, soil

[3]Given that these interactions may take place theoretically over any space- or time-scale, it is useful here to restrict our discussion to specific scales and the interactions expressed strongest at those scales. We focus here on plot-scale dynamics ($\sim 10^2$ [m^2], or several individuals) occurring over time-scales ranging from hourly to inter-annual. Therefore, dynamics resulting from processes such as evolution and landscape development are ignored.

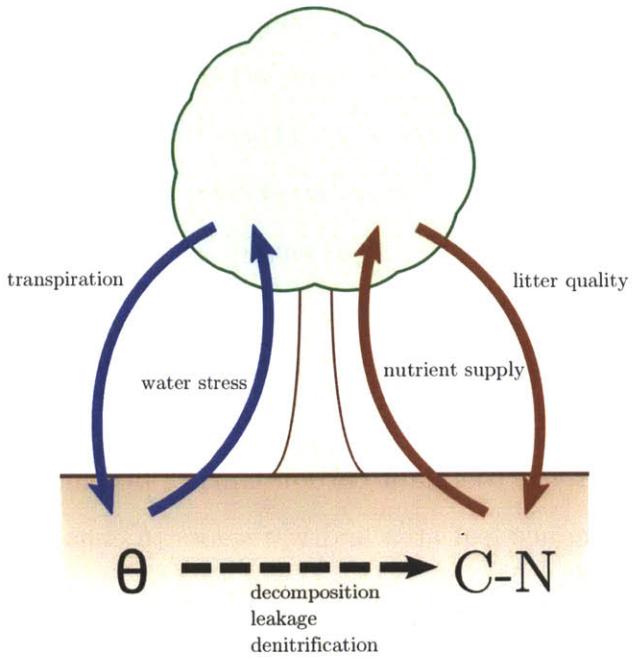

Figure 1-1: Interactions between the water, carbon, and nitrogen cycles at ecosystem scales.

moisture, evaporation, and runoff determines the soil saturation regime and sets the stage for ecosystem processes to do their work.

Transpiration, an ecosystem process modulated by plant physiological activity, interacts with the soil water balance much like the physical processes described above. In order to obtain CO_2 for photosynthesis, plants must necessarily maintain a porous leaf surface, across which CO_2 diffuses to the site of carboxylation. When open, leaf pores, or stomata, inadvertently allow water to evaporate and escape into the atmosphere. Because physiological processes require maintenance of turgor pressure, primary productivity thus requires a continuous supply of soil water. Between rainfall events, the soil water supply is depleted by transpiration, which results in reduced turgor pressure and a condition of plant water stress. Plants have evolved many strategies to cope with water stress, including adjustments to stomatal opening, leaf area, and root structure. These physiological responses modulate a negative feedback between transpiration and soil moisture that is expressed in the character of the soil moisture signal and the land surface carbon and water fluxes.

The most immediate response to water stress is slowing of the transpiration flux. Reduced transpiration is first achieved by stomatal closure, which raises cellular and xylem pressures

to avoid tissue damage [*Kramer and Boyer*, 1995]. Stomatal closure is induced either by (1) hormonal signals from the root that indicate a depleting water supply [*Tardieu et al.*, 1996; *Wilkinson and Davies*, 2002] or (2) a direct mechanical response to decreased turgor pressure in the cells that surround the stomatal opening [*Buckley et al.*, 2003]. The relative importance of these two mechanisms differs among species [*Lambers et al.*, 2008]. As water stress develops further, however, pressure losses are unavoidable. Loss of leaf turgor pressure causes leaves to wilt. Wilting reduces leaf exposure to radiation and turbulence, which contribute to the evaporation process. Under severe stress, the photosynthetic and metabolic machinery itself is degraded and the plant carbon balance becomes negative. At this point, leaves are shed to further reduce leaf area and water loss [*Kramer and Boyer*, 1995]. If the water supply is not replenished by rainfall, mortality is imminent.

In addition to stomatal and leaf area adjustments, plants interact with the soil water balance through root exploration of the soil at depth. Rooting depth is the plant trait that most determines the volume of water available for evaporation. It controls the active soil depth, or the depth that interacts directly with the atmosphere, and increases evapotranspiration beyond that accessible by exfiltration alone. Root growth is driven in part by moisture availability and, therefore, rooting depth can be predicted from the soil and climate characteristics that determine the characteristic infiltration depth for the ecosystem [*Schenk and Jackson*, 2002a; *Laio et al.*, 2006; *Collins and Bras*, 2007; *Sivandran*, 2011].

So far, the water stress responses we have addressed are those that vary at hourly to seasonal scales. These dynamic responses represent plant acclimation to variability in the environment, or the ecosystem phenotype. However, rooting depth, transpiration rates, and water stress responses are also related to plant life history strategy. Thus, these characteristics may be considered part of the ecosystem genotype, which varies by adaptation over ecological and evolutionary time-scales. Plants that complete their entire life-cycle within a single growing season cannot grow fast enough for roots to penetrate deeper than several 10s of centimeters [*Noy-Meir*, 1973]. Therefore, they primarily interact with moisture stored near the surface, which is cycled at the highest frequency, and are found in environments where infiltration depths are limited. These ephemeral species, such as annual grasses, typically follow an intensive growth strategy [*Rodriguez-Iturbe and Porporato*, 2004; *Zea-Cabrera*

et al., 2006], whereby they grow and transpire at high rates, but die-off quickly after water stress initiates. Longer-lived individuals are able to establish deeper rooting systems over multiple growing seasons and, thus, tap into water stored below the surface. Access to lower soil layers and groundwater provides a larger water supply, provides a buffer during periods of drought, and is associated with an overall dampening of the water balance dynamics [*Noy-Meir*, 1973]. These extensive water users, like trees, maintain low growth and transpiration rates and, thus, exhibit a more conservative resource use strategy.

The observed soil water balance and vegetation are inter-related and result from innumerable interactions between soil, vegetation, and climate. At the molecular scale, leaf cell osmotic pressures affect the rate at which CO_2 molecules are captured by Rubisco. At the whole-plant scale, this capture rate determines the amount of carbon available for root and leaf growth, which controls ET and the accumulation of water-storing organic matter. And, at the landscape scale, soil water storage and ET regulate the processes that produce rainfall. These interactions across processes and scales are evident in observable associations between soil moisture and vegetation patterns (see Figure 1-2) and limit our ability to attribute water balance dynamics to a succinct set of independent factors.

Figure 1-2: Examples of vegetation-hydrology organization. At Wai-Ula-Ula, Hawai'i (a) and Konza Prairie, Kansas (b), topographic redistribution of soil moisture leads to two distinct eco-hydrologic regimes. Water drains from divergent slopes, resulting in dry uplands dominated by grasses, and collects in convergent slopes, where wet valleys are dominated by trees.

Soil moisture also supports microbial life and, in so doing, serves as the medium for soil biogeochemical reactions. These reactions, modulated by soil moisture, determine the supply of nutrients available to plants for enzyme synthesis and biomass production. In direct analogy to the plants, the soil water potential establishes the micro-environment in which microbes live. As the soil dries, water potential drops rapidly, creating a hostile environment that slows microbial activity. In addition, soil moisture facilitates the mobility of soluble ions, needed for both plant and microbe metabolism. At low soil moisture, water is tightly bound to soil particles and pores disconnected, such that diffusion through the soil pore space to reaction sites and to root surfaces for plant uptake is limited. This effect on soil connectivity is also expressed at the soil profile or catchment scales, affecting solute delivery to processing zones and export via streamflow. At high soil moisture, the fraction of pore space filled with air is limited and oxygen availability declines. Under oxygen deficit, anaerobic metabolism is energetically favored, which is associated with low decomposition rates and N loss via gases produced during denitrification. All of these factors play a role in microbial activity, rates of C and N transformation in the soil, and the availability of nutrients for plant uptake.

Patterns of soil C and N cycling are related to soil and climate characteristics, consistent with the influence of soil moisture and temperature. In general, soil organic matter and N accumulate in cooler and wetter climates [*Kern*, 1994]. Decomposition rates increase over a wide range of temperature and precipitation; however, decomposition is inhibited by the anaerobic conditions of saturated soils and at extreme temperatures. Across a precipitation gradient, this uni-modal decomposition effect is superimposed by a monotonic increase in biomass production [*Sala et al.*, 1988]. Biomass C:N ratios also increase with precipitation, as wetter soils enhance non-productive N losses via runoff and denitrification [*Brady and Weil*, 2004; *Aranibar et al.*, 2004; *McCulley et al.*, 2009]. To the extent that they affect the soil water balance, soil properties also play a role in the soil C-N cycle. Fine and poorly drained soils are typically near saturation and are associated with high productivity, low decomposition, and, thus, high organic matter accumulation [*Brady and Weil*, 2004].

While soil organic matter dynamics seem to be well constrained, the internal dynamics of the soil C-N cycle are more uncertain. For example, net N mineralization was observed to be

relatively unaffected by precipitation in the central United States grasslands [*Barrett et al.*, 2002; *McCulley et al.*, 2009], whereas model simulations showed mineralization to increase across the same precipitation gradient [*Burke et al.*, 1997]. This discrepancy may be related to non-linearity in the microbial responses to soil moisture and temperature [*Brady and Weil*, 2004; *Aranibar et al.*, 2004] or a result of an inconsistency in the prevailing conceptual model for soil N cycling [*Schimel and Bennett*, 2004]. Despite this uncertainty, observations clearly demonstrate the importance of soil environmental conditions in the fate of C and N in the plant-soil system.

In addition to the soil environment, decomposition and mineralization rates also depend on the "quality" of the organic substrate, composed of plant and microbe litter. Litter quality denotes the ease of which microbial decomposition proceeds and partially depends on litter N content. Litter with high N content decomposes more quickly and releases more mineral N than litter with low N content [*Booth et al.*, 2005]. Plant tissue and litter N content have been observed to depend on vegetation type [*Tilman*, 1990; *Wedin and Tilman*, 1990; *Craine et al.*, 2002]. In a reciprocal manner, the nutrient supply rate, determined by the litter quality, also influences tissue N content. Therefore, in addition to that associated with the soil water balance, plants and soil are engaged in a second feedback by which high (low) productivity, decomposition, and N supply rates are self-sustaining [*Ehrenfeld et al.*, 2005]. Within this feedback, the relationships between plant life history strategy and the rate of N cycling are similar to those of the intensive/extensive water users introduced above. That is, annual grasses tend to grow faster, to have lower C:N ratios, and to promote higher mineralization rates than long-lived perennial grasses or woody shrubs and trees [*Ehrenfeld et al.*, 2005, and references]. Similarly, plants found in cold and/or wet environments, where decomposition and N supply rates are low, tend to exhibit high C:N ratios and conservative resource-use strategies [*Aerts and Chapin*, 1999]. Through these mechanisms, soil biogeochemistry is organized with both climate as well as vegetation characteristics. As in the case of the soil water balance, the complexity of this system is such that it is extremely difficult to establish a causal relationship between any two factors.

While the role of soil moisture in the C-N cycle, and resulting N supply rates, is well-recognized, it is less obvious whether there is a complementary effect of N supply on the soil

water balance. Indeed, this question has been studied from a wide range of perspectives. Soil N supply and corresponding plant tissue N concentrations are known to affect many vegetation characteristics that control ET, including leaf area index, stomatal conductance, and root structure. However, the range of hydrologic conditions studied and the scales at which these studies were conducted rarely match those needed to construct a comprehensive theoretical understanding commensurate with existing ecohydrological models.

In N-limited ecosystems, leaf area index varies with soil N supply. This supply is reflected in leaf N content, the majority of which is used to produce and maintain the photosynthetic and metabolic machinery. Thus, soil N supply controls rates of photosynthesis and growth [*Evans*, 1989; *Poorter et al.*, 1990]. Growth rates are often correlated with leaf area index – that is, plants that grow faster have larger canopies [*Anten et al.*, 1995; *Cowling and Field*, 2003]. As discussed earlier, leaf area index represents the surface area over which transpiration occurs and, thus, controls plant water use.

At the leaf scale, leaf N content influences stomatal conductance and the water stress response. A meta-analysis of leaf-scale measurements indicated that net CO_2 assimilation generally increases linearly with leaf N content under adequate water supply [*Field and Mooney*, 1986; *Evans*, 1989]. Since net CO_2 assimilation also scales linearly with stomatal conductance [e.g. *Leuning*, 1995], the hypothesis that stomatal conductance scales linearly with leaf N content naturally follows. This hypothesis has been verified under well-watered conditions [e.g. *Hunt et al.*, 1985a; *Sage and Pearcy*, 1987]; however, experiments under natural hydrologic regimes are limited. Those that do exist suggest physiological responses to N and water supplies interact to produce the stomatal response, which may decrease with increased N supply [*Ewers et al.*, 2000; *Bucci et al.*, 2006]. This behavior has been speculated to result from simultaneous optimization of leaf water and N use [*Wright et al.*, 2003]. Leaf N content also affects the soil moisture conditions under which plants experience water stress. *Radin and Parker* [1979] and *Radin* [1981] observed the leaf water potential at incipient stomatal closure to increase under N deficiency in individual, glasshouse grown cotton plants; however, fertilized plants wilted earlier. A more recent modeling study suggested the opposite, that fertilized plants are more susceptible to water stress [*Emanuel et al.*, 2007]. Together, these studies demonstrate the influence of N in stomatal dynamics, but fail to

create a consistent picture of the underlying mechanisms.

Below-ground, plant water and nutrient uptake is controlled by the size and structure of the root system. Plants scavenge for soil nutrients by extending their root systems, implying that root size and structure are related to nutrient availability. Plants respond to low N supply by increasing the total fraction of biomass allocated below-ground to the roots [*Poorter et al.*, 2012] and by generating new roots in zones with the greatest N concentrations *Lambers et al.* [2008]. Both strategies may simultaneously enhance plant water uptake and, thus ET.

Much evidence exists for the dependence of ET on soil N supply. The question has held the attention of ecologists, plant physiologists, agronomists, and hydrologists for several decades. However, general relationships between soil moisture, nitrogen supply, and ecosystem water use, as well as a mechanistic understanding of these relationships, remain open questions in ecology and hydrology.

It should now be clear that ecosystems are governed by at least two important feedback loops linked by soil moisture. Plant-soil interactions regulate both the soil water balance and soil biogeochemical cycles. These plant-water and plant-biogeochemistry interactions are not entirely independent as (1) soil moisture and temperature affect biogeochemical process rates and (2) nutrient supply affects ET (Figure 1-1). These linkages suggest that the soil C-N cycle may be an indirect factor in the surface water-energy balance, with both hydrological and biogeochemical implications. This leads to the following broad hypothesis (depicted in Figure 1-3):

> Given the N-sensitivity of plant traits that control ET, exogenous N supply from fertilization or atmospheric deposition may alter plant-water interactions and the soil water balance.

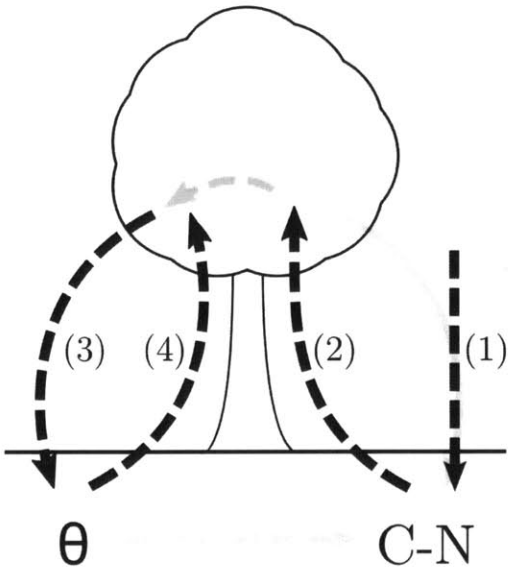

Figure 1-3: Visual depiction of the hypothesized indirect control of nitrogen fertilization on plant-water interactions: (1) exogenous ecosystem nitrogen input is increasing from fertilizer use and atmospheric deposition; (2) increased nitrogen supply increases productivity and aboveground biomass; (3) increased productivity and aboveground biomass may increase transpiration and reduce bare soil evaporation; and (4) altered evapotranspiration affects soil moisture regimes which may feedback onto transpiration.

Ecosystems are highly complex entities composed of soil, micro-organisms, plants, and animals that import, process, and export energy and matter. Their energy, water, and biogeochemical cycles are closely linked. These links result in apparent correlations between soil, climate, and ecosystem structure and function. Therefore, a perturbation to any one of the underlying processes (e.g. a change in N deposition, radiation, or precipitation regime) may cascade through the others. It is these potential unintended, and so-far unknown, consequences that require a detailed mechanistic understanding of ecosystem complexity and the capability to predict outcomes of global change. In the next section, we will look at how such ecosystem interactions have been addressed quantitatively in the study of dryland ecosystems, an intensely studied ecotone immensely relevant to human welfare.

1.3 Quantitative dryland ecohydrology

Of all the ecosystems covering the surface of the earth, drylands may be the most in need of critical attention. Drylands are generally defined as regions receiving less than 500 mm of rainfall per year [*Noy-Meir*, 1973] or those that receive annual rainfall insufficient to satisfy evaporative demand [*Budyko*, 1986].[4] They are often referred to as "water-controlled" ecosystems as it is assumed that water is the primary factor limiting energy flow through the ecosystem [*Noy-Meir*, 1973]. Drylands cover approximately 41% of the earth surface and support almost 2.5 billion people [*Reynolds et al.*, 2007]. Approximately 80% of grassland, a common ecotype in semi-arid regions, has been converted for human use [*White et al.*, 2000]. People in these areas are often poor [*White et al.*, 2002] and are highly vulnerable to the consequences of forecasted climate change [*Wilbanks et al.*, 2007]. Recent work suggests that productivity in many of these regions may be near irreversible thresholds [*Schlesinger et al.*, 1990], beyond which recovery may be impossible. For these reasons, dryland ecosystem processes have a long history of study.

In 1973, *Noy-Meir* [1973] published a comprehensive review whose conceptual framework still stands as the foundation in ecohydrology. The early picture of dryland structure and

[4]Note, the UN Convention to Combat Desertification defines this threshold as precipitation equal to 65% of evaporative demand.

function that emerged from his work emphasized intermittency and uncertainty in resource availability (i.e. rainfall) and a complex, dynamic coupling between soil, vegetation, and climate. With this recognition of the coupling between plants and the soil water balance, the modeling of vegetation activity took a central role in quantitative hydrology.

Eagleson [1978a;b;c;d;e;f;g] was the first to develop a quantitative framework for the study of coupled soil-vegetation-climate systems, with the objective of predicting the mean annual water balance for a region, considering the influence of vegetation. In his classic statistical-dynamical annual water balance model he applied an *a priori* assumption of ecological optimality as a constraint for model closure. The notion of ecological optimality assumes that the vegetation function in the model is optimized with respect to some indicator of ecological fitness. In Eagleson's case, maximum transpiration was used as a surrogate for maximum photosynthesis that could be described entirely in terms of the water balance and its parameters. The assumption represents the idea that observed vegetation in a given region is the outcome of a history of evolutionary and ecological processes, whereby the most successful growth strategy has out-competed all other possibilities. This assumption simplified the rather difficult effort inherent in the explicit mathematical treatment of vegetation activity. Later work lead to hypotheses suggesting that soil and vegetation properties co-evolve to an optimal state, given a prevailing climate [*Eagleson*, 1982; *Eagleson and Tellers*, 1982; *Eagleson and Segarra*, 1985]. Although this approach has received its share of criticism [*Hatton et al.*, 1997; *Kerkhoff et al.*, 2004], it did spur two research directions proven to be invaluable in our understanding of and ability to predict earth system dynamics: (1) the incorporation of plant physiological processes in quantitative hydrology and climate studies [*Sellers et al.*, 1997]; and (2) the further investigation of the co-evolution of the biotic and abiotic components of the earth system. The latter direction has contributed to more parsimonious models of land-atmosphere exchange [e.g. *Kleidon*, 2004; *Schymanski et al.*, 2009] and improved land management practices [*Folke et al.*, 2004]

More recently, a similar water balance model was developed for application in water-controlled ecosystems. This framework included a simplified functional representation of vegetation-soil moisture interaction in place of Eagleson's optimality assumption [*Rodriguez-Iturbe et al.*, 1999a; *Laio et al.*, 2001a] and successfully reproduced characteristics of the soil

water balance [*Rodriguez-Iturbe and Porporato*, 2004]. The model has supported a mechanistic interpretation for many observed landscape patterns. As an example, the Kalahari Transect in central Africa covers a rainfall range from approximately 250 to 1600 [mm yr^{-1}], with grasses predominant in the drier, southern region and trees predominant in the wetter, northern region [*Scanlon and Albertson*, 2003]. Simulations of the water balance demonstrate that the observed vegetation is that which experiences a minimum of a theoretically derived water stress, or deviation from the maximum ET rate [*Porporato et al.*, 2003a; *Scanlon and Albertson*, 2003]. In a separate study, it was argued that spatial interactions between trees and grasses in mixed savanna ecosystems produce an ecosystem structure that minimizes the time-averaged water stress of the system [*Rodriguez-Iturbe et al.*, 1999b]. Further analysis of the water balance model shows that perceived water stress is a function of soil hydraulic properties, rooting depths, maximum ET rates, and water stress responses [*Porporato et al.*, 2001; *Laio et al.*, 2001a]. In all of the cases described here, we see that the model provides a theoretical basis for *Noy-Meir*'s [1973] conceptualization of dryland ecohydrology.

While the initial focus of this work was on improving predictability in the hydrologic sciences, more recent studies have extended the theory to include the biogeochemical cycles. The soil water balance model has been coupled to similarly complex models of photosynthesis [*Daly et al.*, 2004a;b; *Porporato et al.*, 2004; *Williams and Albertson*, 2004], soil respiration [*Riveros-Iregui et al.*, 2011; 2012], and soil C-N cycling [*Porporato et al.*, 2003b; *D'Odorico et al.*, 2003]. These studies elucidate the tight coupling of surface water and carbon fluxes imposed by their coincident stomatal transport and patterns of spatial and temporal variability. Landscape variability in respiration was attributed to variability in soil moisture driven by underlying topographic gradients [*Riveros-Iregui and McGlynn*, 2009; *Riveros-Iregui et al.*, 2011]. The temporal dynamics of the soil C-N cycle were shown to exhibit lower frequency variability than that of the soil moisture dynamics, due to microbial sequestration of N and the long decomposition times required to release C and N from recalcitrant organic compounds [*D'Odorico et al.*, 2003]. Despite this progress in the mechanistic understanding and modeling of dryland ecosystems, these studies only consider a uni-directional causality between the soil water and C-N cycles – that is, the C-N dynamics are controlled by soil moisture, but not vice versa.

Given the ubiquity of N limitation in terrestrial ecosystems and the scale of anthropogenic modification of the N cycle, the most conspicuous assumption in the studies summarized here seems to be that of exclusive water control on ecosystem structure and function. As stated by *Rodriguez-Iturbe et al.* [2001a],

> "Although other sources of stress (fire, grazing, nutrient availability, etc.) are certainly also present, in many of the world [sic] ecosystems soil moisture is the most important resource affecting vegetation structure and organization."

and *Eagleson* [2002],

> "We propose that the optimum foliage state will be that giving maximum canopy conductance, because that will provide maximum water-borne nutrient flux from soil to plant."

This assumption is certainly well justified. Soil moisture controls nearly every aspect of mineral N delivery, from decomposition rates to the advective and diffusive fluxes of N to the root surface. In so-called water-controlled ecosystems, the correlation between water and N supply is so strong that the attribution of their observed effects on ET and productivity is highly impractical [*Burke et al.*, 1997; *Craine*, 2009]. However, evidence exists that primary productivity is often co-limited by water and N availability, even in water-controlled ecosystems [*Hooper and Johnson*, 1999]. Co-limitation suggests addition of either water or N to the system will increase productivity. In human-dominated landscapes, where atmospheric N deposition and N fertilization are commonplace, not all plant-available N is delivered by soil moisture-controlled decomposition rates. Therefore, it would seem likely that, at least under conditions where water and N supply are decoupled, N could play an indirect role in plant-water interactions. One very basic outstanding research question in dryland ecohydrology, that echoes the hypothesis in section 1.2 above, is thus: *what is the role of nitrogen supply in the structure and function of dryland ecohydrological systems?*

In a research track parallel to that discussed above, the land surface models (LSMs) applied in global climate prediction and weather forecasting have evolved to incorporate dynamic vegetation models [*Sellers et al.*, 1997] and fully coupled C-N dynamics [*Schimel et al.*, 1997; *Dickinson et al.*, 2002; *Tague and Band*, 2004; *Sokolov et al.*, 2008]. In contrast

to the ecohydrological approach, whereby mechanism has been inferred from the emergent properties of a model grossly simplified with respect to its ecophysiological features, LSM development followed a reductionist approach to the representation of vegetation dynamics and associated water and carbon fluxes. The primary approach is based on the observed correlation between leaf gas exchange and net carbon assimilation [*Collatz et al.*, 1991; *Leuning*, 1995]. Therefore, stomatal dynamics and their control on ET are parameterized through the behavior of the leaf photosynthetic machinery in response to various environmental states at the leaf surface (temperature, humidity, wind speed, radiation). While earlier models treated vegetation cover of the land surface as static or varying with a prescribed seasonality, more recent versions incorporate a prognostic representation of coupled vegetation-soil moisture dynamics [*Sellers et al.*, 1997]. One such model was specifically developed for application in dryland ecosystems and predicts many of the previously noted plot- and landscape-scale patterns of organization in the carbon and water cycles [*Ivanov et al.*, 2008a;b]. For example, the authors show how terrain-modulated water and energy inputs lead to niches of favorability for primary production.

While the full coupling of water, C, and N dynamics has yet to be explored in the ecohydrological framework, several LSMs have fully coupled the soil C-N cycle with vegetation dynamics and the surface water-energy balance [*Schimel et al.*, 1997; *Dickinson et al.*, 2002; *Tague and Band*, 2004; *Sokolov et al.*, 2008]. The application of these models has lead to many intriguing hypotheses on the organization of hydrology and biogeochemistry in ecosystems and its significance within the earth system dynamics. *Schimel et al.* [1997] used output from their model to show the emergence of correlations between ET, NPP, and N mineralization, demonstrating the pervasive influence of energy and water availability on ecosystem processes. At the global scale, models coupling soil C and N cycles generated the hypothesis that N limitation to primary productivity may modulate the soil-atmosphere CO_2 flux and resulting atmospheric CO_2 concentrations [*Sokolov et al.*, 2008]. Model results have also suggested that, in environments where water and N co-limit productivity, observed vegetation characteristics are those that simultaneously optimize the use of both resources for the acquisition of CO_2 [*Mackay*, 2001; *Hwang et al.*, 2009]. Despite the intrigue and novelty of these hypotheses, few studies have explored the applicability and accuracy of the model

assumptions with respect to ET within the context of site-specific experiments. The primary objective of this thesis is to develop an ecohydrological model that effectively couples the water, carbon, and nitrogen cycles and to evaluate model performance with experimental observations.

1.4 Thesis outline

This thesis utilizes physically-based modeling and data analysis to understand the role of the nitrogen cycle in ecohydrology. Specifically, the following questions are addressed for the Loma Ridge field experiment:

1. What vegetation characteristics that interact with the water balance respond to variability in nitrogen supply rates?
2. Are these responses expressed in the surface water-energy balance?
3. How do various modeling assumptions capture this sensitivity?

Experimental data collected in a grassland with varying water and nitrogen experimental treatments are analyzed in *Chapter 2*. These data are interpreted within the context of previous empirical results and the prevailing eco-hydrological theory. In *Chapter 3*, a new parameterization to model coupled water, carbon, and nitrogen dynamics is developed and validated. Subsequently, this model is applied in *Chapter 4* to investigate how productivity and root-leaf biomass allocation responds to variability in the coupled water and nitrogen supply rates and whether this vegetation sensitivity to the nitrogen balance influences the surface water-energy balance. The experimental data are discussed within the context of this new model. The thesis then concludes with a summary and prospectus for future work in *Chapter 5*, including a proposal for where accurate knowledge of nitrogen dynamics is necessary for modeling land surface processes.[5]

[5]For further reading on the commonly held material presented in this chapter, see the following texts that have contributed to my understanding of these topics: *Bonan* [2002]; *Brady and Weil* [2004]; [*Bras*, 1989]; [*Jenny*, 1994]; *Lambers et al.* [2008]; [*Liou*, 2002]; [*Madigan et al.*, 2002].

Chapter 2

The Ecohydrology of Loma Ridge

From the work of *Noy-Meir* [1973] and *Eagleson* [1978a;b;c;d;e;f;g] to the present, many studies have quantified the interactions between soil, vegetation, and climate. Below, assumptions commonly used to model the vegetation-modulated water balance are introduced along with corresponding diagnostics used to infer optimality in ecosystem function. Observations from the Loma Ridge field experiment, which includes factorial water and nitrogen addition treatments, are then described and analyzed within the context of the ecohydrological model. This model analysis suggests a hypothesis of organization in the soil-plant-atmosphere continuum under conditions of varying nitrogen supply.

2.1 Ecohydrologic water balance theory

A recent series of papers have provided insight into the co-organization of ecological and hydrological processes [*Laio et al.*, 2001a;b; *Porporato et al.*, 2001; *Rodriguez-Iturbe et al.*, 2001a]. Their soil water balance model subsequently served as the basis for studies investigating the role of soil texture, plant water use characteristics, and climate in the dynamics of the water cycle and plant populations [*Fernandez-Illescas et al.*, 2001; *van Wijk and Rodriguez-Iturbe*, 2002; *Porporato et al.*, 2003b; 2004; *Fernandez-Illescas and Rodriguez-Iturbe*, 2004]. This model is described here and follows closely the development of *Rodriguez-Iturbe et al.* [2001a] and *Laio et al.* [2001a] with some minor modifications.

2.1.1 Soil water balance model

The daily-scale, vertically-averaged soil water balance is shown conceptually in Figure 2-1 and written as,

$$nz_r \frac{ds(t)}{dt} = P(t) - I(t) - R[s(t), t] - E[s(t)] - L[s(t)] \tag{2.1}$$

where n [m^4 m^{-3}] is the soil porosity, z_r [m] is the root-zone depth, s [-] is the relative soil saturation (i.e. $s = \theta/n$), P is precipitation, I represents the evaporative losses due to interception by the canopy, R is surface runoff, E is soil evaporation, T is transpiration, and L is leakage below the soil column (all in units of [mm d^{-1}]). The model is formulated with the following assumptions [*Rodriguez-Iturbe et al.*, 2001a]:

1. The model is applied at the plot scale, an area with a characteristic scale of a few meters and represents a single tree or a small patch of grasses, shrubs, or bare soil.

2. The model only considers water fluxes in the vertical direction and, thus, best represents a horizontal plot. While R and L may exit (or enter) the modeled control volume laterally, the horizontal components of these fluxes are driven by topographic effects, which may be neglected for a flat plot.

3. The model is aggregated, or "lumped," in the vertical direction, such that heterogeneity in the vertical profiles of root density and soil moisture is averaged. Soil moisture is characterized by a single average value and the intricacies of root structure are captured in a single parameter, z_r.

4. Only saturation-excess runoff is permitted, there is no mechanism for infiltration-excess runoff production.

5. The saturated zone is assumed to be located far enough below the root zone such that it does not interact with the modeled soil moisture dynamics.

Rainfall and infiltration. The model is forced with a daily rainfall time-series generated either from observations or from a suitable probabilistic model of the processes governing rainfall arrival and intensity. Rainfall is commonly modeled as a poisson process,

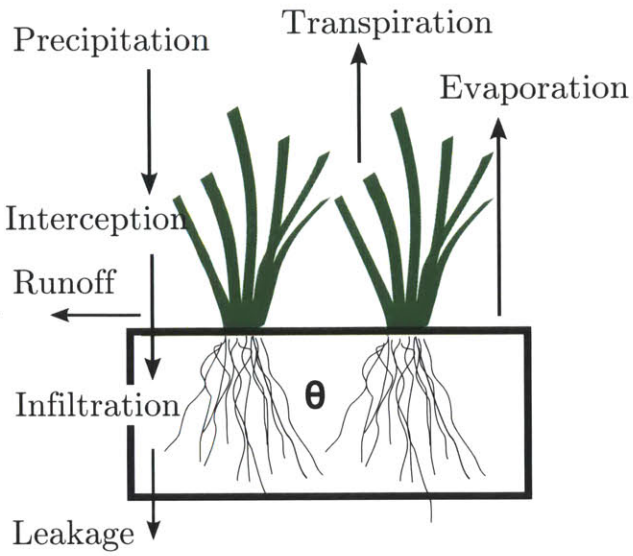

Figure 2-1: Conceptual bucket water balance model.

whereby the times between the arrivals of successive rainfall events, τ [d], are assumed to be independent and identically distributed following the exponential distribution,

$$f_T(\tau) = \lambda \exp(-\lambda\tau) \text{ for } \tau \geq 0 \tag{2.2}$$

where λ [d^{-1}] is the mean storm frequency, or the inverse of the mean inter-arrival time. Similarly, rainfall depths are assumed to be exponentially distributed with mean α [m].

Rainfall partitioning for a storm of depth h [m] is determined instantaneously at the event arrival time $t = t*$. Canopy interception losses are determined as a function of the vegetated ground fraction v,

$$I(t*) = \min[h(t*), i_{max}v] \tag{2.3}$$

where i_{max} [m] is a parameter describing the interception loss for a fully vegetated ground surface (v is defined below). Infiltration and R are then determined from the remaining rainfall volume ($h' = h - I$) by the antecedent soil moisture condition $s(t*)$. Infiltration is taken as the minimum of $h'(t*)$ and the capacity of the soil to hold additional moisture at that time, $nz_r[1 - s(t*)]$. If $nz_r[1 - s(t*)] < h'(t*)$ the remainder is partitioned to runoff.

Thus, the effective rainfall, or infiltration depth, is

$$P_e(t*) = P(t*) - I(t*) - R(t*) = \min\{h'(t*), nz_r[1 - s(t*)]\} \tag{2.4}$$

and

$$R(t*) = \max\{0, h'(t*) - nz_r[1 - s(t*)]\} \tag{2.5}$$

Evaporation and transpiration. The water balance in equation 2.1 is coupled with a mechanistically simple evapotranspiration model. The daily average transpiration rate T [mm d^{-1}] is defined as the product of a climate- and vegetation-specific potential transpiration rate T_p [mm d^{-1}] and a linear scaling factor β_v that accounts for soil water deficit,

$$T(s) = T_p \cdot \beta_v = T_p \cdot \begin{cases} 0 & s \leq s_w \\ \dfrac{s - s_w}{s^* - s_w} & s_w < s \leq s^* \\ 1 & s > s^* \end{cases} \tag{2.6}$$

where s_w [-] is the permanent wilting point, below which transpiration ceases, and s^* [-] is the incipient stress point, above which transpiration occurs at the potential rate.

T_p in equation 2.6 can be expressed in terms of observable canopy characteristics. Net carbon assimilation, transpiration, and stomatal conductance vary with depth in the canopy as light is extinguished by upper canopy layers. The energy available for photosynthesis decreases exponentially with cumulative leaf area index (LAI, L_a [m^2 leaf m^{-2} ground]) [*Monsi and Saeki*, 2005] and stomatal conductance is proportional to the local irradiance through the carbon assimilation rate [*Leuning*, 1995]. The total canopy water vapor conductance G_c [mol H_2O m^{-2} ground s^{-1}] is then,

$$G_c = \int_0^{L_a} g_s^{max} \beta_v \exp(-kl) dl = g_s^{max} \beta_v k^{-1} [1 - \exp(-kL_a)] \tag{2.7}$$

where g_s^{max} [mol H_2O m^{-2} leaf s^{-1}] is the light-saturated leaf-specific stomatal conductance measured at the top-of-canopy and k [m^2 ground m^{-2} leaf] is the canopy light extinction

coefficient. Under the diffusion analogy,

$$T = G_c D = g_s^{max} \beta_v k^{-1} \left[1 - \exp\left(-kL_a\right)\right] D \tag{2.8}$$

where D [kPa kPa^{-1}] is the vapor pressure deficit normalized by atmospheric pressure.

Bare soil evaporation is defined similarly,

$$E(s) = E_p \beta_s \exp\left(-kL_a\right) \tag{2.9}$$

where β_s takes the same form as equation 2.6, but E varies linearly between a maximum at s_w and 0 at the hygroscopic point, s_h, and the factor $\exp\left(-kL_a\right)$ accounts for the fraction of energy that penetrates the canopy to the soil surface.

Leakage. Leakage below the root zone is assumed to depend on water content in a fashion similar to the unsaturated hydraulic conductivity,

$$L(s) = k_s s^c \cdot \frac{\exp\left[\beta(s - s_{fc})\right] - 1}{\exp\left[\beta(1 - s_{fc})\right] - 1} \tag{2.10}$$

where k_s [mm d^{-1}] is the saturated hydraulic conductivity, $c = 2b + 3$ represents the decay of conductivity with saturation, where b is the soil pore size distribution index, s_{fc} is the soil moisture at field capacity, and $\beta = 2b + 4$.

Although this model is very simple with respect to its representation of the underlying physical and ecological processes, it does have its advantages. First, analytical solutions exist for the statistical behavior of the water balance, when a poisson process is assumed for rainfall generation. Second, the parameterizations are physically relevant, easy to understand, and, when analytical solutions are not sought, lend themselves to rapid numerical integration. Lastly, various indicators of ecological success can be derived directly from the water balance output. These indicators are useful for the identification of optimal (or deviations from optimal) ecosystem structure and function.

2.1.2 Optimality hypotheses

Vegetation optimality hypotheses are a useful modeling approach and an interesting lens through which to examine organization in nature. Some authors have used the idea to simplify the modeling of extremely complex ecophysiological processes underlying vegetation influence on land-atmosphere exchange [*Eagleson*, 1978a;b;c;d;e;f;g; *Schymanski et al.*, 2009; *Sivandran*, 2011]. In place of modeling the underlying process, these models represent the outcome of that process and assume its dynamics conform to some pre-defined optimality principle. For example, *Sivandran* [2011] models root dynamics under the assumption that the rate of growth is that which maximizes β_v at a given time. In contrast, root growth rates are certainly determined by countless physical processes – roots sense and grow toward water and nutrients [*Nobel*, 2009] (models of this behavior exist [*Diggle*, 1988; *Dunbabin et al.*, 2002]) and respond to gravity [*Knight*, 1806] – but it is the aggregate behavior that is ultimately important for hydrologic modeling purposes. Others have combined the predictions of these ecophysiological process models (of varying levels of complexity) with optimality hypotheses to demonstrate optimality in the observed environment [*Caylor et al.*, 2004; 2005; 2009; *Collins and Bras*, 2007; *Ivanov et al.*, 2008a;b; *Hwang et al.*, 2009].

Several hypotheses have been suggested to govern the optimal organization of ecohydrological systems, all stemming from Eagleson's original work. Eagleson initially proposed two assumptions that allowed him to reduce the dimensionality of his annual water balance model. First, within and between years, ecosystems achieve an equilibrium canopy density that maximizes soil moisture (i.e. minimizes water stress) and, correspondingly, minimizes evapotranspiration. Secondly, over evolutionary[1] time-scales, given the equilibrium canopy density, the species composition adjusts such that the transpiration rate per unit leaf area is maximized. Together, these assumptions imply simultaneous maximization of the mean growing season soil moisture and transpiration rate. The inconsistency of this proposal with reality was quickly uncovered as the two objectives are in competition with one another – simply put, the maximum soil moisture is always associated with zero transpiration [*Salvucci and Eagleson*, 1992]. Indeed, observed vegetation characteristics correspond to a soil moisture value of moderate stress that is lower than the theoretical maximum [*Salvucci*

[1]Eagleson's terminology, but may also be interpreted as ecological time-scales

and Eagleson, 1992; *Kochendorfer and Ramirez*, 2010]. This indicates a potential trade-off between transpiration and water stress, confirmed elsewhere in the literature [e.g. *Kerkhoff et al.*, 2004] on the basis that although transpiration must occur for plant growth, it simultaneously depletes soil moisture and induces water stress.

The growth-stress trade-off can be represented by properties of the water balance alone, without invoking an additional model for the ecosystem carbon balance. *Caylor et al.* [2009] expressed the trade-off as the maximum "stress-weighted transpiration" hypothesis, which balances transpiration with water stress by maximizing their product, a surrogate for NPP,

$$\zeta = \overline{T}(1 - \overline{\chi}) \tag{2.11}$$

where the bar represents a temporal mean and χ is the dynamic water stress defined below.

Water stress may be interpreted as the magnitude of an excursion below the maximum transpiration rate, or,

$$\xi(s) = \begin{cases} 1 & s \leq s_w \\ \left(\dfrac{s^* - s}{s^* - s_w}\right)^q & s_w < s \leq s^* \\ 0 & s > s^* \end{cases} \tag{2.12}$$

where q is a parameter that accounts for possible non-linearities in the water stress response. Because water stress affects photosynthesis and growth, stress effects are cumulative over time. To address this point, a "dynamic" water stress was also proposed [*Porporato et al.*, 2001],

$$\overline{\chi} = \begin{cases} \left(\dfrac{\overline{\xi}'\overline{T}_{s^*}}{kT_{seas}}\right)^{1/\sqrt{\overline{n}_{s^*}}} & \overline{\xi}'\overline{T}_{s^*} < kT_{seas} \\ 1 & \text{otherwise} \end{cases} \tag{2.13}$$

where $\overline{T}_{s^*}$ [d] is the mean duration of each period spent below s^*, $\overline{n}_{s^*}$ is the mean number of times the water stress threshold is crossed, k is a parameter, and T_{seas} [d] is the length of the growing season. This formulation accounts for the fact that plants respond to the frequency, duration, and severity of water stress.

The maximum stress-weighted transpiration hypothesis makes several predictions for the

optimization of plant water-use traits. In its original application [*Caylor et al.*, 2009], it was shown that tree-grass coexistence in an African savanna achieves a greater ζ than either a homogeneous woodland or grassland for a climate with high inter-annual rainfall variability. In addition, the spatial distribution of trees, grasses, and shrubs along a large topographic gradient in a semi-arid river basin was shown to be similar to that which maximizes ζ. The theory also predicts an optimal ratio of lateral root radius to canopy radius for trees. Therefore, ζ seems to integrate the organization of plant-water interactions across a wide range of scales [*Caylor et al.*, 2009].

Other empirical evidence for ecohydrological optimality does exit. First, several examples demonstrate that a minimum modeled water stress is associated with vegetation patterns similar to those that are observed [*Porporato et al.*, 2003b; *Caylor et al.*, 2004; 2005]. Secondly, simultaneous observations of evapotranspiration and soil moisture, across a wide range of ecosystem types, show that the most likely soil moisture state is that which maximizes evapotranspiration [*Emanuel et al.*, 2007]. In addition, model simulations were used to argue that observed root distribution are those that confer maximum transpiration under given soil and climate properties [*Collins and Bras*, 2007]. Lastly, when these optimality conditions are assumed *a priori* to aid in dynamic simulations, modeled energy, water, and carbon fluxes match well with observations [*Schymanski et al.*, 2009; *Sivandran*, 2011]. Yet, despite such comprehensive evidence for the optimization of ecosystem water use, the effect of nutrient supply has yet to be studied from this perspective.

The role of soil nutrient supply in the plant-modulated soil water balance may be understood through variations in the canopy characteristics, L_a and g_s ($= g_s^{max}\beta_v$, equation 2.7). Eagleson's [1978a; 1978f] maximum transpiration hypothesis was originally expressed as a maximization of the canopy conductance, or the product of the canopy density, M, and transpiration efficiency, k_v (i.e. Mk_v). This product is analogous to the canopy conductance given by equation 2.7, when normalized by β_v. In equation 2.7, g_s^{max} plays the role of k_v and $k^{-1}\left[1-\exp\left(-kL_a\right)\right]$ plays the role of M. If an optimal transpiration rate exists, this constraint implies a trade-off between L_a and g_s. This trade-off is confirmed by the model in Figure 2-2 and will become a central part of our interpretation of the Loma Ridge field observations below.

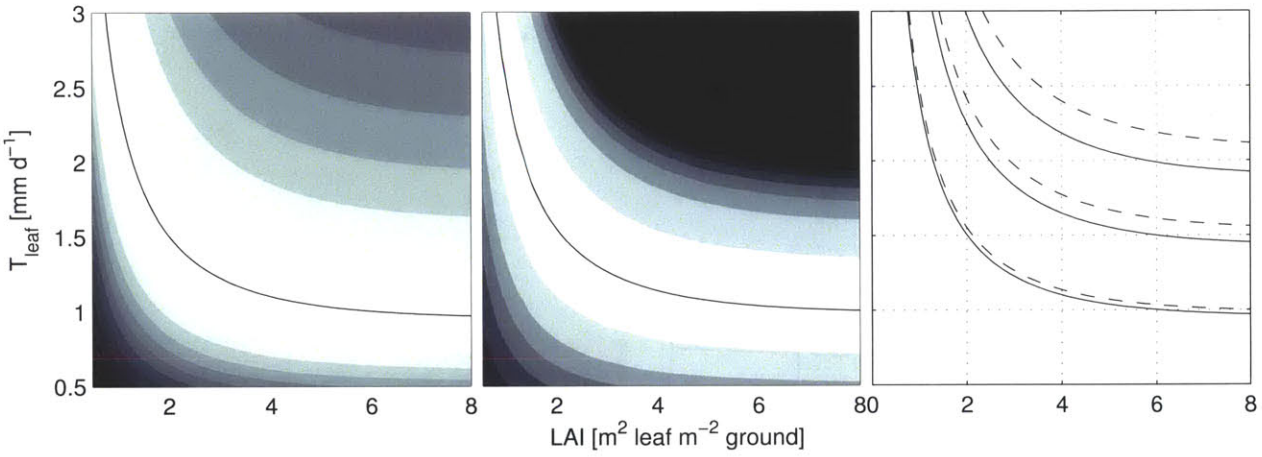

Figure 2-2: Optimal leaf area index and stomatal conductance. Static (a) and dynamic (b) stress-weighted transpiration as a function of leaf area index and transpiration per unit leaf area (i.e. $g_s D$) for the soil, climate, and vegetation parameters: $\alpha = 15$ mm, $\lambda = 0.1$ d^{-1}, E_p=0.1 mm d^{-1}, $s_w = 0.24$, $s^* = 0.57$, $b = 5.39$, $k_s = 200$ mm d^{-1}, $n = 0.45$, $s_h = 0.19$, $s_{fc} = 0.65$; and (c) optimal $L_a - g_s$ combinations for several values of annual rainfall ($\lambda \in [0.1, 0.15, 0.2]$ d^{-1}). In (a) and (b), the color scale varies from black (minimum) to white (maximum). In (c), the solid lines correspond to ξ and the dashed lines correspond to χ.

2.2 Loma Ridge

The Loma Ridge experimental site is located in the Santa Ana foothills in central Orange County, California (33.742°N, 117.704°W) (Figure 2-3). The site is managed under the auspices of the Irvine Ranch Conservancy (http://irvineranchconservancy.org) and operated and maintained by the University of California, Irvine (UCI). The experiment was established in 2006 and contributes to a broader effort to understand the impact of environmental change on the function of California's ecosystems. The data analyzed and presented here were collected and made freely available by members of the Michael Goulden Laboratory at UCI (to which the present author is profoundly indebted and without which none of this work would have been possible).

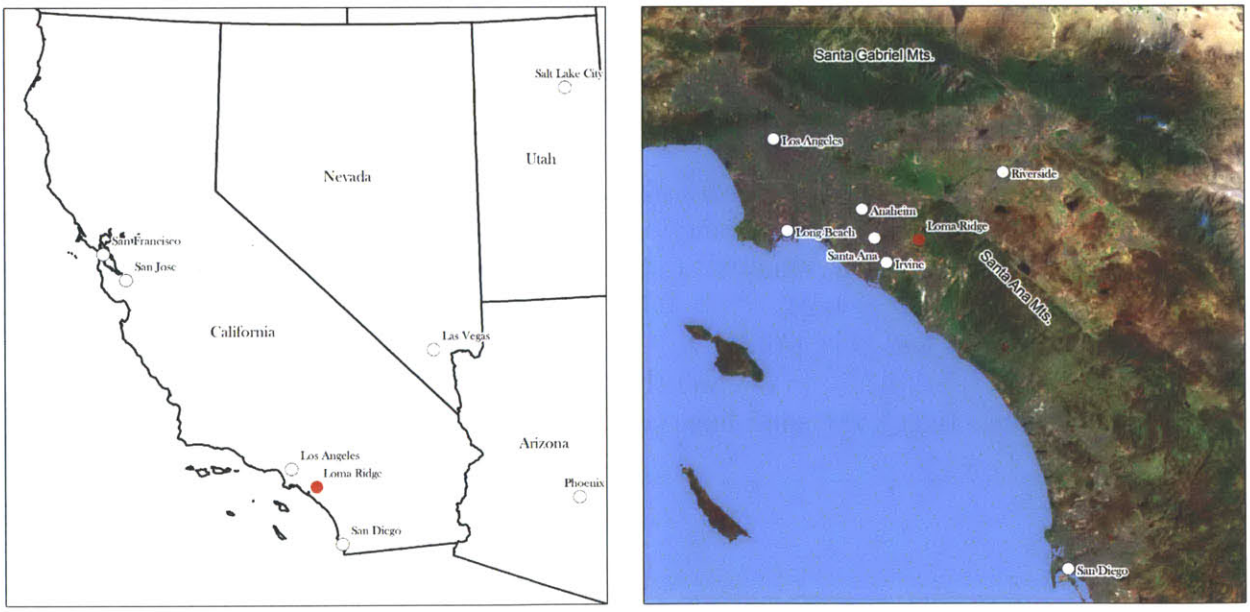

Figure 2-3: Loma Ridge regional and local context.

2.2.1 Soil, climate, vegetation, and disturbance

A brief review of the prevailing vegetation-environment relationships at Loma Ridge provides insight into the function of this ecosystem and a basis for interpretation of the following data analysis. Loma Ridge refers to a region of the foothills separating the alluvial outwash known as the Los Angeles basin (to the west) and the Santa Ana Mountains (to the east). The Los Angeles basin is generally a few meters above sea level and hosts substantial urban and suburban development. Within just a few kilometers of the experimental site are the densely developed cities of Tustin, Irvine, and Lake Forest, some agricultural land, and major transportation corridors. These land uses contribute to some of the highest N deposition rates in the United States [*Fenn et al.*, 2003]. By contrast, the Santa Ana Mountains are generally undisturbed by human activity, protected as part of the Cleveland National Forest. The vegetation is primarily composed of coastal sage scrub and chapparal communities, characterized by dense stands of evergreen or drought-deciduous shrubs [*Schoenherr*, 1995]. The highest elevation is found at the 1,700 m summit of Santiago Peak.

Between the plain and mountains, the foothills rise to approximately 500 m, the highest elevation of Loma Ridge. The experimental plots are located on a northwest facing hillslope, just below the ridge. The elevation of the 200 m hillslope ranges between 345 and 370 m with a slope of approximately 12°. Below the hillslope, the site is dissected by two branches of a deep-cut ephemeral stream with steep banks a few meters high. Soil sampling and analysis indicate Loma Ridge grassland soils typically contain 67% sand, 14% clay, and 18% silt and are relatively homogeneous with depth at least up to 2 m (unpublished data). This soil composition is characterized as sandy loam (USDA), with properties as listed in Table 2.2 below.

A wide range of vegetation communities are found at Loma Ridge – including mixed annual and perennial grassland, coastal sage scrub, evergreen shrubs, and larger trees. Trees are exclusively found in the ephemeral channels, consistent with moisture accumulation in convergent areas of the landscape. On the hillslope, aerial photographs clearly show a marked contrast between the grass and coastal sage scrub communities (Figure 2-4). This pattern is ostensibly related to topography, with the coastal sage scrub primarily found at

higher elevations and grassland found near the channels. However, it does not seem to be simply a result of topographic moisture redistribution. Heterogeneity in soil composition likely dominates topographic redistribution in generating soil moisture patterns within the experimental area because the adjacent hillslope is relatively flat (no curvature) and has a relatively low slope of 12°. In addition, previous work has shown a localized patch of higher soil moisture near the center of the experimental area within a surrounding homogeneous field (data not shown). Alternative hypotheses for the vegetation patterning at this site include: (1) greater clay content beneath coastal sage scrub; (2) the existence of a permeable soil layer limiting infiltration and/or rooting depths beneath the grass community; or (3) a founder control effect.

Figure 2-4: Aerial photograph of Loma Ridge experimental area, showing the grass, shrub, and tree communities and their relationship to topography.

In addition to spatial patterning in topography, soil moisture, and vegetation, the dynamics of this ecosystem are driven by the temporal fluctuations of climate. The climate in Southern California is of a Mediterranean-type with cool, wet winters and dry, hot summers. Annual rainfall is marked by high inter-annual variability that follows a lognormal distribution with median 282 mm yr^{-1} (Figure 2-5). In a typical year, approximately 90% of this rainfall occurs between November and April, when net radiation and evaporative demand are low (Figure 2-6). As the winter subsides, the oncoming summer is characterized by rising net radiation, temperature, and evaporative demand. Rainfall is almost absent during the summer months, May through September.

The primary growing season straddles this transition between wet and dry seasons, during which water availability is high and temperatures have warmed to a level ideal for plant growth. The first winter rains in October and November create a moist soil environment, which initiates the germination of annual grass seeds. By the next substantial rainfall, seedlings are prepared to begin a period of rapid growth [*Barbour et al.*, 2007]. After the end of the rainy season, the surface soil moisture store is no longer replenished, water stress is induced, and the grasses enter their reproductive stage. During this time, biomass is allocated

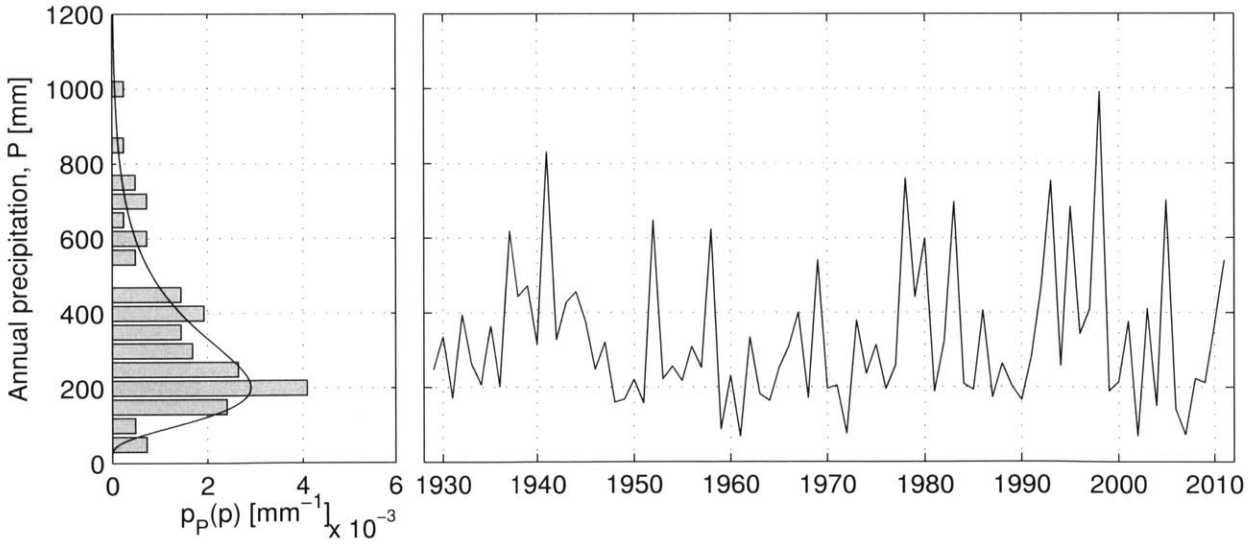

Figure 2-5: Rain gage observations summarized for the Santa Ana Fire Station, Tustin Irvine Ranch, and Loma Ridge rain gages, providing 83 years of data. Annual rainfall follows a log-normal distribution with $\mu = 332$ mm and $\sigma = 208$ mm (med=282 mm).

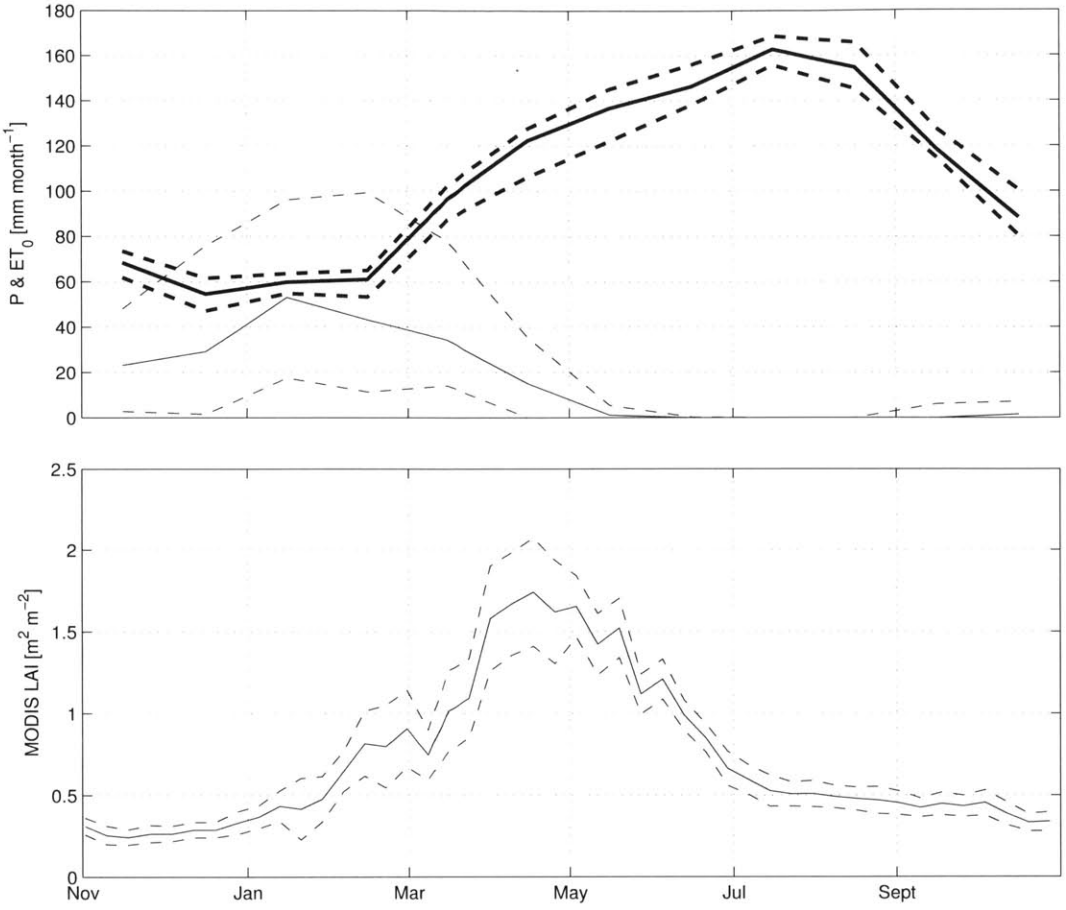

Figure 2-6: Typical seasonal dynamics of climate and vegetation activity at Loma Ridge: (a) reference evapotranspiration (ET_0, bold black lines, obtained from the California Irrigation Management System (http://wwwcimis.water.ca.gov/)) and precipitation (P, thin black lines, Santiago Dam) and (b) LAI as measured by the MODIS satellite. For ET_0 and P, the solid lines denote median values and the dashed lines denote the 25% and 75% percentiles. For LAI, the solid line is the mean value and the dashed lines denote $\pm\sigma$.

to seed production and leaf and root tissues senesce. Eventually, evapotranspiration is limited by severe soil water deficit, surface temperatures increase, and both water and temperature stresses cause physiological damage and mortality.

Although the seasonal dynamic is dominated by this rapid growth / rapid death behavior of the annual grasses and drought-deciduous shrubs, evergreen shrubs and trees also contribute. Their activity can be characterized as consistent, but relatively low rates of pho-

tosynthesis and transpiration. Growth of these functional types is supported by moisture stored in deep soil layers and the saturated zone, such that their activity has a minimal influence on the surface moisture dynamics. For these reasons, it is practical to ignore the deeper-rooted species for the ecohydrological analysis of the grass community.

Finally, disturbance, including drought, fire, and grazing, is a common element of this ecosystem. Historically, cattle and sheep grazed the site until the mid-1990s [*Potts et al.*, 2012]. A natural fire regime is often associated with the coastal sage scrub and chapparal communities. Toward the end of the dry season, plant tissues desiccate and become susceptible to fires stoked by the warm air brought from the desert by the Santa Ana winds [*Schoenherr*, 1995]. Fire return intervals at Southern California sites range between 5 and 100 years and average 30-40 years over the region [*Keeley and Fotheringham*, 2001]. It has been argued whether these fire frequencies have been reduced by modern fire suppression activities [*Minnich*, 1983; *Keeley and Fotheringham*, 2001]. In addition to fire, high inter-annual variability in rainfall imposes frequent drought on this ecosystem. Using the log-normal model introduced above, the return interval for drought 25% below the long-term median is 31 yr. Both a severe drought (rainfall was 20% of the median and the minimum on record) and a fire (that destroyed much of the experimental setup) occurred in October 2007, shortly after the start of the experimental program. This somewhat fortuitous event provides a unique opportunity to study the dynamics of disturbance recovery in this ecosystem.

2.2.2 Experimental setup

Factorial plot experiments were established in 2007 to study ecosystem responses to changing climate and increased nitrogen deposition. Twenty-four plots (approx. 6.1x8.5 m) are arranged within each of the grassland and coastal sage scrub communities, as shown by the solid dots and squares in Figure 2-7. All plots were burned in the October 2007 Santiago wildfire.

The plots are divided into eight groups of three water input treatments: ambient, ambient minus 40% (dry), and ambient plus 40% (wet). Rainfall is excluded from dry plots with retractable polyethylene roofs that were closed during approximately half of the rain events

(closed < 5% of the days during a year). Water draining from the roofs was collected in polyethylene tanks for subsequent application to the wet plots using pressure compensated drip tubing. Excluded events and irrigation rates are chosen to simulate observed patterns in storm frequency and intensity.

Each plot is split lengthwise and half of the ground area is fertilized and half remains unfertilized (control). Plots are fertilized with 2 gN m^{-2} immediate release calcium nitrate (15.5-0-0+19% Ca) prior to the growing season and 4 gN m^{-2} 100-day release calcium nitrate during the growing season. These deposition rates are similar to those occurring in the more urbanized areas of Los Angeles and Orange Counties [*Fenn et al.*, 2003].

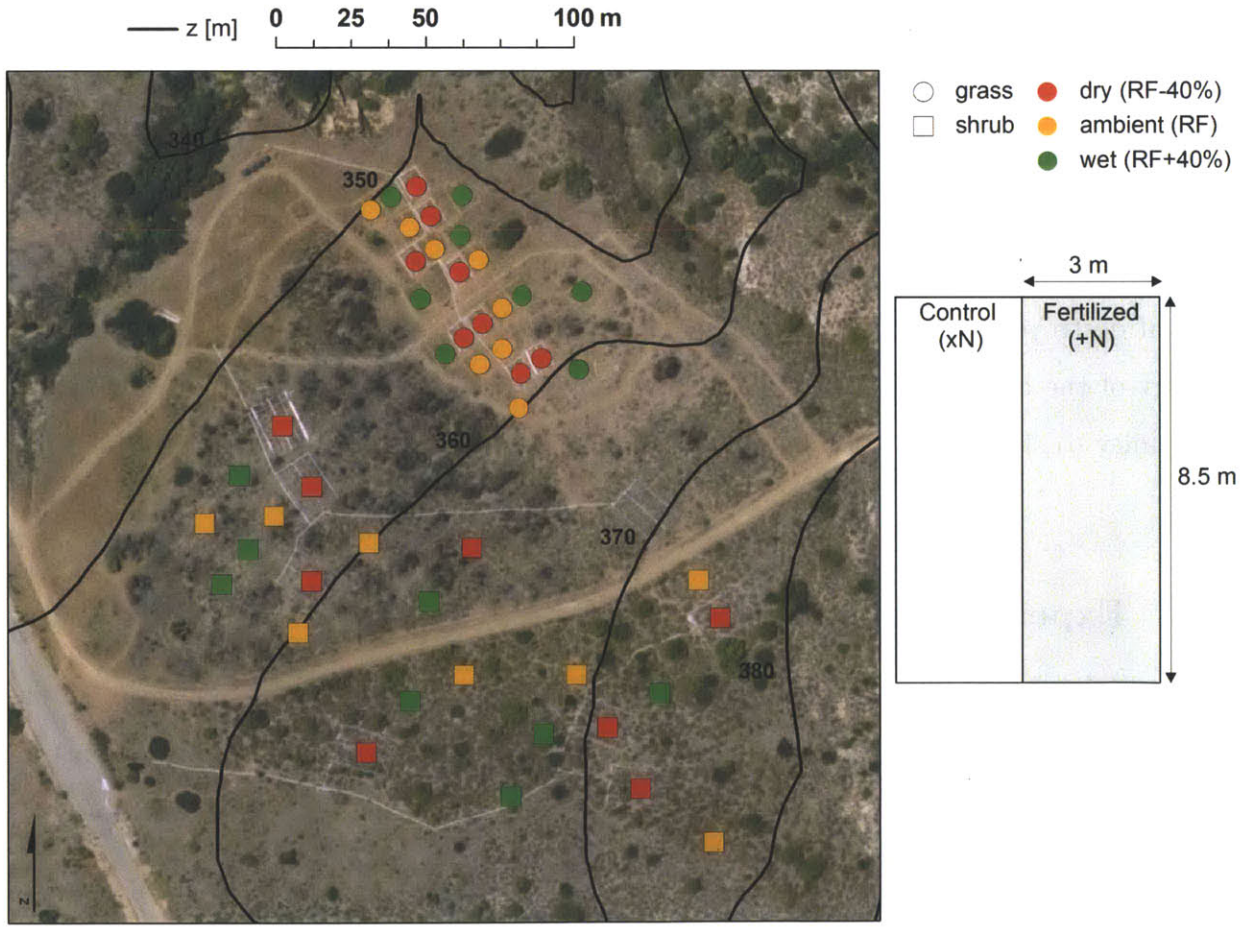

Figure 2-7: Loma Ridge experimental site layout.

Several physical and ecophysiological observations are collected within the experimental plots and are summarized in Table 2.1. In addition to these plot-level measurements, an eddy covariance tower is located in a similar grassland community approximately 1 km from the experimental site. These observations are used below to investigate the role of nitrogen supply in the ecohydrologic dynamics of this ecosystem (and to validate model results in subsequent chapters).

Table 2.1: Plot-scale observations collected at Loma Ridge 2007-present.

Observation		**Method**	**Frequency**
Species composition		point-intercept method with 100 points selected in a 1.5x0.5 m area	annually at the end of the growing season
Soil water content	$\overline{\theta}_{15}$	15-cm TDR[1] (MiniTrase, ICT Intl.)	$\sim 2-4$ weeks, x3 per plot
	$\overline{\theta}_{30}$	30-cm TDR[1] (HydroSense, Campbell Sci.)	$\sim 2-4$ weeks, x4 per plot
Precipitation	P	Tipping bucket rain gage	30 min
Leaf area index	L_a	PAR[2] measured by SunScan Canopy Analysis System (Dynamax)	$\sim 2-4$ weeks during the growing season
Leaf gas exchange	g_s, A_n	Open-path gas analyzer (LI-6400, LiCor)	$\sim 2-8$ weeks, March through July
ANPP[3]		harvest two 14x50 cm biomass strips	annually following the growing season

[1]Time-domain reflectometer
[2]Photosynthetically active radiation
[3]Above-ground net primary productivity

2.2.3 Data analysis and model parameters

The data summarized in Table 2.1 were used (1) to identify the response of grassland ecosystem characteristics to varying water and nitrogen supplies; (2) to constrain the water balance directly from the observations; and (3) to estimate parameters for the stochastic water balance model. Methods used to convert some of the direct observations into modeled parameters (e.g. PAR to LAI), to estimate rainfall model parameters, and to estimate observational errors are described in this section. The remaining parameters needed for the water balance model are summarized in Table 2.2 with references.

Leaf area index. Leaf area index, L_a, is estimated from direct observations of photosynthetically active radiation (PAR). Subcanopy PAR [mmol m^2 s^{-1}] was measured in each plot with the SunScan Canopy Analysis System (Dynamax). To compute a plot-scale value, a single measurement was taken at the top of the canopy and 5 evenly spaced measurements were taken below the canopy. For each independent below-canopy observation, i, L_i was calculated from PAR assuming exponential light attenuation within the canopy,

$$L_i = -k^{-1} \ln \left(f_{PAR}^i \right) \tag{2.14}$$

where $f_{PAR}^i = PAR_{below}^i / PAR_{above}$ [-] is the fraction of PAR transmitted through the canopy and $k = 0.5$ for grassland [*Monsi and Saeki*, 2005]. Random observational error at the plot scale was then estimated as the standard error of the 5 independent measurements,

$$SE_L^{plot} = \frac{\sigma_L}{\sqrt{n}} \tag{2.15}$$

To compute an LAI error estimate at the landscape scale, the 8 values computed above in each plot are combined,

$$SE_L^{land} = \frac{1}{n} \sqrt{\sum \left(SE_L^{plot} \right)^2} \tag{2.16}$$

In both cases, average values are taken as the arithmetic mean. This method of plot- and landscape-scale mean and random error estimates is applied to each of the observations – soil water content, leaf gas exchange, and ANPP.

Scaling leaf gas exchange measurements. Instantaneous stomatal conductance to water vapor was collected under conditions of peak sunlight and vapor pressure deficit between 10 am and 2 pm. Because the water balance model is applied at the daily scale, these measurements must be scaled to a daily average value. To do this, it is assumed that stomatal conductance and leaf transpiration follow an assumed diurnal pattern related to incoming solar radiation [*Daly et al.*, 2004a],

$$\phi(t) = \frac{4}{\delta}\left[-t^2 + (\delta + 2t_0)t - t_0(t_0 + \delta)\right] \tag{2.17}$$

where ϕ_t [-] is the fraction of the observed maximum mid-day value, t is the hour of the day, $t_0 = 6$ is the time of sunrise, and $\delta = 12$ is the day length. To convert stomatal conductance to transpiration rate per leaf area, g_s is multiplied by the vapor pressure deficit, D, calculated from air temperature and relative humidity collected at the time of measurement. Daily leaf transpiration, T_{leaf} [mm d^{-1}] plotted in figures 2-15, 2-16, and 2-17 is thus,

$$T_{leaf} = g_s^{obs} D(T_a^{obs}, q_a^{obs}) \int_0^{24} \phi(t)dt \tag{2.18}$$

Water stress correction for Mediterranean ecosystems. Because Loma Ridge experiences a Mediterranean climate, water stress (equation 2.12) must be corrected to account for the antecedent moisture condition at the beginning of the growing season that results from early winter rains. This correction is related to the mean first passage time, $T_{s^*}^0$, for soil moisture to cross s^* given an initial soil moisture s_0 and is given by [*Rodriguez-Iturbe et al.*, 2001b],

$$\chi' = \chi \cdot \frac{T_{s^*}^0 - T_{seas}}{T_{seas}} \tag{2.19}$$

.

Rainfall model. An exponential distribution is assumed for rainfall depth and interstorm arrival time at the daily scale. The parameters α and λ are estimated from the Santa Ana Fire Station daily rainfall record. The exponential model fit is demonstrated in Figure 2-8. The model reproduces the majority of rainfall variability, capturing approximately 99% of the mass of the storm depth distribution and approximately 90-95% of that of the inter-

storm duration distribution. The model tends to over-predict the depths of high-intensity storms and the durations of long inter-storm periods, both of which rarely occur. At the annual scale, these effects compensate each other and the model reproduces the median annual rainfall to within 2.5% ($\overline{P} = \alpha\lambda T_{seas} = 11.3 \cdot 0.17 \cdot 150 = 289$ mm). This behavior is typical for the exponential model and may be improved by either applying a minimum storm aggregation time [*Restrepo-Posada and Eagleson*, 1982] or by applying a multi-scale model [*Islam et al.*, 1990]. Regardless, the model performs very well for its relative simplicity, which will be further demonstrated in the results below, and, for that reason, is retained here.

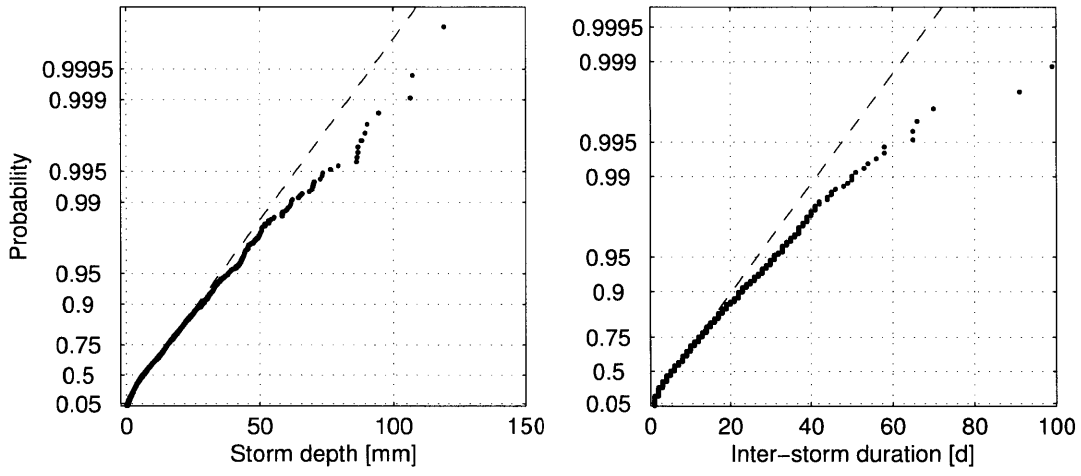

Figure 2-8: Exponential rainfall model fit. The dashed lines represent the theoretical probability density functions for an exponential distribution with mean $\alpha = 11.3$ mm (left) and $\lambda^{-1} = 5.9$ d (right). The black dots are daily observations from Santa Ana Fire Station.

Table 2.2: Soil water balance model parameters.

Parameter		Value	Units	Reference
Vegetation				
Point of incipient stress	s^*	0.46		*Laio et al.* [2001a]
Wilting point	s_w	0.18		"
Stress response exponent	q	3		*Porporato et al.* [2001]
Dynamic stress parameter	k	1		
Active soil depth	z_r	40	cm	*Holmes and Rice* [1996] *Schenk and Jackson* [2002a]
Climate[1]				
Mean rainfall depth	α	11.3	mm	Figure 2-8
Mean storm frequency	λ	0.17	d^{-1}	Figure 2-8
Maximum soil evaporation	E_p	0.1	mm d^{-1}	*Porporato et al.* [2001]
Growing season length	T_{seas}	150	d	Figure 2-6
Soil				
Porosity	n	0.43	m^2 m^{-2}	*Rawls et al.* [1982]
Field capacity	s_{fc}	0.56		"
Hygroscopic point	s_h	0.14		"
Saturated hydraulic conductivity	k_s	80	cm d^{-1}	"
Pore-size distribution index	b	4.9		"

2.3 Results

Loma Ridge experimental data are presented in the following section.[2] The discussion begins by looking at vegetation responses to varying water and nitrogen inputs, within and between years (2007-2011). Then, observations of the water balance are analyzed to ascertain the hydrologic response to varying water and nitrogen inputs. This includes direct observations of soil water content and indirect estimates of transpiration, derived from leaf gas exchange and leaf area index measurements. Finally, the observations are compared to the optimal vegetation characteristics determined from the stochastic water balance model output.

2.3.1 Experimental observations

ANPP and leaf area production are co-limited by water and nitrogen availability (Figure 2-9). In general, ANPP and LAI responded positively to fertilization. However, this effect is not consistent between years or between water input treatments. Under conditions of strong water limitation, fertilization had almost no effect. This occurs in all water input plots during the drought year of 2007 and in the dry water input plots when water input is below approximately 200 mm. In the next two growing seasons, 2008 and 2009, ANPP and LAI exhibited the largest response to fertilization. The response was lower in 2010 and not consistently present in 2011,[3] despite the fact that rainfall increased from 2009 to 2011 (Figure 2-5). A similar decay is also apparent in the LAI time-series derived from the Moderate Resolution Imaging Spectroradiometer (MODIS) aboard the Terra satellite (Figure 2-10). These observations indicate a decrease in productivity and its response to fertilization with time following fire (and/or drought) that does not seem to be linked with annual rainfall.

It is hypothesized that this effect may be due to (1) a pulse of nitrogen availability following fire and/or drought or (2) the removal of litter by fire, factors reminiscent of the transient maxima hypothesis [*Seastedt and Knapp*, 1993]. Both fire and drought may

[2]Some of the data and conclusions presented here were previously presented in conference or seminar presentations.

[3]Only ANPP data was available in 2011 because the LAI meter malfunctioned.

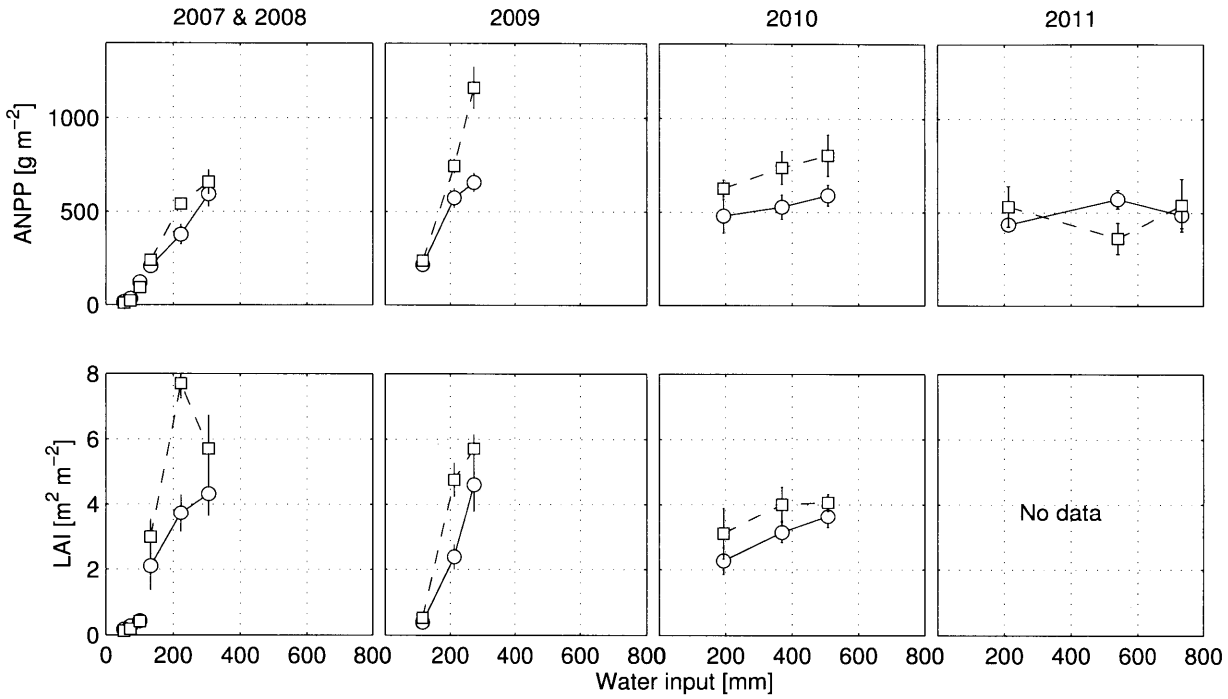

Figure 2-9: Plot-scale ANPP and LAI measured over the multi-year experiment. The solid lines denote control plots and the dashed lines denote fertilized plots.

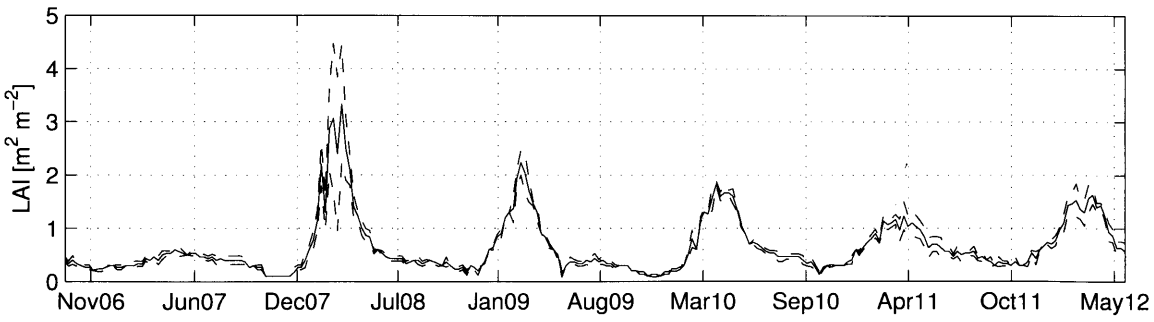

Figure 2-10: Seasonal and inter-annual dynamics of LAI derived from MODIS. The solid line represents the mean of three 1 km pixels within 1.5 km of the eddy covariance tower and the dashed lines indicate one standard deviation from the mean.

cause a short-term abundance of nitrogen availability. When fire is absent from the system, nitrogen accumulates in the soil as light availability above-ground is the primary factor limiting productivity and the nitrogen uptake rate is therefore less than the potential rate. This accumulated nitrogen then becomes available when fire removes accumulated litter and light limitation is released. Also, because productivity depends strongly on water availability, drought may also increase nitrogen availability in subsequent years by limiting mineralization and uptake during the drought year. These effects are diminished in following years as either nitrogen is sequestered in organic matter or litter re-accumulates on the surface.

In addition to ANPP and LAI measured at the plot-scale, leaf-scale gas exchange observations also exhibited a response to fertilization (Figure 2-11).[4] Stomatal conductance to water vapor, g_s, and net carbon assimilation, A_n, were measured with an open-path leaf gas exchange system (LiCor, LI-6400). In general, A_n increased and g_s decreased with fertilization, with a stronger effect in the ambient and wet plots as compared to the dry plots. A_n only increased in the ambient plots, consistent with ANPP and LAI responses. The positive response of ANPP and LAI, which is greatest in ambient plots, can therefore be partially attributed to an observed increase in leaf-level rates of photosynthesis.

From Figures 2-9, 2-10, and 2-11, it is clear that Loma Ridge grasses respond to both water and nitrogen availability by increasing photosynthesis, producing more biomass and leaf area, and simultaneously decreasing leaf-level transpiration rates. Leaf area determines the surface area over which water evaporates and becomes available for transport into the atmosphere and, thus, controls transpiration. Therefore, it is expected that the fertilizer-induced increase in LAI will be accompanied by an increase in transpiration. However, the leaf gas exchange measurements suggest that the LAI increase may be partially or fully offset by decreased g_s. This hypothesis is now tested with estimates of the components of the Loma Ridge soil water balance.

The surface soil water content, θ, describes the cumulative behavior of the terrestrial water balance. Each of the surface water fluxes (evaporation, transpiration, runoff, and

[4]Gas exchange data is presented for 4 days during the 2008 growing season, for which data quality was acceptable. I am indebted to Matt Gilbert of the Holbrook Lab at Harvard University for assistance in evaluating the usefulness of this data. It is fortunate that this data aligns with the year in which the largest LAI response to fertilization was observed.

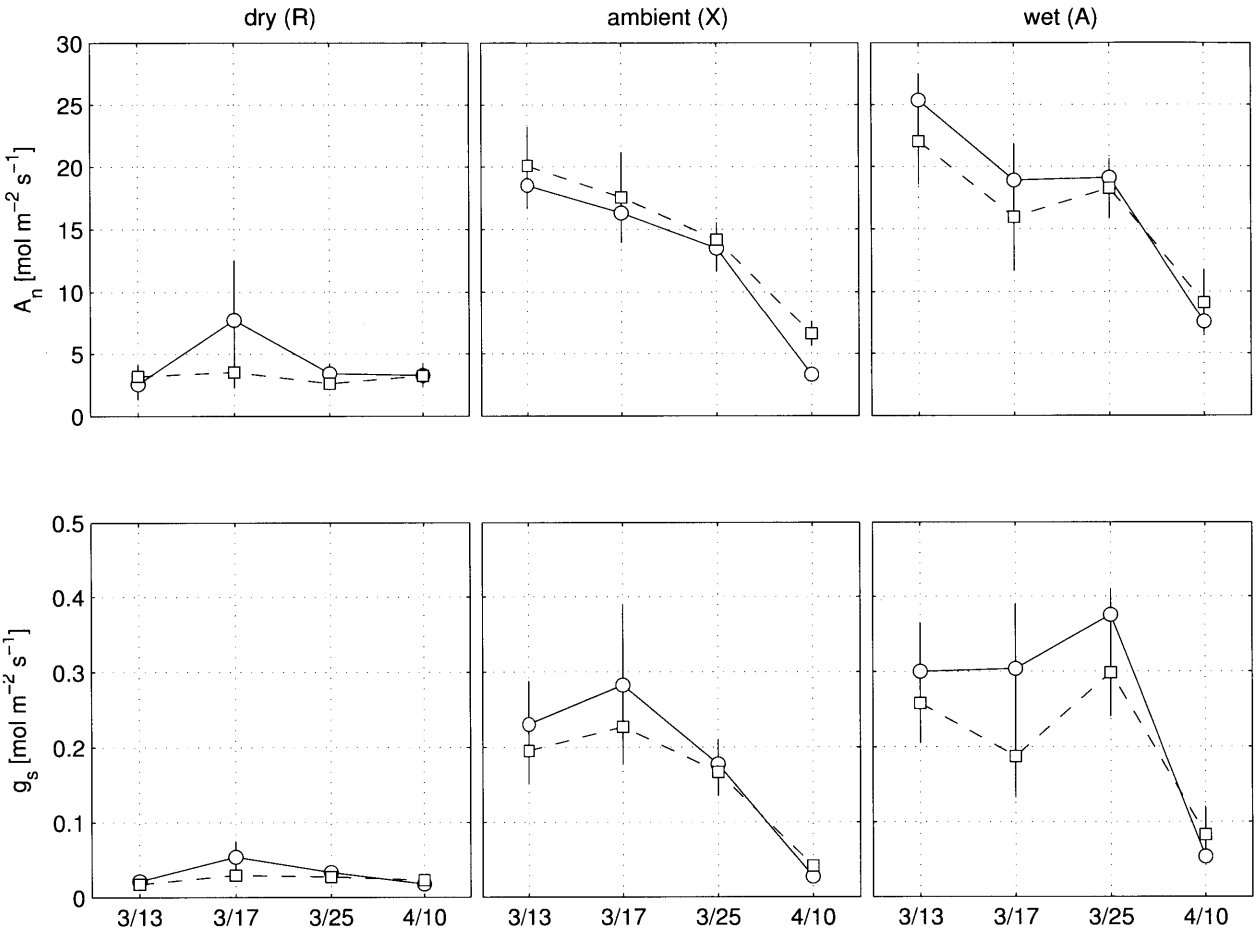

Figure 2-11: Leaf gas exchange observations. g_s and A_n measured at mid-day of 4 days during the 2008 growing season. March 13, 17, and 25 are near the peak LAI and April 10 is after water stress has developed.

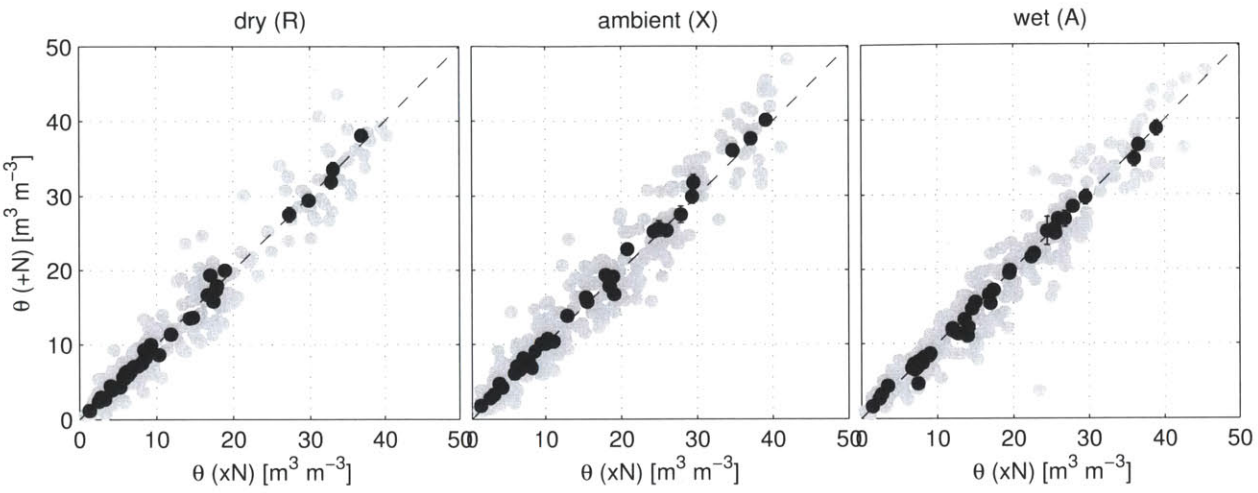

Figure 2-12: Soil water content in control and fertilized plots. The gray dots represent side-by-side comparisons within each of the 24 experimental plots and the black dots represent hillslope-scale averages ($\mu \pm SE$, $n = 8$). These plots combine 15-cm and 30-cm TDR data collected between 2007 and 2011.

leakage) depends on this quantity through the soil hydraulic properties. Measurements of $\overline{\theta}_{15}$ and $\overline{\theta}_{30}$ indicate no significant influence of fertilization in all water input treatments (Figure 2-12). Equivalent θ suggests at least the sums of the water fluxes are equivalent among ambient and fertilized plots. The scale of these observations is likely smaller than the rooting depth of the grass species at this site [*Holmes and Rice*, 1996], so it is not an exact representation of the root zone water content as defined in equation 2.1. Also, note the substantial variability in the side-by-side comparison around the 1:1 line (gray dots). This scatter is attributed to landscape variability in soil hydraulic properties. Although single plots may demonstrate a fertilization effect on θ, when taken together these effects are not discernible at the landscape scale.

To determine whether this consistency in soil moisture observations can be explained by transpiration, G_c is calculated from the canopy characteristics that control transpiration, L_a and g_s (Figure 2-13). Two distinct regimes are evident in the data. When water is strongly limiting, canopies exhibit low LAI and g_s in both control and fertilized plots. This occurs in the dry plots (circles) and late in the season (10 April, closed symbols). When water is less limiting, LAI increases (a), but g_s decreases (b) in fertilized plots. These canopy changes offset one another, leading to a similar G_c (c). Therefore, under conditions of low water

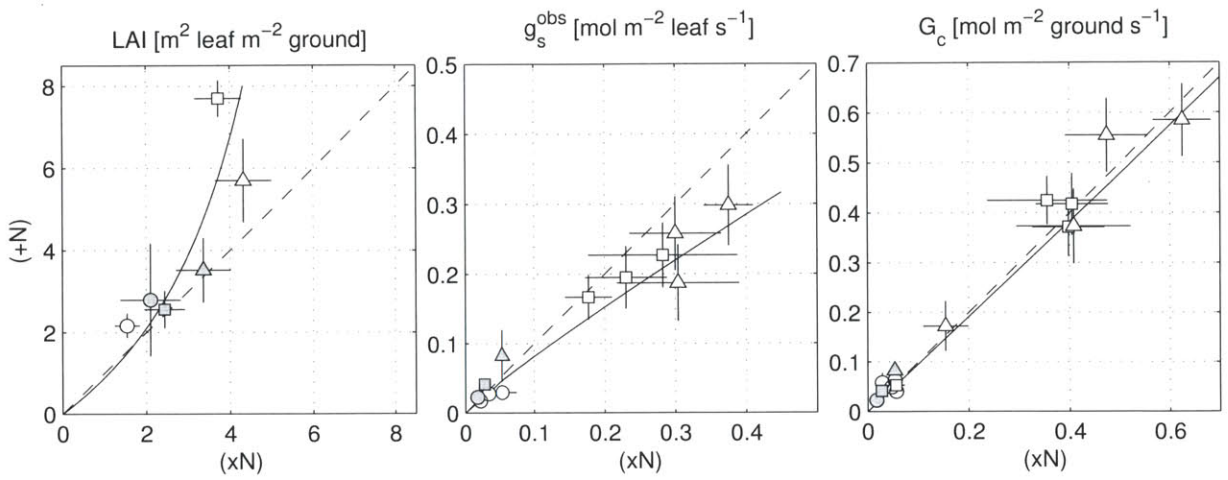

Figure 2-13: Comparison of canopy attributes in control (xN) and fertilized (+N) plots: (a) LAI, (b) light-saturated top-of- canopy stomatal conductance, and (c) canopy-scale conductance ($\mu\pm$ SE, n = 8). The symbols indicate water input treatment (○=dry; □=ambient; △=wet) and the shading indicates the date of measurement (open symbols: 13, 17, and 25 March; shaded symbols: 10 April). The black dashed line indicates $y = x$ and the black solid lines represent interpreted relationships between the variables.

stress, the unfertilized and fertilized grasses achieve the same G_c via unique $L - g_s$ pairs. Unfertilized plots are characterized by low L_a, high g_s canopies; whereas fertilized plots are high L_a and low g_s.

In addition to the calculation of G_c, canopy-scale transpiration can be estimated from the plot- and leaf-scale measurements using the Penman-Monteith equation,

$$\lambda E = \frac{\Delta R_n + \rho C_p D g_a}{\Delta + \gamma \left[1 + g_a / G_c\right]} \tag{2.20}$$

where Δ [kPa K^{-1}] is the slope of the Clausius-Clapeyron relationship, ρ_a [kg m^{-3}] is the density of air, C_p [J kg^{-1} K^{-1}] is the specific heat capacity of air, g_a [m s^{-1}] is the atmospheric conductance (see Chapter 3, equation 3.7), and $\gamma = 0.067$ [kPa K^{-1}] is the psychrometric constant.

Canopy-scale λE estimates may contain substantial errors attributable to both instrument error in the underlying measurements and landscape variability within and between plots. To understand the effect of these errors on this analysis, the λE estimates upscaled

from leaf-scale measurements are compared to canopy-scale λE as measured by the nearby eddy covariance tower in Figure 2-14. Eddy covariance estimates are associated with an error of 10-20% [*Goulden et al.*, 1996; *Wilson et al.*, 2002] and uncertainty in G_c at the landscape scale is of a similar order (Figure 2-13). Given these uncertainties, the upscaled estimates are a reasonable approximation of the λE flux, which is indistinguishable between the control and fertilized plots on the first three days of measurement. On these days, LAI is at its peak and grass transpiration likely dominates the water balance. On April 10, however, the upscaled estimate is much lower than that measured by eddy covariance. At this point in the season, grass photosynthetic activity has slowed substantially (Figure 2-11), and the eddy covariance tower is thus likely measuring soil evaporation and/or transpiration from nearby evergreen trees.

Finally, in addition to addressing the errors, we must also be cognizant of the fact that at any time λE may be limited by either the atmospheric water demand or the soil-vegetation water supply. The equivalence of the control and fertilized fluxes is only interesting from the perspective of ecological organization if indeed the vegetation controls λE. Otherwise, if it is climate controlled, the fluxes should be the same, because the plots experience the same climate. In Figure 2-14, the stomatal, leaf boundary layer, and atmospheric conductances are plotted for the 4 days with observations. Here, we see that at the time of measurement, the stomatal conductance is always lower than the others during daylight hours, indicating it as the most limiting factor in the soil-vegetation-atmosphere pathway.

The analysis above demonstrates that the soil water balance in Loma Ridge grassland is relatively insensitive to nitrogen fertilization. Although the ecosystem clearly responds to fertilization by various mechanisms at the leaf- and plot-scales, their cumulative effect results in a similar water balance. These observations are now compared to results from the stochastic water balance model to determine whether they are consistent with the optimality hypothesis of maximum stress-weighted transpiration.

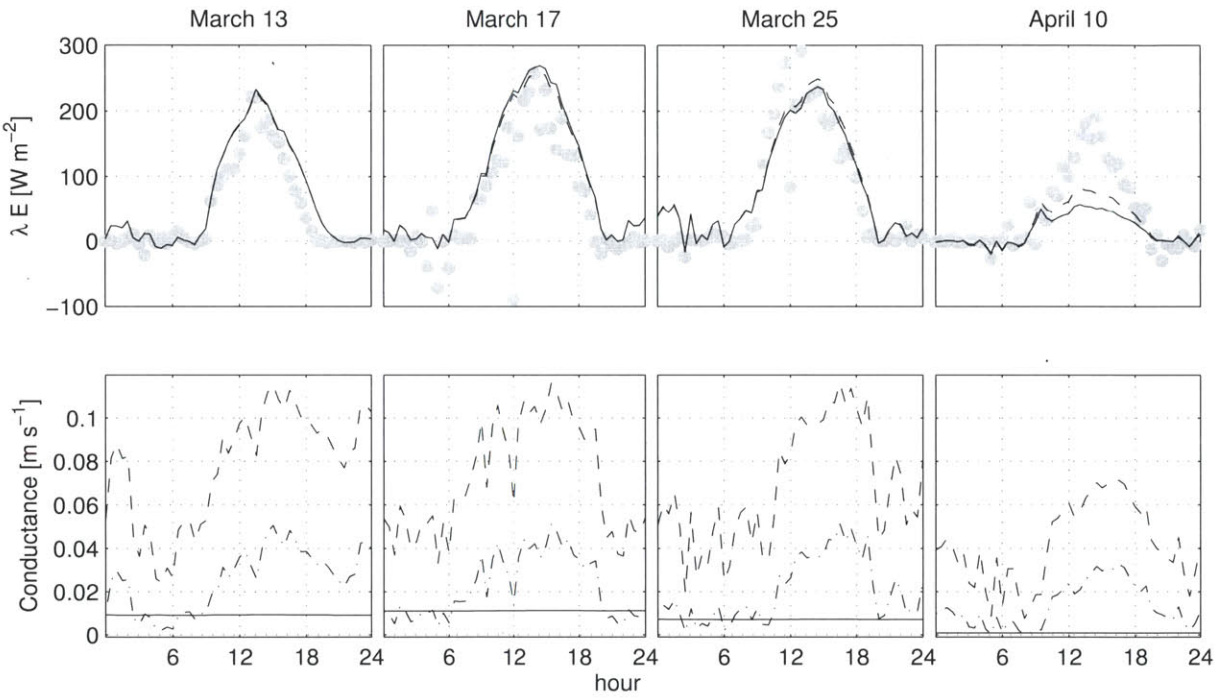

Figure 2-14: Canopy-scale evapotranspiration estimates and relative limitation by surface water supply and atmospheric water demand. In the top panel, eddy covariance estimates (gray dots) are compared to λE estimates from leaf- and plot-scale data (black lines). In the bottom panel, g_s (solid line), g_b (dashed line), and g_a (dot-dashed line) are compared.

2.3.2 Model results

Optimal $L_a - g_s$ curves derived from water balance simulations with the parameters listed in Table 2.2 are drawn in Figure 2-15. Given the estimated landscape variability, the observed $L_a - g_s$ pairs for the ambient and wet water input treatments fall within an optimal range defined by the long-term median annual rainfall and bracketed by water stress parameter $q = 1$ and $q = 3$. This result indicates the Loma Ridge canopy seems to exhibit an optimized state with respect to transpiration and water stress, regardless of the level of nitrogen input. This state is characterized by (1) a transpiration rate, controlled by water supply under the prevailing soil and climate conditions, and (2) canopy characteristics L_a and g_s, modulated by nitrogen supply. The existence of a single optimal $L_a - g_s$ state with respect to water supply and demand was hypothesized and calculated by *Eagleson* [2002] (see his Figure 7.10). The data here suggests that, while the optimal transpiration rate is constrained by hydrological mechanisms, changes in nitrogen supply move the realized state along this constraint line.

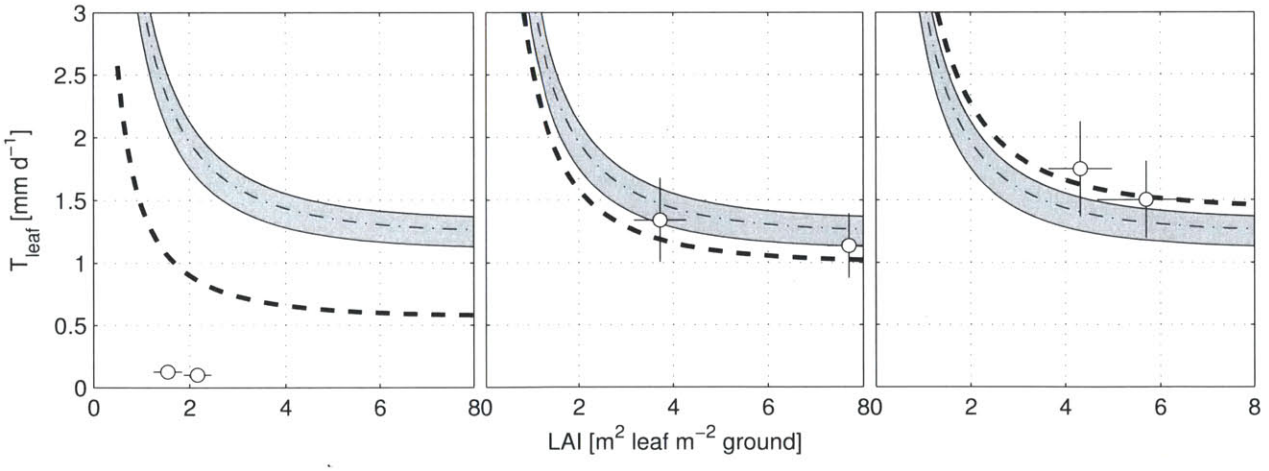

Figure 2-15: Maximum stress-weighted transpiration curves compared with $L_a - g_s$ observations (open symbols $\mu \pm$SE). The shaded areas represent a range of simulations under conditions of median rainfall, bounded below by $q = 1$ and above by $q = 3$. The dashed lines represent $q = 2$. In each case, a stochastic realization of the exponential rainfall model was scaled to match the water input volume for the 2008 growing season (133, 223, and 305 mm, respectively) and denoted by the bold dashed lines ($q = 3$).

The observations are not entirely consistent with the optimality hypothesis, however. First, canopy characteristics in the dry plots are much lower than those predicted by the model. This is likely due to the fact that the dry plots received 133 mm of rainfall in 2008, less than that needed to support a measurable level of productivity as shown in Figure 2-9. Secondly, although the ambient and wet predictions correspond fairly well with the observations given the simplicity of the model, the model tends to over-predict the observed state in the ambient plots and under-predict in the wet plots. The shaded region is defined for an annual rainfall of 289 mm, whereas the ambient and wet plots received 223 and 305 mm in 2008, respectively. When the model simulations are conducted with the actual 2008 water input (bold dashed line, $q = 3$), the prediction is improved in the wet case and performs equally well in the ambient case. However, in the ambient case, the prediction decreases substantially from the median rainfall condition.

The discrepancy between the observed and modeled data can be partially explained by evaluating the choice of rooting depth, z_r. $z_r = 40$ cm for all simulations shown in Figure 2-15, a value chosen based on observations of annual grass rooting depth in other ecosystems. *Holmes and Rice* [1996] observed the roots of *Bromus spp.* to be primarily located above 30 cm in a similar California ecosystem that received twice as much rainfall (609 mm). The global mean root depth for annual grasses is approximately 50 cm and the global mean for an annual rainfall of 300 mm is approximately 40 cm [*Schenk and Jackson*, 2002a]. z_r varies with climate and between seasons, mostly responding to climate and soil factors that determine infiltration depths [*Schenk and Jackson*, 2002a; *Laio et al.*, 2006; *Collins and Bras*, 2007; *Sivandran*, 2011]. Thus, it is reasonable to expect z_r to vary between the ambient and wet water input treatments. Although direct observations of rooting depth are not available at Loma Ridge, we can combine the canopy observations and the optimality hypothesis to generate an estimate. The following problem is therefore posed – identify the z_r such that ζ is maximized at the observed transpiration rate, or formally,

$$F = \max_{z_r} \left[\overline{T}(1 - \overline{\chi}) \right] \tag{2.21}$$

subject to the constraint $T_p = T_{obs}$. The state-space of this optimization problem is depicted

in Figure 2-16. As z_r increases, ζ increases and the optimal T_p decreases. The z_r values that correspond to T_{obs} are 30 cm and 40 cm for ambient and wet water input treatments, respectively, which fall within the observed range and increase with water input, as expected. Note the $\zeta(T_p)$ curves exhibit a plateau at their maximum, indicating a potentially wide range of transpiration rates and root depths consistent with this hypothesis. Results from the water balance model using the optimized values of z_r are shown in Figure 2-17 and correspond well with the observations. This procedure may offer a novel method for inferring root depth from more easily collected above-ground observations.

This synthesis of data collected in the Loma Ridge semi-arid annual grassland demonstrates that a suite of ecophysiological traits respond simultaneously to water and nitrogen supplies. For constant water supply, several lines of evidence from observations and theory suggest that ecosystem water use is balanced such that a consistent growth-stress trade-off is achieved in both the control and fertilized plots. A trade-off between canopy density and leaf conductance, dependent on the nitrogen supply rate, facilitates this balance. When rainfall varies, model simulations confirm rooting depth and its effect on water supply modulate the optimal transpiration rate. Therefore, both root and canopy characteristics are important to

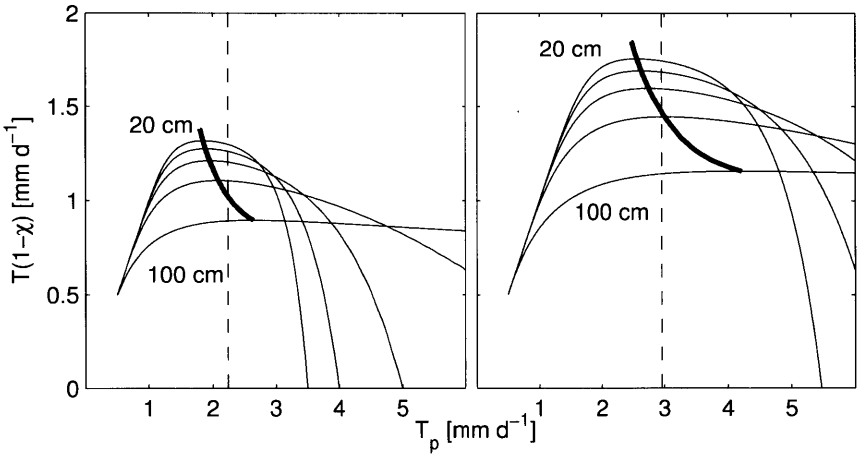

Figure 2-16: Stress-weighted transpiration as a function of T_p for several values of z_r, $q = 3$, and ambient (left) and wet (right) water input treatments. The solid lines correspond to $z_r \in [20, 40, 60, 80, 100]$ cm and the dashed line indicates the observed transpiration rate. The bold lines delineate the maximum T_p for each z_r.

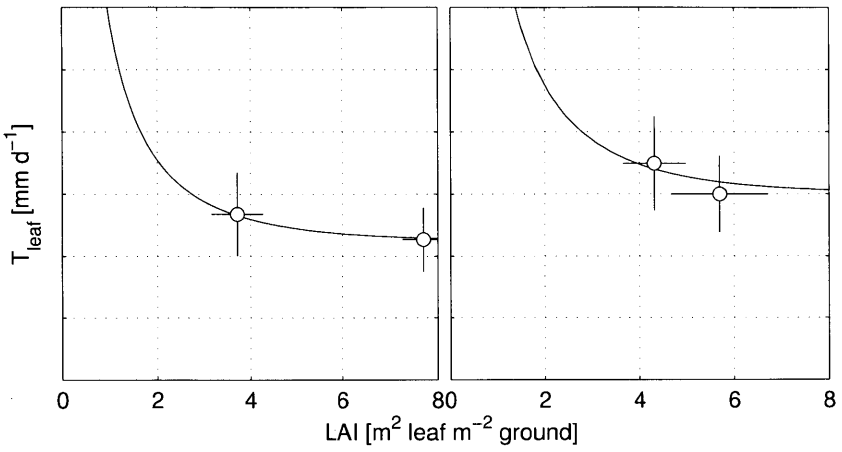

Figure 2-17: Maximum stress-weighted transpiration curves with the optimal z_r compared with $L_a - g_s$ observations ($\mu \pm$SE). $z_r = 30$ for the ambient plots (left), $z_r = 40$ cm for the wet plots (right), and $q = 3$.

understanding the ecohydrological response to varying water and nitrogen supplies. While not directly observed, a chain of physical and biochemical mechanisms likely underlie the coordination of plant traits with water and nitrogen supplies. Plausible mechanisms are introduced below as the Loma Ridge results are discussed in the context of other similar studies.

2.4 Discussion

Plant ecophysiological traits and environmental stimuli vary in concert over a range of temporal scales. For example, at the leaf scale, stomatal aperture and rates of photosynthesis respond to high frequency fluctuations of radiation and humidity within seconds to minutes. These leaf traits, as well as root and canopy development at the individual and community scales, also respond to variability in soil moisture and nutrient supplies, which evolve at the daily to seasonal time-scales. Between seasons and generations, ecological processes such as competition, disturbance, and succession lead to changes in species composition and, over even longer time-scales, evolutionary processes alter the genetic make-up of the species pool. The observed canopy characteristics and fluxes at Loma Ridge are thus an integrated

expression of multi-scale interactions occurring over the entire history of the ecosystem. Mechanisms underlying these interactions, that can be tested with existing modeling tools, are introduced here as alternative hypotheses to explain the observations.

Few generalizations can be made regarding the hydrologic response to fertilization in other experiments at sites similar to Loma Ridge. In a Northern California annual grassland (receiving 1318, 766, 721, and 566 mm during the four observed growing seasons), mean 30-cm soil moisture across eight plots decreased approximately 1-2% in fertilized plots [*Zavaleta et al.*, 2003]. However, this minor decrease was only observed briefly during the summer of two of the four years. LAI and g_s were not measured in this study, but NPP did respond positively to fertilization [*Shaw et al.*, 2002]. In another annual grassland only a few miles from Loma Ridge, mean 15-cm soil moisture across four plots decreased approximately 2% in fertilized plots during one growing season [*Harpole et al.*, 2007]. This decrease was associated with increased above-ground biomass and LAI and was also observed in irrigated plots. Gas exchange measurements were only collected at the end of the growing season in May and, therefore, are likely a better characterization of the fluxes during the reproductive or senescent phases, rather than during the growing phase as observed at Loma Ridge. Interestingly, ET was lower in the fertilized plots at this time. Neither study reported landscape variability in soil moisture. The former study did not report an aggregate spatial scale, whereas the latter study was conducted over an area approximately 1.5x10 m. Loma Ridge observations were replicated in eight plots over an area approximately 50x150 m. Despite these differences in experimental methods, the observed changes in soil moisture are consistent. The observed soil moisture differences account for no more than 6 mm water ($\Delta\theta \cdot z_{tdr} = 0.02 \cdot 30 = 6$), or only 1-2% of rainfall at these sites.

While the observed increases in photosynthesis, productivity, and LAI are consistent with other nitrogen addition studies, consensus regarding the mechanisms behind the simultaneous decrease in stomatal conductance is lacking. In early studies conducted under well-watered, controlled laboratory conditions, g_s increased linearly with leaf nitrogen content [*Hunt et al.*, 1985a; *Sage and Pearcy*, 1987] and canopy-scale transpiration increased with nitrogen supply rate [*Polley et al.*, 1999]. These plant water use results were associated with corresponding canopy changes, either increased above-ground biomass allocation [*Sage*

and Pearcy, 1987; *Polley et al.*, 1999] or increased leaf area [*Hunt et al.*, 1985b] and are consistent with the observed linear relationships between g_s, photosynthesis, and leaf nitrogen content [*Evans*, 1989]. More recent studies conducted under natural hydrologic regimes indicate a more complex picture, in which plant water use depends on the response of several traits to both nitrogen and water supply rates. g_s in fertilized *Pinus taeda* stands completely compensated for increased LAI under natural soil moisture conditions, but was not affected when irrigation was also applied [*Ewers et al.*, 2000]. Reduced g_s in this study was associated with reduced root and leaf hydraulic conductivity. In another study, hydraulic conductance and g_s decreased in fertilized woody savanna species, but whole plant water use increased due to a larger relative increase in LAI [*Bucci et al.*, 2006]. These changes resulted in decreased leaf water potential, but fertilized trees were also less susceptible to xylem cavitation. Thus, from a mechanistic viewpoint, fertilization responses are likely mediated by the hydraulic conductivity and status of the soil-plant water pathway. Mechanisms of hydraulic limitation are simulated in a number of theoretical and operational models [*Sperry et al.*, 1998; *Williams et al.*, 2001; *Katul et al.*, 2003; *Hickler et al.*, 2006] and would account for feedback between LAI and g_s if it is hydraulically driven.

While the exact underlying physical mechanisms are just recently being uncovered, a mature theory of stomatal optimization does exist. For example, observations from "low nutrient" woodland in Australia suggest g_s decreases with leaf nitrogen content, when compared between high and low rainfall sites [*Wright et al.*, 2003]. This behavior is explained as an optimal trade-off between water and nitrogen use, an idea also discussed by several others [*Cowan and Farquhar*, 1977; *Hunt et al.*, 1985a;c; *Fredeen et al.*, 1991]. Optimization of g_s can be interpreted at diurnal [*Cowan and Farquhar*, 1977] and ecological [*Fredeen et al.*, 1991; *Wright et al.*, 2003] time-scales and, given the rapid acclimation capable of Loma Ridge annual grasses, may explain the result in Figure 2-13.

Moving from the leaf to the whole plant scale, the relative allocation of biomass between below-ground (roots) and above-ground (stems, shoots, and leaves) tissues also responds to water and nitrogen supplies and may alter the ecosystem water balance. As compared to the rapid response of stomatal conductance, changes in allocation typically occur over days to weeks, or on the order of carbon turnover rates in leaf and root tissues. Allocation is thought

to be controlled by the relative growth limitation of environmental resources. The "balanced growth hypothesis" assumes plants allocate more biomass to the organs that acquire the most limiting resource [*Shipley and Meziane*, 2002, and references]. For example, when water is the resource most limiting to growth, plants allocate more biomass to roots to search for more water. This occurs toward the end of the growing season in seasonally-dry ecosystems like Loma Ridge. Root-leaf allocation also depends on the balance between above-ground light availability and below-ground nutrient availability and the level of competition for the two resources [*Reynolds and Pacala*, 1993; *Vincent and Vincent*, 1996; *Shipley and Meziane*, 2002]. Observed allocation patterns have been explained under the assumption that plants compete most strongly for the most limiting resource. Therefore, a deficit in soil nitrogen supply relative to light supply will induce an increase in root allocation (and vice versa). It is plausible that Loma Ridge grasses respond to fertilization by increasing biomass allocation above-ground as the limiting resource shifts from below-ground (nitrogen) to above-ground (light). In this way, the soil water balance may depend on nitrogen supply through the root-leaf allocation strategy. This topic is investigated further in Chapter 4.

Beyond these root and leaf responses, environmental fluctuations also interact with ecological processes, such as competition, disturbance, and succession, and evolutionary processes (an idea fundamental to Eagleson's hypotheses). Of all the existing species, the collection found in a given ecosystem arises through competition for limiting resources and the avoidance or tolerance of disturbance and stresses. In annual grassland, these processes can lead to inter-annual variability in species composition. At Loma Ridge, species composition varies between all experimental treatments, but during the 2008 growing season annual grasses and forbs with presumably similar water use and growth rates were dominant in all treatments (96% cover on average). Thus, these changes are likely not important for the single growing season analysis conducted here. The same can be said of evolutionary processes, because their effects are likely only observed over several generations. Therefore, a mechanistic explanation for the hydrologic response to fertilization in this ecosystem can focus on organ- to plant-scale mechanisms.

2.5 Conclusions

In this chapter, observations from a unique factorial water and nitrogen addition experiment in a semi-arid annual grassland were analyzed to identify the effect of nitrogen fertilization on the relationships between ecological and hydrological processes. It was concluded that the surface soil water balance was relatively insensitive to nitrogen fertilization, owing to the opposing responses of canopy density and leaf conductance. Further, results from a simplified soil water balance model provide evidence that the observed responses may be associated with an optimal trade-off between photosynthesis and water stress. However, natural variability in rooting depth and water stress response, not captured by the model parameterization, limits the interpretation of these results. While the model analysis provides an interesting null hypothesis for ecosystem interactions between the water, carbon, and nitrogen cycles, it does not provide any further insight into the underlying mechanisms governing these interactions. The remainder of this thesis seeks to characterize these underlying mechanisms while demonstrating the importance of viewing ecosystems as integrated hydrologic and biogeochemical systems.

Chapter 3

Ecosystem modeling with coupled water, carbon, and nitrogen dynamics

The analysis in *Chapter 2* suggests that the observed water balance at Loma Ridge results from the simultaneous optimization of LAI and g_s with respect to the competing objectives of maximum transpiration and minimum water stress. This inference was made using information from the water balance only and did not explicitly account for the ecosystem carbon and nitrogen balances. In *Chapter 3*, a modeling approach coupling the water, carbon, and nitrogen balances is introduced to investigate the mechanistic basis underlying the observed fertilization responses. The objectives for the model developed here are (1) to effectively couple the water, carbon, and nitrogen cycles at the daily scale and (2) to provide an acceptable approximation of the seasonal variability in biomass accumulation, from which the relative ecological success of various resource use strategies can be inferred. Daily-scale model parameterizations are derived from a physically-based model of the diurnal surface energy, water, and carbon fluxes validated against eddy covariance measurements. The resulting functional relationships between net primary productivity, plant nitrogen content, and soil moisture are shown to be applicable to the seasonal and inter-annual dynamics of this ecosystem.

3.1 A daily-scale parameterization for photosynthesis as a function of stomatal conductance and leaf nitrogen content

3.1.1 Ecosystem control of surface fluxes: stomatal conductance and leaf gas exchange

With respect to the first objective above, the most important feature that must be addressed is the dependence of leaf water vapor and carbon dioxide exchange on water and nitrogen availability. The influence of vegetation in land-atmosphere exchange is typically modeled through a semi-empirical representation of g_s and net carbon assimilation, A_n, which control the diffusion of water vapor and CO_2 across the stomata. These models attempt to capture the basic features of stomatal movement – stomata open to capture CO_2 for photosynthesis and close in response to either low soil water supply or high atmospheric water demand – and apply at the time-scale of typical leaf gas exchange or eddy covariance observations, on the order of several minutes to one hour.

The choice of models for this study is now justified. Model parameterizations are only detailed here in cases where they are needed to demonstrate a critical point in the approach or where they were not previously published. In all other cases, the appropriate references are included. The reader is referred to *Daly et al.* [2004a], *Ivanov* [2006], and *Oleson et al.* [2010] for examples of the models discussed here.

Two general g_s models have been adopted in the literature, hereafter referred to as the "Leuning" and "Jarvis" approaches. The Leuning model developed from the work of *Ball et al.* [1987], *Collatz et al.* [1991], and *Leuning* [1995] and explicitly represents the observed correlation between g_s and A_n [*Leuning*, 1995]. This model is commonly implemented in land surface models (LSMs) [e.g. *Sitch et al.*, 2003; *Krinner et al.*, 2005; *Oleson et al.*, 2010; *Zaehle and Friend*, 2010; *Niu et al.*, 2011]. The Jarvis model was proposed by *Jarvis* [1976] and applied by *Federer* [1979; 1982]. It treats g_s as mathematically independent of A_n, although their correlation may be preserved under some conditions. The Jarvis model is much less common in the LSMs (e.g. the Noah LSM offers the Jarvis parameterization as a user-specified option [*Niu et al.*, 2011]).

The Leuning model relates g_s to A_n and has the general form,

$$g_s = m\frac{A_n\left(R_n, T_l, c_i, \psi\right)}{c_s - \Gamma^*} f_D(D) \tag{3.1}$$

where m [-] is a parameter that links g_s and A_n, which is a function of environmental parameters (R_n [W m^{-2}], leaf temperature, T_l [K], leaf internal CO_2 concentration, c_i [mol mol^{-1}], and ψ is a generic variable representing the soil water status), c_s [mol mol^{-1}] is the leaf surface CO_2 concentration, Γ^* [mol mol^{-1}] is the CO_2 compensation point, and D [kPa] is the vapor pressure deficit. $f_D(D)$ represents the stomatal sensitivity to atmospheric water demand and is assumed to be, $f_D(D) = (1 + D/1.25)^{-1}$. Equation 3.1 is also constrained by the diffusion of CO_2 across the leaf surface,

$$A_n(R_n, T_l, c_i, \psi) = g_{sba}^{CO_2}(c_a - c_i) \tag{3.2}$$

where g_{sba} is the combination of stomatal, leaf boundary layer, and atmospheric conductances for CO_2, acting in series, and is scaled appropriately with LAI. Alternative parameterizations for $A_n(R_n, T_l, c_i, \psi)$ and leaf-to-canopy scaling are described in *Daly et al.* [2004a] and *Ivanov* [2006]. Solving equations 3.1 and 3.2 simultaneously with the surface energy balance yields g_s and A_n.

The Jarvis model is similar in form to the Leuning model, but relies on a maximum stomatal conductance parameter, $g_{s,max}$, which is mathematically independent of A_n,

$$g_s = g_{s,max} f_{R_n}(R_n) f_{T_a}(T_a) f_\psi(\psi) f_D(D) \tag{3.3}$$

In this model, g_s is first determined from equation 3.3 and then substituted into equation 3.2 to calculate A_n, as opposed to solving equations 3.1 and 3.2 simultaneously. In both cases transpiration is,

$$T = g_{sba} D \tag{3.4}$$

where g_{sba} is the canopy-scale combined stomatal, leaf boundary, and atmospheric conductance to water vapor.

The effect of water supply is represented in the Leuning approach by the dependence of A_n on ψ and in the Jarvis approach by the function $f_\psi(\psi)$. In both cases, $f_\psi(\psi)$ takes a similar functional form as β_v in equation 2.6, however, there are subtle differences in its implementation. In the Leuning approach, β_v multiplies the maximum carboxylation capacity, $v_{c,max}$, a parameter in one of three factors (carboxylation, energy/light supply, carbon export) that may limit photosynthesis at any given time. In this case, β_v is usually defined as a linear function of soil moisture, as in equation 2.6, but is also sometimes defined as a non-linear function or a function of soil water potential, ψ_s, instead of soil moisture [*Mahfouf et al.*, 1996]. In the Jarvis approach, as implemented by [*Federer*, 1979; 1982], $f_\psi(\psi)$ is defined as a function of leaf water potential, ψ_l, which is modulated by hydraulic constraints in the soil-plant pathway [*Katul et al.*, 2003; *Daly et al.*, 2004a]. In this formulation, T is not only constrained by g_{sba} and D, but by the soil-leaf hydraulic gradient (i.e. $\psi_s - \psi_l$) and the conductance of soil, root, and plant tissues, g_{srp},

$$T = g_{sba}(\psi_l, D)D = g_{srp}(\psi_s, \psi_l)(\psi_s - \psi_l) \tag{3.5}$$

g_{srp} is defined by *Katul et al.* [2003] and *Daly et al.* [2004a] and generally decreases with both ψ_s and ψ_l.

In either model, the effect of nitrogen supply can be represented assuming a linear relationship between the maximum carboxylation capacity, $v_{c,max}$ [μmol m^{-2} s^{-1}], and the leaf nitrogen content, N_l [g N m^{-2} leaf] [e.g. Oleson et al., 2010]. However, examples of this assumption in operation are limited. This assumption is based on laboratory studies demonstrating a correlation between N_l and the rate of CO_2 assimilation [Evans et al., 1989],

$$v_{c,max} = k_n N_l \tag{3.6}$$

where k_n [μmol CO_2 g^{-1} N] is the slope of the $v_{c,max} - N_l$ relationship. Again, see *Daly et al.* [2004a], *Ivanov* [2006], or *Oleson et al.* [2010] for examples of how $v_{c,max}$ control of leaf gas exchange is modeled in LSMs.

Inspecting equations 3.1–3.6, two points can be made regarding the suitability of these parameterizations for the task at hand. First, since the Leuning approach requires a mono-

tonic increasing relationship between g_s and A_n, it follows that it also requires a monotonic increasing relationship between g_s and N_l (i.e. $g_s \propto A_n \propto N_l$). Assuming fertilization increased N_l in the Loma Ridge field experiment, this model would be inconsistent with the observation that g_s decreases with increased N_l and, by this logic, would not be applicable here. The Jarvis approach allows g_s to vary independently of A_n and N_l. Note, this does not necessarily imply that g_s and A_n are uncorrelated. The model allows for correlations to arise from the two variables responding simultaneously to the same environmental conditions or from the dependence of A_n on g_s (equation 3.2). Secondly, when $f_\psi(\psi) = \beta(\theta)$, the model does not consider the possible limitation of soil, root, or xylem transport on transpiration. Therefore, transpiration is tightly linked to the canopy demand and is only reduced when θ is depleted. The additional constraint in equation 3.5 allows the soil-root-plant supply to limit transpiration and reduces transpiration sensitivity to increased LAI through ψ_l [*Sperry et al.*, 1998]. This model artifact is also supported by the Loma Ridge experimental observations. For these reasons, the Jarvis approach with hydraulic limitation is the preferred model choice for this analysis.

The model assumptions presented here are valid at sub-daily time-scales only. Due to diurnal variability in the environmental conditions (i.e. temperature, radiation, humidity, etc.) and the non-linear dependence of ecophysiological processes on these environmental conditions, the assumed relationships between photosynthesis, leaf nitrogen content, and soil moisture may not hold at the daily scale. To develop a function $A = f(g_{s,max}, v_{c,max})$ applicable at the daily scale, the sub-daily model is first validated against half-hourly observations from the Loma Ridge eddy covariance tower and then upscaled to the daily level (following the approach of Daly et al. [2004a], but now including the effect of N_l).

3.1.2 Surface energy, water, and carbon flux validation

Before the daily-scale parameterization is developed, the Jarvis model performance is validated against ecosystem-scale energy and gas fluxes observed at the Loma Ridge eddy covariance tower. The period 26 February through 30 April 2008 is chosen as the validation period and resource supply conditions correspond to the ambient water input and nitrogen control treatments. Validation begins just prior to the peak of the growing season, when soil

moisture is plentiful and vegetation exert a strong control on land-atmosphere exchange, and it concludes with the end-of-season drying of the soil column, which induces water stress. The validation exercise therefore covers the key periods of plant-water interactions.

Validation simulations are forced with environmental conditions measured at the nearby eddy covariance tower. Air temperature, windspeed, relative humidity, and precipitation are measured at a half-hour frequency at the tower. Missing data are filled by linear interpolation between the nearest valid observations in the time-series (approximately 2.8% of T_a values and 1.6% of u values were missing). In addition to the meteorological forcing, the validation simulations must be initialized at the observed level of soil water content. Using the TDR data as a guide, the root zone average water content is initialized at $\theta_i = 0.26$ (or $s = 0.57$). Validation parameters are summarized in Table 3.1. Physical constants required for the photosynthesis model listed in *Daly et al.* [2004a] are not listed here.

While the *Daly et al.* [2004a] model assumes constant g_a and g_b, the model implemented here calculates these parameters based on representations of the dominant transport mechanisms. A conductance for the rate of turbulent atmospheric transport between the surface and an arbitrary measurement height, z [m], can be written as,

$$g_a^{-1} = \frac{1}{\kappa^2 u} \ln\left(\frac{z - d_0}{z_{0m}}\right) \ln\left(\frac{z - d_0}{z_{0v}}\right) \tag{3.7}$$

where $\kappa = 0.41$ is von Karman's constant [-], u [m s^{-1}] is windspeed, and the surface roughness is characterized by d_0 [m], the height of zero momentum flux, and z_{0m} and z_{0v} [m], the roughness lengths for momentum and water, respectively. Before turbulence transports water vapor in the atmosphere, water vapor must first diffuse across the leaf boundary layer. The following form for g_b is assumed [*Choudhury and Monteith*, 1988],

$$g_b = \frac{0.02}{\alpha} \sqrt{\frac{u(H)}{d_{leaf}}} \left[1 - \exp\left(-\frac{\alpha}{2}\right)\right] \tag{3.8}$$

where α [-] is an extinction coefficient for windspeed, H [m] is the vegetation height, and d_{leaf} [m] is the leaf width.

Table 3.1: Jarvis stomatal conductance and photosynthesis model parameters for annual grassland at Loma Ridge. Where references are not included, these parameters were used by *Daly et al.* [2004a].

Parameter		Value	Units	Reference
Vegetation				
Atmospheric CO_2 concentration	c_a	380	μmol mol^{-1}	NOAA ESRL
Maximum carboxylation capacity	$v_{c,max}$	50	μmol m^{-2} s^{-1}	
Maximum electron transport capacity	J_{max}	75	μmol m^{-2} s^{-1}	
Point of incipient assimilation stress	$\psi^*_{l,A}$	-0.5	MPa	
Point of complete assimilation shut-down	$\psi^*_{l,A}$	-4.5	MPa	
Leaf area index	LAI	3.5	m^2 m^{-2}	observed
Root area index	RAI	5.6	m^2 m^{-2}	
Active soil depth	z_r	0.5	m	calibrated
Maximum plant conductivity	$g_{p,max}$	11.7	μm MPa^{-1} s^{-1}	
Xylem vulnerability parameter	c	2	[-]	
Xylem vulnerability parameter	d	2	MPa	
Point of incipient stomatal closure	ψ^*_l	-0.05	MPa	
Wilting point	$\psi_{l,w}$	-4.5	MPa	
Root soil moisture response factor	a	9	[-]	
Atmospheric transport				
Zero-plane displacement height	d_0	$0.67H$	m	*Ivanov* [2006]
Momentum roughness length	z_{0m}	$0.123H$	m	"
Water vapor roughness length	z_{0v}	$0.1z_{0m}$	m	"
Windspeed attenuation coefficient	α	3	[-]	"
Leaf width	d_{leaf}	0.1	m	"
Soil				
Porosity	n	0.453	m^3 m^{-3}	*Rawls et al.* [1982]
Saturated hydraulic conductivity	k_s	80	cm d^{-1}	
Air-entry pressure	ψ_b	-210	mm	
Initial soil moisture	θ_i	0.26	m^3 m^{-3}	

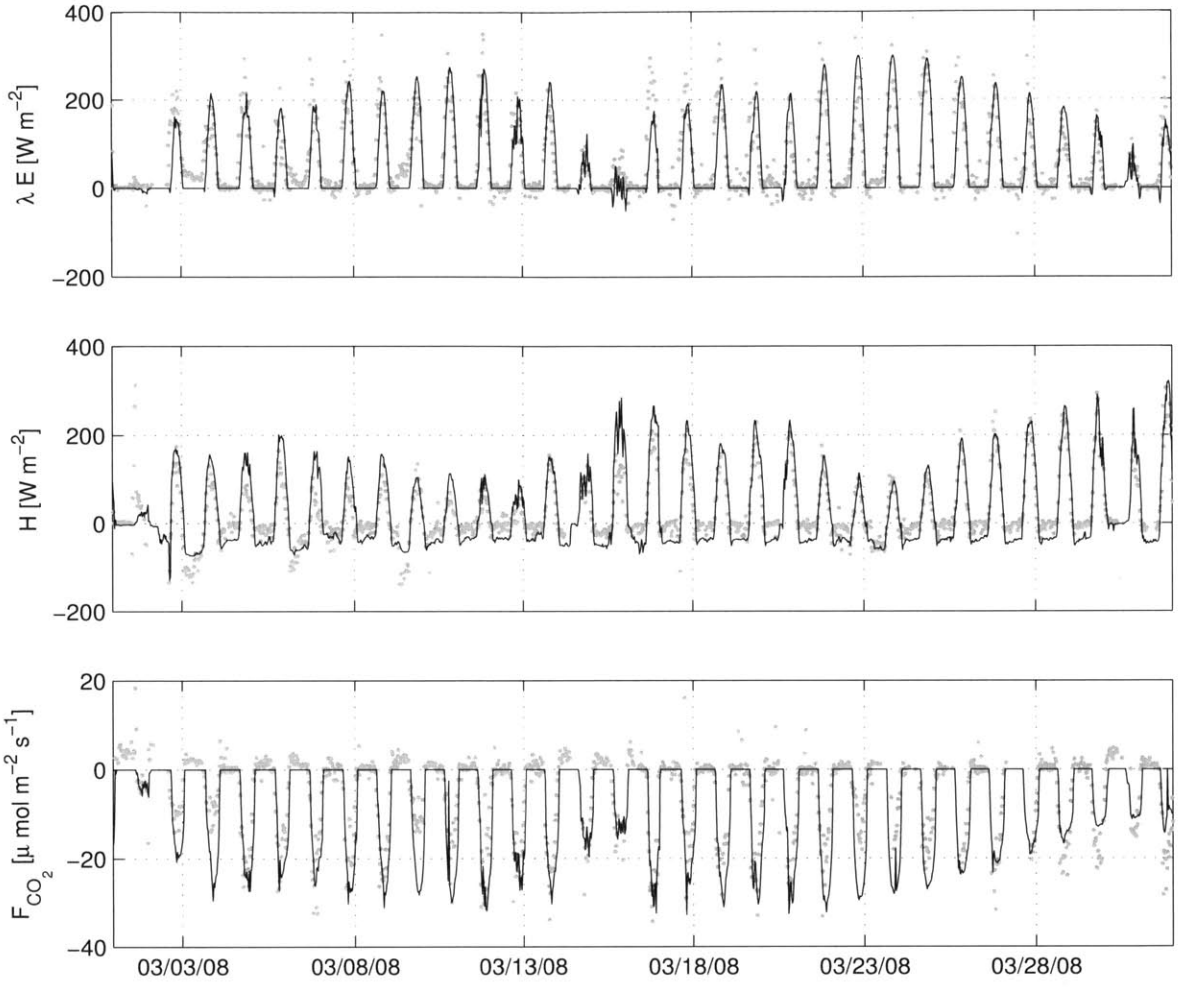

Figure 3-1: Comparison of observed (gray dots) and modeled (black lines) λE, H, and F_{CO_2} during the 2008 growing season at Loma Ridge.

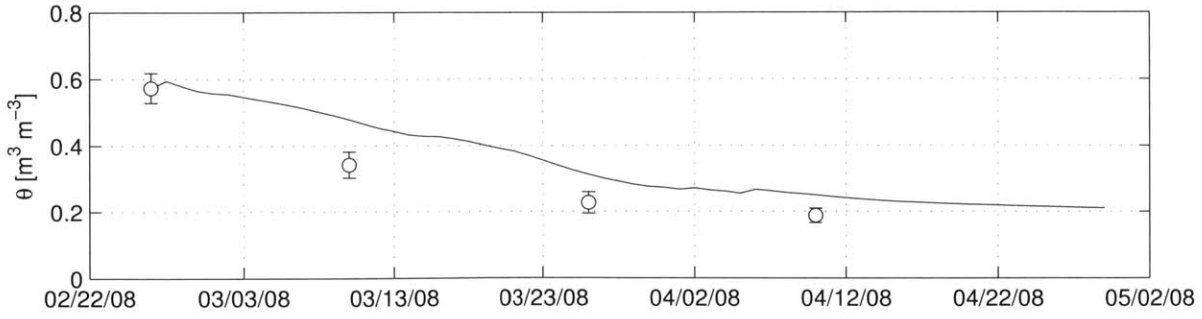

Figure 3-2: Comparison of observed (open circles) and modeled (line) soil moisture. The observations are averaged over the top 15 cm of soil, whereas the simulated values represent the average over the entire 50 cm active soil depth.

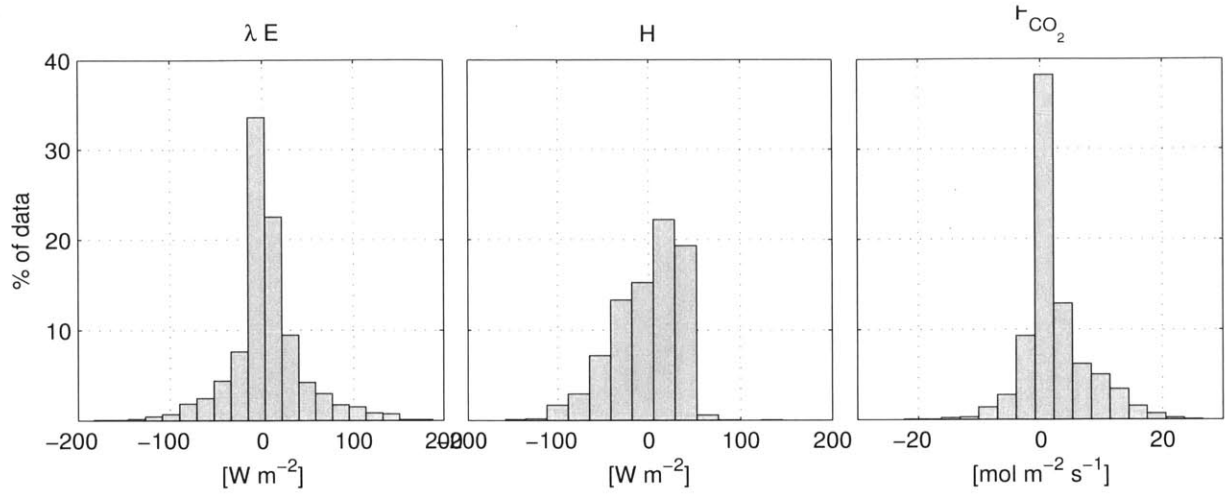

Figure 3-3: Histograms of error between measured and modeled fluxes. The error is defined as the measured value minus the modeled value.

As demonstrated in Figures 3-1, 3-2, and 3-3, the Jarvis model performs well during the 2008 growing season at Loma Ridge. These results are qualitatively similar to other energy balance validation studies using the Leuning approach [*Bisht*, 2010; *Sivandran*, 2011]. However, there are some inconsistencies in the model prediction. Latent heat is generally under-predicted at the peak of the day and negative sensible heat during the night is generally over-predicted. This latter discrepancy may be attributable to poor eddy covariance accuracy during calm night conditions. The CO_2 flux is always predicted equal to 0 at night, while a small positive flux is observed. This night-time flux is respiration, a process not explicitly represented by the model. Lastly, the predicted soil water content is always greater than the measured value. This results from a difference between the measurement depth, 15 cm, and the parameterized active soil depth, 50 cm. Although the correct volume of water is extracted from the soil column, it is distributed over a greater depth and, thus, the change in the average θ over time is less. This discrepancy is even larger for evaporation, which typically can only access water stored in the top 5-10 cm of soil. The larger root depth parameter is needed to provide a large enough water reservoir to sustain transpiration throughout the growing season. In reality, plant roots likely utilize water near the surface first and then explore lower soil depths later in the season. Hence the rapid decline in the surface θ and the continuation of water vapor flux after the surface soil moisture is depleted.

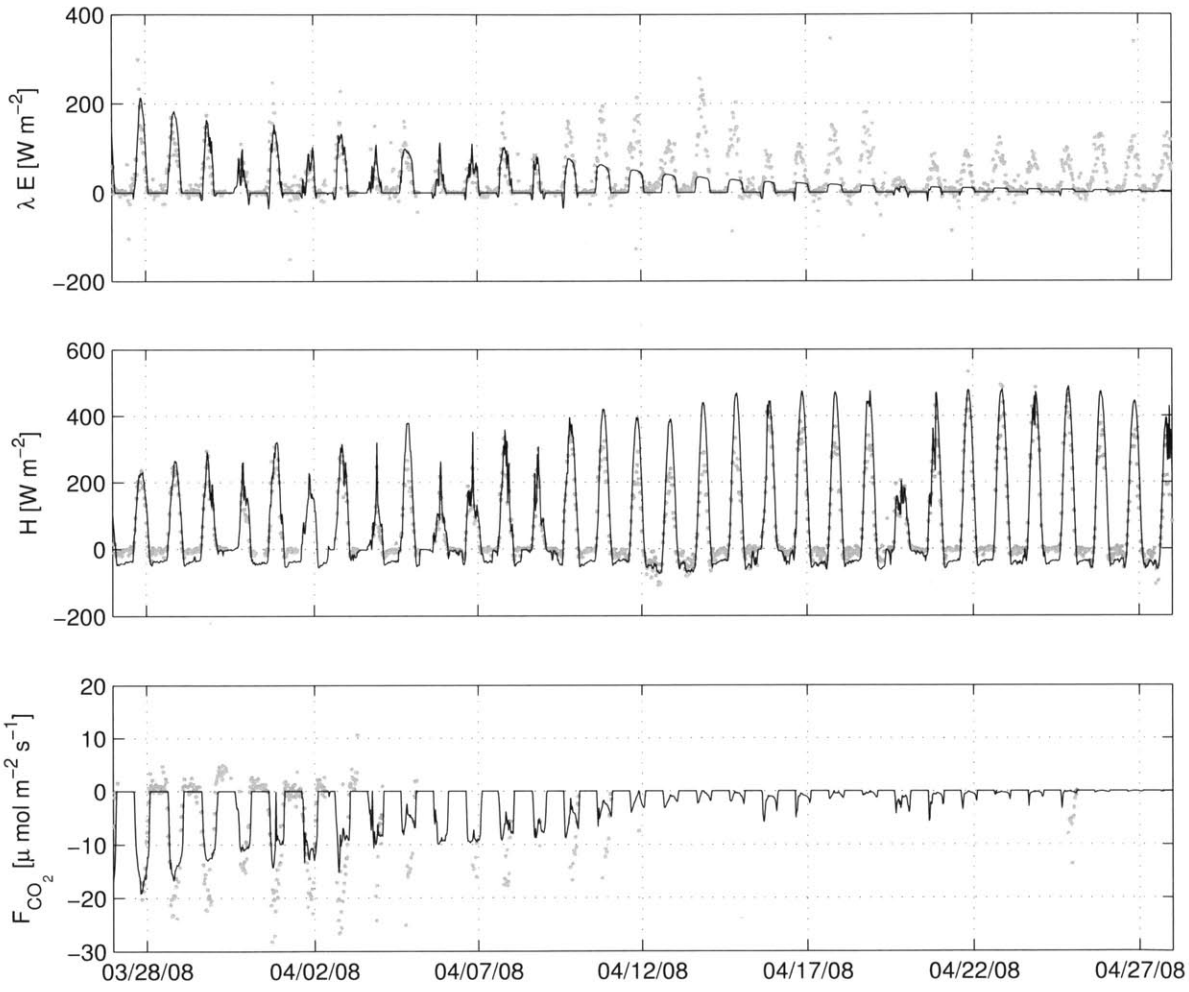

Figure 3-4: Comparison of observed (gray dots) and modeled (black lines) λE, H, and F_{CO_2} at the end of the annual grassland growing season.

These inconsistencies are recognized as a consequence of the aggregated soil column modeled here.

To gain a better understanding of the surface energy balance at Loma Ridge, it is instructive to also evaluate the end-of-season stress period for the annual grass community, shown in Figure 3-4. Note that the modeled latent heat fluxes begin to decrease around April 10, whereas the eddy covariance device continues to measure water vapor flux. Minimal transpiration and photosynthetic activity from annual grasses on April 10 is corroborated by the leaf gas exchange measurements shown in Chapter 2 (Figure 2-11). During this transition period, the annual grasses are in their senescence phase, while deeper-rooted trees and evergreen shrubs are active. Given that the eddy covariance tower fetch likely includes surfaces other than annual grasses, it is plausible that the device is measuring transpiration from vegetation communities not well represented by the model as parameterized. The CO_2 flux shows a similar result, although observations are almost all missing after April 2.

3.1.3 Scaling surface fluxes from the sub-daily to the daily level

With confidence in the sub-daily model performance, the daily parameterization can now be developed. For this analysis, maximum stomatal conductance, $g_{s,max}$, and maximum carboxylation capacity, $v_{c,max}$, are assumed to be free parameters. These parameters represent the soil resource controls on photosynthesis. First, $g_{s,max}$ responds to, and thus is a surrogate for, soil water availability and controls the rate of CO_2 supply to the photosynthetic machinery by diffusion across the stomatal opening. $g_{s,max}$ is also partially responsible for N_l and $v_{c,max}$ as nitrogen acquisition depends on both the transpiration rate and soil moisture level (see section 3.2.3 below). Similarly, $v_{c,max}$ integrates both soil nitrogen and water availability, which simultaneously control the rate of nitrogen uptake, and controls the photosynthetic demand for CO_2. $v_{c,max}$ also plays a role in CO_2 supply, which is inter-dependent with CO_2 demand (equation 3.2). Therefore, these two leaf parameters link carbon, nitrogen, and water within the leaf.

Simulations were performed with several pairs of $g_{s,max}$ and $v_{c,max}$ (which scales linearly with N_l) values. These simulations were forced by a repeating diurnal course of net radiation and coupled to a convective boundary layer model to allow the atmospheric conditions,

humidity and temperature, to co-evolve with the vegetation and soil moisture states [*Daly et al.*, 2004a]. The half-hourly model output was then aggregated to the daily scale to produce the numerical estimate of the function $a_{max} = f(T_{leaf}, v_{c,max})$. a_{max} [g C m^{-2} d^{-1}] is defined as the leaf-scale assimilation rate when the soil water supply is not limiting.

The effect of the parameters $g_{s,max}$ and $v_{c,max}$ on daily-scale leaf gas exchange is demonstrated in Figure 3-5. Note the different relationships between the parameters and the fluxes. T_{leaf} saturates with $g_{s,max}$, but does not depend on $v_{c,max}$ at the leaf scale (left panel, latter relationship not shown). The lack of a control of $v_{c,max}$ on T_{leaf} was expected because there is no functional relationship between these two parameters in the Jarvis model. Had the Leuning model been applied here, a positive relationship between $v_{c,max}$ and T_{leaf} would have been expected. Saturation of T_{leaf} with $g_{s,max}$ is due to the relative control of stomatal, leaf boundary layer, and turbulent transport on the surface-atmosphere water flux. When $g_{s,max}$ is less than g_a and g_b it controls T_{leaf}. As $g_{s,max}$ increases, leaf boundary layer and/or atmospheric transport become relatively more limiting and T_{leaf} no longer increases with $g_{s,max}$. A negative feedback between T_{leaf} and D may also contribute here. As T_{leaf} increases, humidity increases, D decreases, and T_{leaf} subsequently decreases accordingly.

a_{max} saturates with both $g_{s,max}$ and $v_{c,max}$ (right panel), an outcome that is controlled by CO_2 supply or demand under different resource use conditions. When $g_{s,max}$ is small, a_{max} is strongly limited by CO_2 diffusion and is approximately constant with $v_{c,max}$. As $g_{s,max}$ increases, the diffusion supply of CO_2 to the photosynthetic apparatus and a_{max} increase. However, under constant $v_{c,max}$, a_{max} becomes limited by CO_2 demand such that no further increase in supply can increase photosynthesis. When $g_{s,max}$ is sufficiently large, a_{max} also saturates with increasing $v_{c,max}$. Photosynthesis is limited by energy availability in addition to $v_{c,max}$ and N_l. Therefore, a_{max} cannot increase beyond this additional limitation, hence the saturation with $v_{c,max}$.

The proposed daily-scale parameterization for a_{max} is now described. The saturation of a_{max} with $v_{c,max}$ is assumed to follow the Michaelis-Menten reaction kinetic expression,

$$a_{max} = a\frac{v_{c,max}}{H_n + v_{c,max}} = a\frac{k_n N_l}{H_n + k_n N_l} \tag{3.9}$$

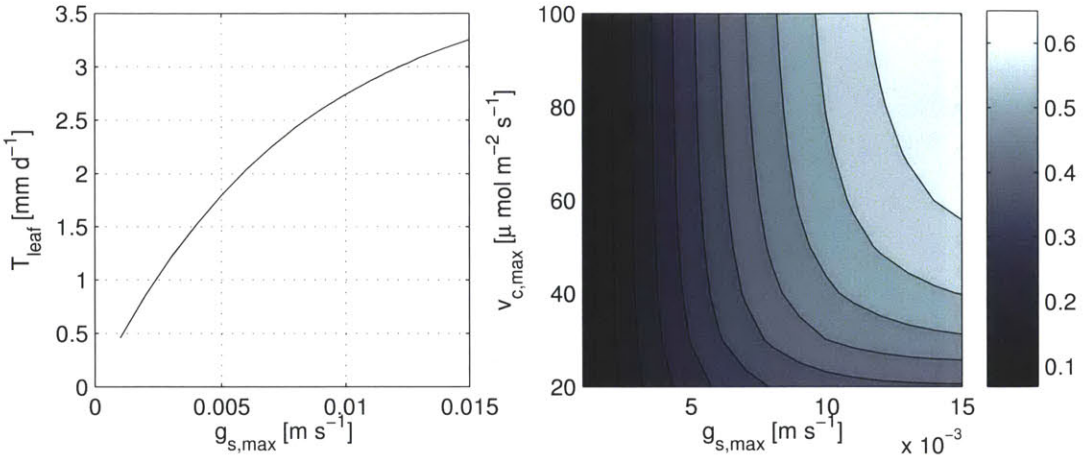

Figure 3-5: The dependence of daily leaf-scale transpiration, T_{leaf}, (left panel) and daily leaf-scale assimilation, a_{max} [mol C m^{-2} leaf d^{-1}], (right panel) on Jarvis model parameters $g_{s,max}$ and $v_{c,max}$.

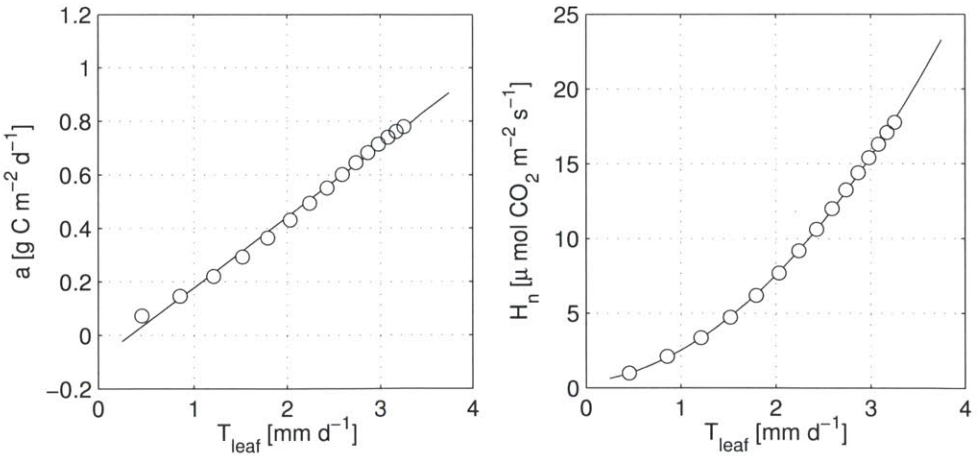

Figure 3-6: Variation of daily-scale photosynthesis parameters a and H_n with T_{leaf}.

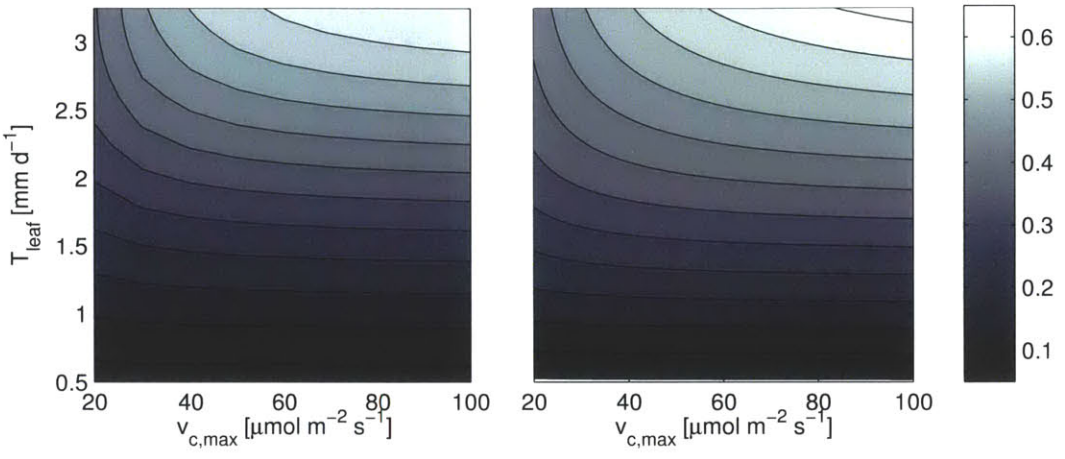

Figure 3-7: Comparison of $a_{max} = f(T_{leaf}, v_{c,max})$ calculated with the full model (left panel) and with the daily-scale parameterization (right panel). The contours represent a_{max} [mol C m^{-2} leaf d^{-1}].

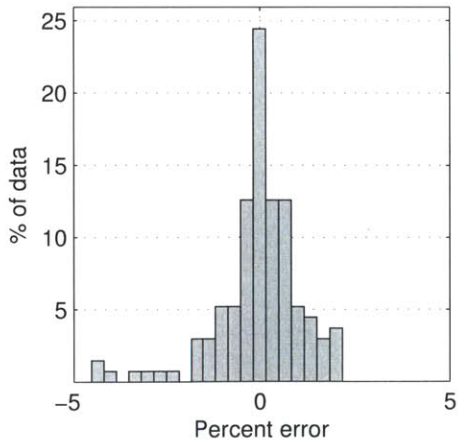

Figure 3-8: Performance of the daily-scale a_{max} parameterization. Percent error is defined as $100 \cdot (A_{Jarvis} - A_{est})/A_{Jarvis}$.

where H_n [μmol m^{-2} s^{-1}] is a half-saturation constant for a_{max} with $v_{c,max}$ and a [g m^{-2} d^{-1}] is the maximum possible assimilation rate when $v_{c,max}$ is not limiting. The parameters a and H_n were estimated using a minimum root mean square error technique and found to vary with T_{leaf} as shown in Figure 3-6. a increases linearly and H_n increases quadratically with T_{leaf}. Parameters estimated for these functions are,

$$a(T_{leaf}) = 0.27T_{leaf} - 0.089 \tag{3.10}$$

and

$$H_n(T_{leaf}) = 1.44T_{leaf}^2 + 0.71T_{leaf} + 0.36 \tag{3.11}$$

Comparison of equation 3.9 with the results of the full simulation (Figures 3.7 and 3.8) shows that equation 3.9 provides an estimate of the upscaled Jarvis model within $\pm 5\%$ for the parameter combinations simulated here. Equation 3.9 is implemented in the coupled ecosystem water-carbon-nitrogen balance discussed in the next section.

3.2 A simple model for the coupled water, carbon, and nitrogen balances

In this section, models for the ecosystem carbon and nitrogen balances are introduced and coupled to the soil water balance (equation 2.1). This coupled water-carbon-nitrogen model is inspired by population models used to study ecological systems [e.g. *Hastings*, 1997]. Similar models have been introduced and applied in a hydrologic context by *Zea-Cabrera et al.* [2006], *Nordbotten et al.* [2007], *Collins and Bras* [2008; 2010], *Istanbulluoglu et al.* [2011], and *Feng et al.* [2012], while others considered limited aspects of the fully coupled system [*Porporato et al.*, 2003b; *D'Odorico et al.*, 2003; *Manzoni et al.*, 2004; *Manzoni and Porporato*, 2007; *Everard et al.*, 2010]. The framework presented here builds on these models by including (1) the water, carbon, and nitrogen balances and (2) dynamic vegetation with above- and below-ground carbon allocation. The model is validated here with observations from Loma Ridge and analyzed in Chapter 4 to develop an understanding of allocation strategies applicable in this and similar ecosystems.

3.2.1 Modification to the soil water balance forcing

To prepare the coupled model for comparison with observed ecosystem carbon and nitrogen dynamics, the previously introduced climatic forcing and its interaction with vegetation must be modified. In Chapter 2, no distinction was made between potential evapotranspiration (PET) and precipitation (P) forcings during wet and dry seasons. Seasonality was addressed using a probabilistic analysis of the growing season antecedent moisture condition (i.e. equation 2.19 [Rodriguez-Iturbe et al., 2001]). However, this stochastic approach does not apply to the temporal dynamics within a single growing season, which is needed to verify the applicability of the proposed model.

To address this issue, the seasonality of PET and P are explicitly represented. The year is separated into distinct wet and dry seasons. During the wet season, the model is forced with either observed daily P (for validation) or P generated from the exponential rainfall model (for sensitivity analyses). No rainfall is assumed to occur during the dry season. The seasonal course of PET is approximated by a sinusoidal wave fit to the average values on record,

$$E_p(t) = E_p + \Delta E_p \sin \omega t \tag{3.12}$$

where E_p [mm d^{-1}] is the annual average daily PET, ΔE_p [mm d^{-1}] is the amplitude of E_p, and $\omega = \frac{2\pi}{365}$ [d^{-1}] is the angular frequency [Milly, 1994]. PET estimates are obtained over well-watered grass by the California Irrigation Management Information System (CIMIS) at a nearby site in Irvine, CA (Site 075). Time-series of P and PET during the experiment (2007-present) are shown in Figure 3-9.

With these assumptions, E and T in equation 2.1 are now defined slightly differently,

$$E = E_b \beta_e = E_p \cdot k_s \cdot \exp\left(-kL_a\right) \cdot \min\left(\frac{s - s_h}{s_{fc} - s_h}, 1\right) \tag{3.13}$$

and

$$T = T_p \beta_v = E_p \cdot k_v \left\{k^{-1}\left[1 - \exp\left(-kL_a\right)\right]\right\} \beta_v \tag{3.14}$$

where k_v [-] is the transpiration efficiency [Eagleson, 2002], which represents the fraction of PET satisfied by the soil-plant-atmosphere continuum. Therefore, $k_v \cdot PET$ replaces $g_{s,max} \cdot D$

in equation 2.8. β_v is defined as in equation 2.6 and the term in the curly brackets is the leaf-canopy scaling factor previously derived in equation 2.8. Note that E is now allowed to vary between s_h and s_{fc} and is preceded by a calibrated constant factor, k_s [-], representing the soil-imposed physical limitation to surface evaporation [*Istanbulluoglu et al.*, 2011].

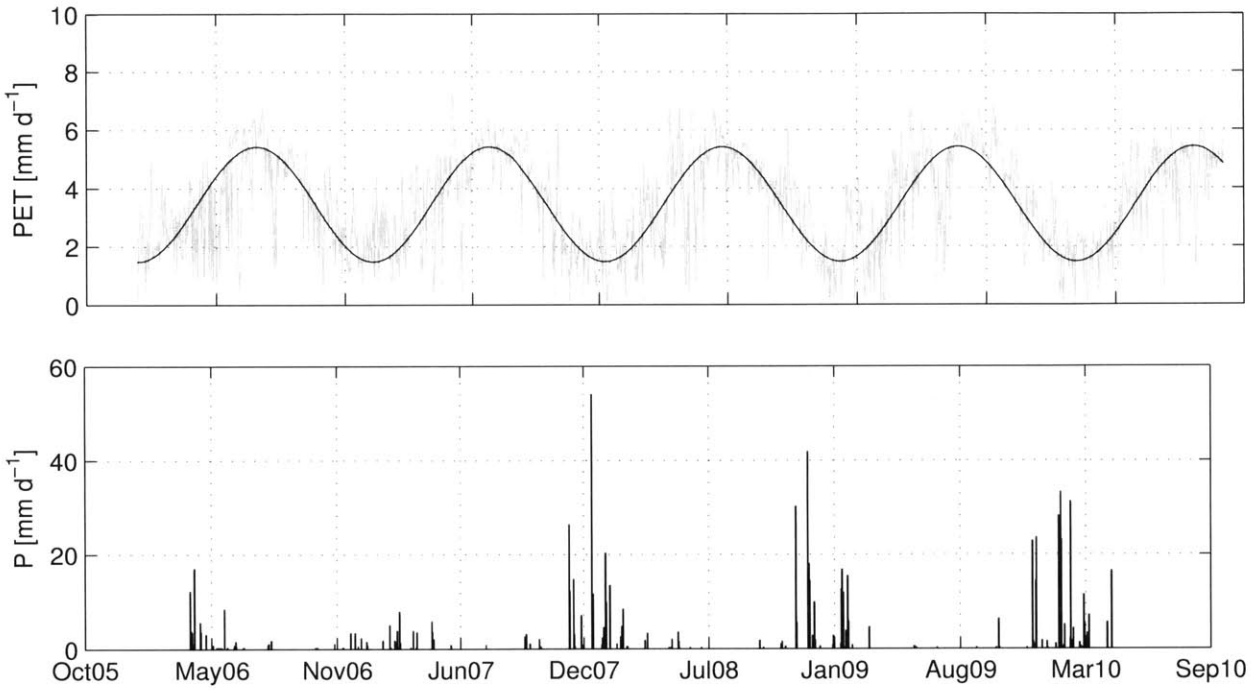

Figure 3-9: Time-series of climatic forcing during the Loma Ridge experiment: precipitation (P, bottom panel) and potential evapotranspiration (PET, top panel). P is measured by a tipping bucket rain gauge at the field site. PET is obtained from a nearby well-watered grassland managed by the California Irrigation Management Information System (CIMIS). The gray lines indicate these estimates and the black line indicates the sinusoidal approximation with $E_p = 3.5$ and $\Delta E_p = 2.0$ [mm d^{-1}].

3.2.2 Ecosystem carbon balance

For this analysis, the ecosystem carbon balance only considers carbon cycling through the vegetation. Therefore, it ignores the dynamics of litter production and organic matter decomposition, which would be important for determining light availability, heterotrophic respiration, and the longer time-scale dynamics of soil carbon and nitrogen cycling. The latter two issues are not included in this first analysis, which focuses solely on the vegetation.

With respect to light availability, we are implicitly assuming soil shading is entirely due to the plant canopy and not to litter. This assumption is reasonable for the 2008 growing season at Loma Ridge (i.e. fire removed all litter) or cases where decomposition rates are fast enough to inhibit litter accumulation on the surface. With these assumptions, the ecosystem carbon balance is,

$$\frac{dC}{dt} = A - R - M \tag{3.15}$$

where C [g m^{-2}] is the total carbon pool, A is the canopy-scale assimilation rate, R is the whole-plant respiration rate, and M is a mortality rate that accounts for stress and senescence (all in units [g m^{-2} d^{-1}]). Detailed formulations for the carbon fluxes A, R, and M are discussed below.

Canopy-scale assimilation, A, is related to the maximum leaf-scale assimilation rate, a_{max}, the leaf area index, L_a, and soil moisture, s,

$$A = a_{max}\beta_v(s)k^{-1}\left[1 - \exp\left(-kL_a\right)\right] \tag{3.16}$$

This represents the total carbon entering the plant via photosynthesis at the daily scale. Some of this carbon is consumed via respiration, which provides energy to build new tissues (growth respiration) and to regenerate enzymes for resource acquisition and transport (maintenance respiration). Net primary productivity (NPP) is the difference between A and the sum of growth and maintenance respiration, R_g and R_m, respectively. R_g is assumed to be a constant fraction of A_n and R_m is assumed to be linearly related to the plant nitrogen content, N_p [g N m^{-2}] [*Dewar*, 1996]. These assumptions give,

$$NPP = y_g A_n = y_g \cdot (A - R_m) = y_g \cdot (A - rN_p) \tag{3.17}$$

where y_g [-] is the growth yield, which converts assimilated carbon to dry matter, and r [g C g^{-1} N d^{-1}] is the nitrogen-specific respiration rate. Finally, NPP is allocated to above- and below-ground tissues according to the root allocation fraction, f_r, (i.e. ANPP=NPP$(1 - f_r)$).

Mortality is similarly assumed to be a constant fraction of biomass and also a function

of soil moisture stress, increasing linearly with stress [*Collins*, 2006],

$$M = m\xi(s)C_i \tag{3.18}$$

where m [d^{-1}] is the biomass specific mortality rate and the index i refers to either the leaf or root carbon pool.

Combining these assumptions, the leaf and root carbon balances can be written as,

$$\frac{dC_{leaf}}{dt} = [A(s, N_p, C_{leaf}) - rN_p]\, y_g(1 - f_r) - m\xi(s)C_{leaf} \tag{3.19}$$

and

$$\frac{dC_{root}}{dt} = [A(s, N_p, C_{root}) - rN_p]\, y_g f_r - m\xi(s)C_{root} \tag{3.20}$$

Root and leaf carbon are converted to the vegetation parameters, z_r and L_a, thus linking the allocation strategy to carbon and water uptake rates,

$$L_a = SLA \cdot C_{leaf} \tag{3.21}$$

and

$$z_r = SRD \cdot C_{root} \tag{3.22}$$

where SRD [m g^{-1}] is the specific root depth and SLA [m^2 g^{-1}] is the specific leaf area.

3.2.3 Ecosystem nitrogen balance

Similar to the carbon balance, the nitrogen balance described here is simplified. Two nitrogen pools are modeled, the plant (subscript p) and soil (subscript s) pools. While soil N is typically modeled using at least three soil pools to represent the multiple time-scales at which decomposition and mineralization occur [*Schimel et al.*, 1994; *Bolker et al.*, 1998], this model is validated for a single year only and applied to calculate the mean behavior of the system. Thus, inter-annual and decadal variability is not anticipated to affect the qualitative interpretation of these results. This model also does not differentiate between ammonium (NH_4^+), nitrate (NO_3^-), and organic N. With these assumptions, the soil and plant nitrogen

balances are,

$$\frac{dN_s}{dt} = DEP + MIN \cdot f_n(s) - UP(s) - L_n(s) \tag{3.23}$$

and

$$\frac{dN_p}{dt} = UP(s) - m\xi(s)N_p \tag{3.24}$$

where DEP [g m^{-2} ground d^{-1}] is atmospheric deposition by dry or wet mechanisms, MIN [g m^{-2} d^{-1}] is the potential mineralization rate, which depends on soil moisture through $f_n(s)$, UP [g m^{-2} d^{-1}] is the sum of active and passive uptake, described below and also dependent on soil moisture, and L_n [g m^{-2} d^{-1}] represents leakage losses, which are tied directly to $L(s)$,

$$L_n(s) = a\frac{L(s)}{snz_r}N_s \tag{3.25}$$

where a [-] is a solubility coefficient for soluble N.

The soil moisture function $f_n(s)$ represents the dependence of the soil nitrogen supply rate as a function of soil moisture. At low soil moisture, the soil environment is unfavorable for microbial activity and mineralization is inhibited. As moisture increases, however, oxygen begins to limit aerobic activity and the anaerobic decomposition continues at a lower rate. Also, anaerobic conditions promote denitrification, further lowering the effective mineralization rate. A rudimentary representation of these processes has been proposed by several authors [*Schimel et al.*, 1996; *Brady and Weil*, 2004; *Porporato et al.*, 2003b; *Everard et al.*, 2010],

$$f_n(s) = \begin{cases} \frac{s}{s_{fc}} & s \leq s_{fc} \\ \\ \frac{1-s}{1-s_{fc}} & s > s_{fc} \end{cases} \tag{3.26}$$

Plant uptake is assumed to be governed by two processes. Passive N uptake, UP_p, occurs as a result of transpiration. That is, whatever N is dissolved in the transpiration stream is automatically taken up by the plant. Secondly, plants can augment this N supply through an active mechanism, UP_a, which increases diffusion toward the root surface by lowering the N concentration at the root surface [*Lambers et al.*, 2008]. These processes are represented

as,

$$UP_p = a\frac{T(s)}{snz_r}N_s \tag{3.27}$$

and

$$UP_a = a\frac{Fs^d}{snz_r}N_s \tag{3.28}$$

where F [m d^{-1}] is a diffusion coefficient and d [-] represents the tortuosity of the diffusion path from the soil pore space to the root surface. Further, total uptake is limited by a demand, DEM, which effectively sets the maximum possible uptake rate. See *Porporato et al.* [2003b] for further discussion of modeling the mineralization and uptake processes.

3.3 Model calibration and validation

Model parameter estimation and validation for the Loma Ridge grassland are described in this section. The calibrated model will be applied (1) to develop a mechanistic explanation for the canopy observations during the 2008 growing season and (2) to study the variation of plant resource use strategies across hypothetical climate and nitrogen deposition gradients. Therefore, the primary objective of this validation exercise is to develop a parameter set that accurately reproduces both the seasonal course of water, carbon, and nitrogen fluxes and the sensitivity of annual net primary productivity and ecosystem water use to water and nitrogen supplies. To achieve the first goal, model predictions are compared to observations collected during the 2008 growing season. To achieve the second goal, NPP predictions are compared to annual scale observations collected over the six year observational record (2007–2012). Lastly, because disturbance is a strong control on productivity in this ecosystem, the merit and performance of this approach is discussed in light of the fire and severe drought that occurred in 2007.

3.3.1 Parameter estimation

A number of sources inform the parameter estimates described below. Where possible, parameters are estimated from direct observation. However, some parameters were only measured during the drought year of 2007 or not at all. In these cases, data from other

studies is also considered. What follows is a brief justification of values selected for each parameter. Parameters for the carbon and nitrogen balances are summarized in Tables 3.2 and 3.3, respectively. Unless otherwise noted, water balance parameters are the same as in Table 2.1.

Slope of $v_{c,max} - N_p$ relationship, k_n. k_n is estimated from the annual grass data points published in *Evans* [1989] Figure 1. This data was collected in Death Valley, California and an abandoned cornfield near Urbana, Illinois [*Mooney et al.*, 1981]. Although these are quite different ecosystems, the relationship between $v_{c,max}$ and N_l is remarkably consistent. The estimated value of k_n is 19 [μmol CO_2 g^{-1} N s^{-1}] and, given the variability in Evans' [1989] plot, may range between 15 and 22 [μmol CO_2 g^{-1} N s^{-1}].

Root allocation fraction, f_r. For the validation scenarios, f_r takes an assumed constant value. Below-ground biomass was not measured at Loma Ridge, therefore an estimate must be obtained from observations at similar sites. First, define f_r as the ratio of below-ground to total biomass, or $f_r = C_{bg}/C_{tot}$. Using this definition, *Harpole et al.* [2007] observed $f_r = 120/(120 + 400) = 0.23$ in control plots and $f_r = 105/(105 + 590) = 0.15$ in fertilized plots at a site nearby Loma Ridge. These values are at the lower end of the range observed by *Shipley and Meziane* [2002] in several species grown in laboratory conditions.

Specific leaf area, SLA. SLA is the ratio of leaf area to leaf mass and, therefore, was estimated directly from Loma Ridge ANPP and LAI measurements. ANPP was estimated by harvesting two 14 x 50 cm strips at the end of the growing season. In the ambient water plots in 2008, ANPP measured 378 [g m^{-2} ground] and LAI measured 3.72 [m^2 leaf m^{-2} ground]. Therefore, SLA=ANPP/LAI=3.72/378=0.01 [m^2 g^{-1}]. At the time of measurement (late May), LAI measured 1.11 [m^2 m^{-2}]. However, all live and dead biomass is collected within the harvest strip, therefore, the peak LAI is used to compute SLA because it represents the leaf area that was present during that growing season. The computed value compares well with the range of observations found in the literature [*Wright et al.*, 2004; *Lambers et al.*, 2008; *Istanbulluoglu et al.*, 2011].

Specific root depth, SRD. SRD is a new root parameter introduced to link root biomass to ecohydrological function. Root systems are generally characterized by a variety of physical characteristics, including root length, diameter, and mass [*Lambers et al.*, 2008]. However, in land surface modeling schemes, all of these characteristics are typically represented by a single parameter, root depth, at the scale of the entire rooting system. SRD is thus proposed to relate root carbon to water uptake while maintaining this relative simplicity. Neither root biomass or rooting depth were measured at Loma Ridge, therefore this parameter must be estimated from measured ANPP, f_r estimated above, and an assumption for the maximum rooting depth. As discussed in Chapter 2, maximum rooting depth for annual grasses is approximately 30 cm [*Holmes and Rice*, 1996]. With these assumptions,

$$SRD = z_r \left(\frac{f_r}{1 - f_r} \cdot ANPP \right)^{-1} = 0.3 \left(\frac{0.23}{0.77} \cdot 378 \right)^{-1} = 0.0027 \tag{3.29}$$

Respiration and mortality rates (r, m). Respiration and mortality rates vary substantially with environmental conditions and between plant organs. Typical respiration values may range between 10 and 50% of assimilated carbon [*Lambers et al.*, 2008]. The mortality parameter, m, aggregates several processes that result in the decline of root and leaf tissues, including late-season phenology, reproduction, and tissue damage due to water and/or temperature stresses. Because of this wide variability, these parameters are treated as highly uncertain and are chosen to fit ANPP observed in the field and the LAI time-series observed by the MODIS satellite.

Deposition, DEP. The background deposition rate, DEP, is estimated from the National Atmospheric Deposition Program dataset (http://nadp.sws.uiuc.edu/). The average values of wet deposition over the years 2006-2010 at two southern California sites are averaged to estimate the deposition rate at Loma Ridge. Deposition at Tanbark Flats (Los Angeles County) is approximately 2.2 [kg ha^{-1} yr^{-1}] and that at Converse Flats (San Bernardino

County) is 5.3 [kg ha^{-1} yr^{-1}]. Therefore, the model is forced with an average daily deposition rate of 0.0011 [g N m^{-2} d^{-1}].

The deposition rate in fertilized plots, DEP+, is supplemented by the experimental fertilization rate, which is equivalent to 2 [g N m^{-2}] immediately applied before the growing season and 4 [g N m^{-2}] 100-day release, or 0.04 [g N m^{-2} d^{-1}] during the growing season. For the 2008 growing season, both applications occurred on 17 December 2007.

Potential mineralization rate, k_{min}. The potential mineralization rate is calculated by extrapolating observed mineralization rates in 2007 to an estimated value at field capacity using equation 3.27. In-situ soil incubations indicate an average nitrogen production rate of approximately 0.13 [g N m^{-3} d^{-1}] during the 2007 growing season. This measurement was made at a volumetric water content of 0.05 [m^3 m^{-3}]. Therefore, the potential mineralization rate at field capacity is estimated as $k_{min} = 0.13/0.19 = 0.68$ [g N m^{-3} d^{-1}]. Lastly, it is assumed that this rate occurs in the top 30 cm of soil, where most of the soil micro-organisms are located, $k_{min} = 0.68 * 0.3 = 0.21$ [g N m^{-2} d^{-1}]. Mineralization rates obtained from ion exchange resins are also used for model validation in Section 3.3.1 below.

Table 3.2: Carbon balance parameters.

Parameter		Value	Units	Reference
Root allocation fraction	f_r	0.23	[-]	*Harpole et al.* [2007]
Respiration rate	r	0.218	g C g^{-1} N d^{-1}	*Dewar* [1996]
Mortality rate	m	0.019	d^{-1}	calibrated
Specific leaf area	SLA	0.010	m^2 g^{-1}	observed
Specific root depth	SRD	0.0027	m g^{-1}	observed
Soil evaporation coefficient	k_s	0.5	[-]	calibrated
Transpiration efficiency	k_v	0.7	[-]	calibrated

Table 3.3: Nitrogen balance parameters.

Parameter		Value	Units	Reference
$v_{c,max} - N_l$ slope	k_n	19	μmol CO_2 g^{-1} N s^{-1}	*Evans* [1989]
Background deposition rate	DEP	0.0011	g N m^{-2} d^{-1}	NADP
Fertilization rate	DEP+	0.04	g N m^{-2} d^{-1}	observed
Potential mineralization rate	k_{min}	0.21	g N m^{-2} d^{-1}	observed
Solubility coefficient	a	1	[-]	*D'Odorico et al.* [2003]
Active uptake diffusion coefficient	F	5e-4	[-]	"
Active uptake tortuosity factor	d	3	[-]	"

3.3.2 Intra-annual dynamics: 2008 growing season

To evaluate the model's ability to predict the seasonal dynamics at Loma Ridge, model output is compared to observations collected during the 2008 growing season. The seasonal trajectories of soil moisture (upper 15-cm average), root and leaf carbon, leaf area index, and soil and plant nitrogen are shown in Figure 3-10. The model captures the seasonal dynamics of LAI and surface soil moisture very well. Although the seasonal variability in carbon and nitrogen stores was not observed, the peak values of root and leaf carbon and plant nitrogen match the observed values well. Mineral soil nitrogen was estimated from soil cores collected in April 2007 and, due to the dry conditions that year, are expected to be larger than typical for this ecosystem. The range of values predicted by the model is of a similar order of magnitude and consistent with this expectation. Also, the model successfully reproduces the seasonal variability in nitrogen availability (also see Figures 3-11 and 3-12). Given its simplicity, the model provides a good description of the intra-annual water-carbon-nitrogen dynamics in this ecosystem.

In addition to the modeled ecosystem states, the modeled fluxes shown in Figure 3-11 provide insight into the function of this ecosystem. Loma Ridge is typical of ecosystems that experience a Mediterranean climate and is strongly influenced by the asynchronous precipitation and evaporative demand. Early in the wet season, when soil moisture levels are high and the plant canopy has yet to develop, soil water losses are dominated by evaporation and leakage. As the season progresses, the growing canopy causes a shift from bare soil evaporation to transpiration. Eventually, soil moisture reaches a level where physiological

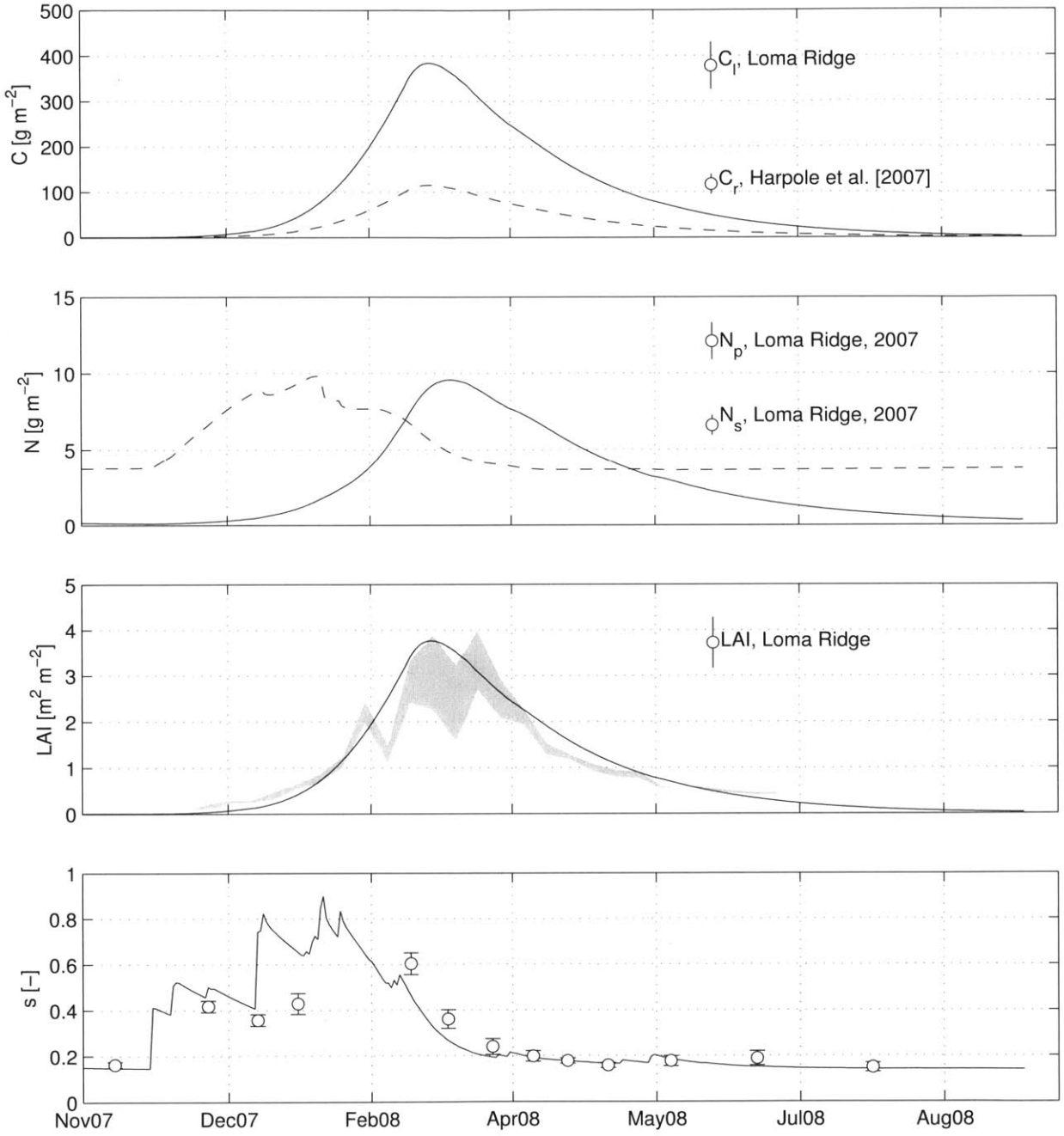

Figure 3-10: Validation of ecosystem water, carbon, and nitrogen balance states: (a) Above-ground (solid line) and below-ground (dashed line) carbon; (b) plant (solid line) and soil (dashed line) nitrogen; (c) LAI; and (d) 15-cm relative soil moisture. Observations are denoted by the open circles except for LAI, where MODIS observations are denoted by the gray region. In cases where error estimates were not available (i.e. soil and plant nitrogen), error was assumed to be 10%.

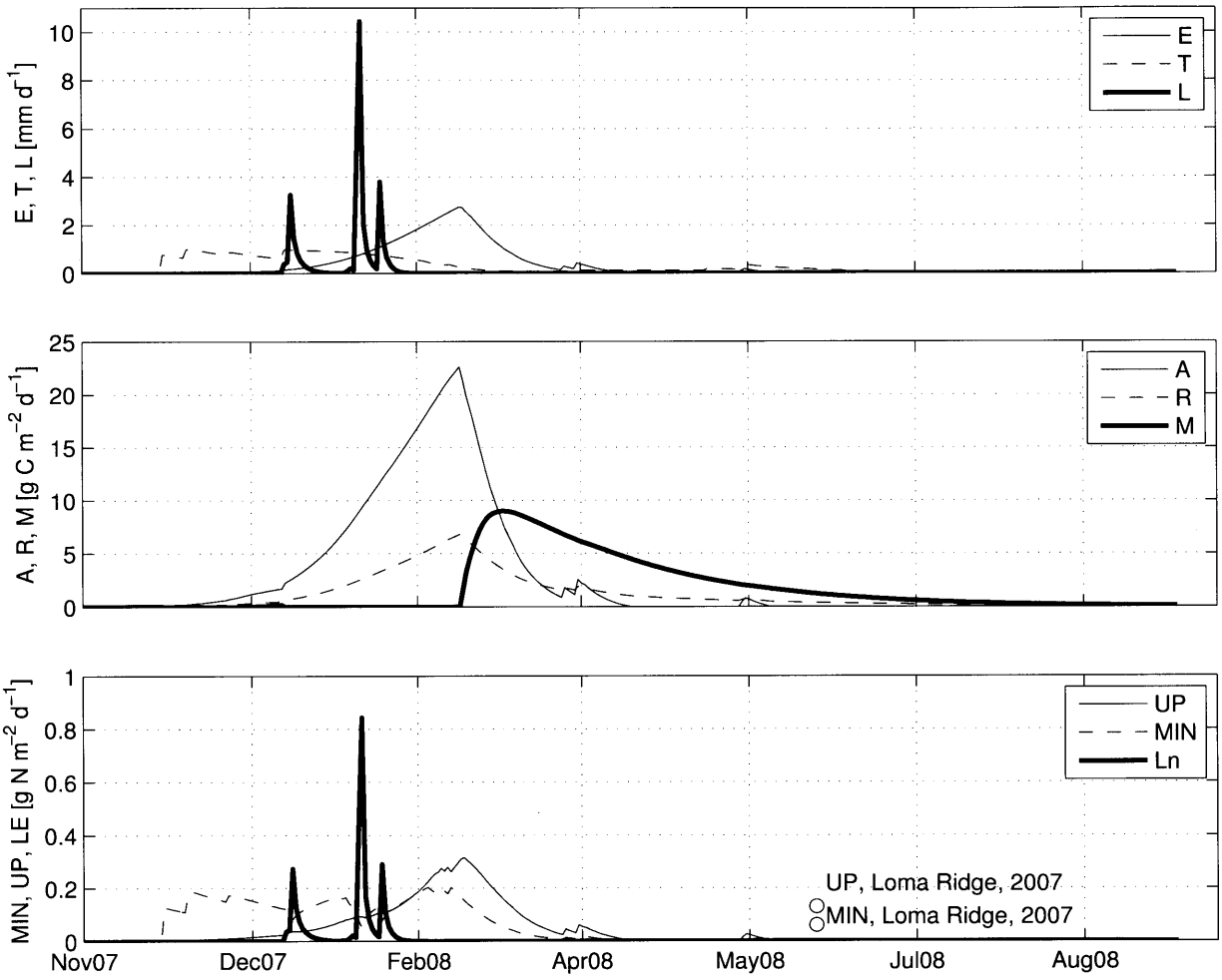

Figure 3-11: Ecosystem water, carbon, and nitrogen balance fluxes: (a) transpiration (solid line), evaporation (dashed line), and leakage (bold line); (b) assimilation (solid line) and respiration (dashed line); and (c) nitrogen uptake (solid line), mineralization (dashed line), and leakage (bold line).

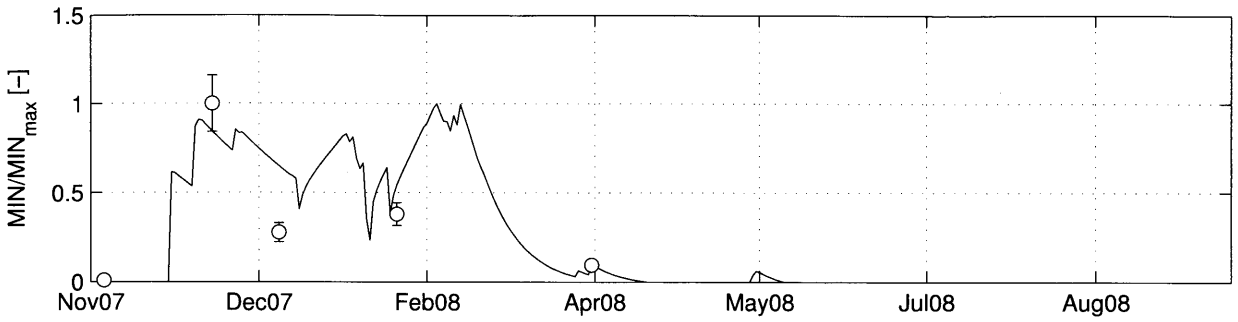

Figure 3-12: Comparison of relative mineralization rates predicted by the model (solid line) and estimated from ion exchange resin sampling (symbols) collected during the 2010 growing season. The observation dates plotted are the mid-points of the resin deployment periods, which were 53, 10, 31, 44, and 75 days from left to right.

stress begins to affect photosynthesis and transpiration, both of which experience a sharp decline. During this period, mortality increases and respiration (a function of nitrogen content and biomass) remains high, leading to senescence and the observed decline in LAI.

A similar trajectory is evident in the soil nitrogen balance. High early-season soil moisture promotes high mineralization and an early pulse of nitrogen availability. During the second pulse of rain events in December and January, which occurs before the canopy is at its maximum density, the saturated soils slow net mineralization and promote nitrogen losses via leakage, leading to a plateau in soil nitrogen availability. As the canopy grows, soil nitrogen losses are dominated by plant uptake. Uptake also experiences a sharp decline at the onset of stress due to its dependence on transpiration and soil moisture.

Together, the modeled water, carbon, and nitrogen balances demonstrate three distinct periods during a typical year at Loma Ridge. The first occurs prior to the growing season and is characterized by high resource availability and high non-productive resource losses. This period is followed by one dominated by vegetation activity, when LAI, transpiration, and photosynthesis are at their maximum. Because the soil resources are no longer replenished during this period, the vegetation enter a final prolonged period of stress that induces reproduction, senescence, and mortality. Note that each of the ecosystem states return to a minimum value during this dry season – live carbon approaches zero, whereas soil moisture and soil nitrogen approach the limiting values required for a positive carbon gain. In the

case of soil moisture, this is the wilting point, whereas for soil nitrogen it represents the level at which uptake ceased. These limiting values have implications for the ecological behavior of this system.

From an ecological perspective, these asymptotes indicate the lowest resource levels at which the modeled resource use strategy can obtain a positive growth rate. The strategy with a positive growth rate at the lowest resource level is the most competitive [*Tilman*, 1994; *Zea-Cabrera et al.*, 2006]. That is, the most competitive strategy reduces resources to a level at which invaders are unable to establish themselves. This suggests that the most competitive strategy is not that which uses resources most efficiently, but that which minimizes resource availability to invaders.

The model also captures the sensitivity of NPP to the experimental fertilization treatment in 2008, as demonstrated in Figure 3-13. For this simulation, the biomass allocation ratio was changed to $f_r = 0.15$ [*Harpole et al.*, 2007] and DEP+ was added to the nitrogen balance forcing. While total NPP increased from 500 to 600 [g m^{-2}], this shift in root allocation resulted in a disproportionate increase in ANPP and almost no change in BNPP. Because allocation information is not available for the dry and wet plots, these resource supply treatments are not simulated here.

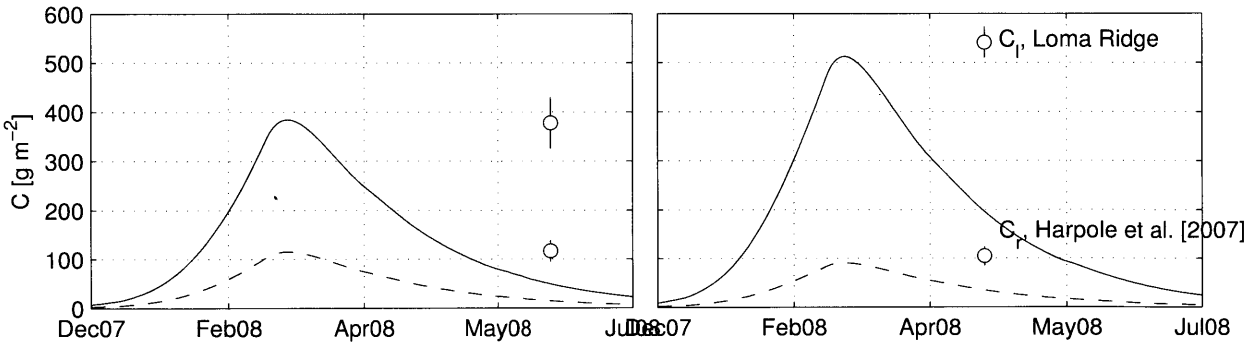

Figure 3-13: Modeled response of above-ground (solid lines) and below-ground (dashed lines) carbon to the experimental fertilization treatment (left, control; right, fertilized).

3.3.3 Disturbance and inter-annual variability

When the model is extended to simulate inter-annual variability, the picture becomes much more complex. ANPP and LAI observations (see Chapter 2) suggest that the coincident fire and severe drought in 2007 imposed a transient response in productivity, as well as its sensitivity to the nitrogen fertilization treatment. In this section, possible explanations for these disturbance effects and the ability of the model to capture them are discussed. It concludes with a best estimate for the typical response of Mediterranean annual grasslands to precipitation and nitrogen deposition gradients.

Considering only the observational evidence, the three data sources characterizing inter-annual variability suggest different responses to the 2007 combined disturbance event (Figures 3-14 and 3-15). First, all datasets show little direct correlation with precipitation, which supports the idea that other factors are controlling productivity in this dry ecosystem. Loma Ridge plot-scale ANPP data show that the ecosystem responds with an intermediate productivity year in 2008, followed by three consecutive high productivity years (2009-2011) and a return to a lower value in 2012. This data is also consistent with the hypothesis that the ANPP response to nitrogen fertilization is transient itself. In the ambient plots, the ANPP fertilization response is only positive and significant in 2008, 2009, and 2010. Interestingly, in the wet plots, the fertilization response is delayed by one growing season, with the most substantial positive effect occurring in 2009 and 2010. The LAI data offer a different perspective. Both MODIS and the plot-scale SunScan LAI estimates show an anomalous peak in 2008 (LAI is elevated in 2008 and 2009 in the wet plots). MODIS also observed a peak in LAI following an earlier drought in 2002. Therefore, when compared to the typical year, the plot-scale ANPP data suggest that 2008 was a low productivity year, whereas the LAI data suggest 2008 was a high productivity year. Analysis of results from other disturbance-response studies may provide a clue as to which is the more likely case at Loma Ridge.

Drought may produce a transient peak in NPP. Several studies have observed increased productivity following drought years [e.g. *Knapp et al.*, 1998; *Bloor and Bardgett*, 2012]. This increase is attributed to enrichment of soil nitrogen. Soil nitrogen availability increases in

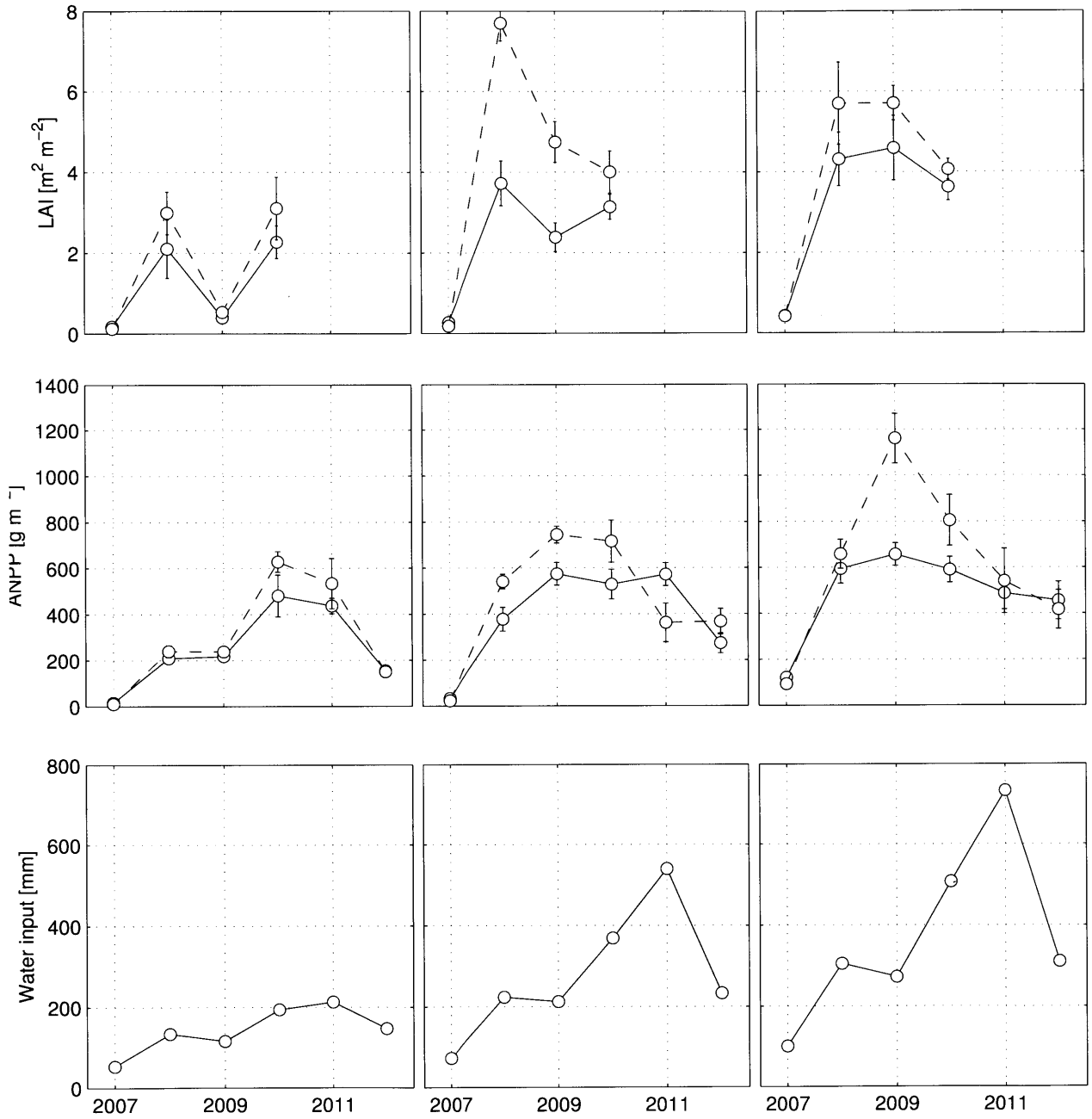

Figure 3-14: Time-series of (a) LAI, (b) ANPP, and (c) water input in dry (left), ambient (middle), and wet (right) water input plots over the course of the Loma Ridge experiment. The solid lines denote control plots and the dashed lines denote fertilized plots..

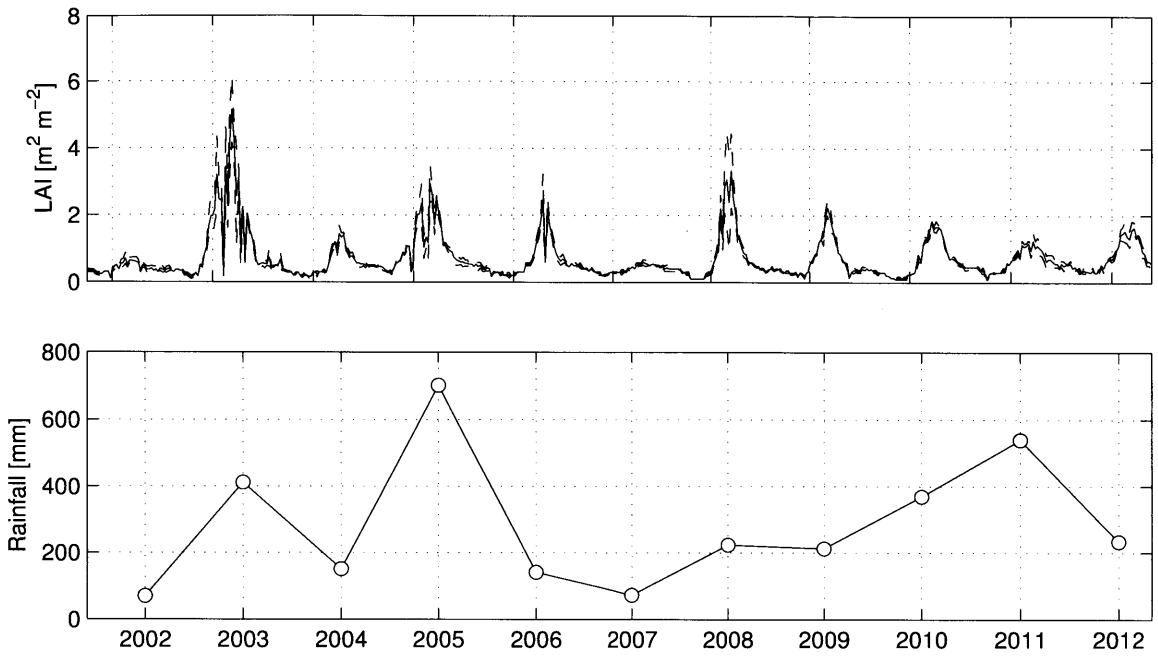

Figure 3-15: Time-series of (a) MODIS LAI and (b) annual rainfall.

drought years because nitrogen loss mechanisms, such as mineralization, plant uptake, and leaching, are strongly limited by water availability. This stored nitrogen is then available in subsequent years to be mineralized and to be taken up by vegetation. This scenario would be consistent with the MODIS observations.

The effect of fire on short-term NPP transients is more uncertain. Fire may have an effect similar to the drought effect described above [*Seastedt and Knapp*, 1993; *Knapp et al.*, 1998]. When fire is absent and water is not limiting, litter accumulates on the surface, canopies are dense, and productivity is primarily light-limited. Soil nitrogen accumulates as plant uptake is determined by the light-limited photosynthesis rate. Fire removes litter (which occurred at Loma Ridge in 2007), shifting the limiting growth factor from light to nitrogen. Therefore, productivity is high in years following fire due to a simultaneous surplus of light and nitrogen. This hypothesis is consistent with the LAI data. However, fire may negatively affect soil nitrogen supplies in some ecosystems [*Harden et al.*, 2004]. In this case, fire releases light limitation, but also volatilizes a fraction of the soil nitrogen stock. At Loma Ridge, it is hypothesized that this would lead to a short-term decline in nitrogen availability during the 2008 growing season. The ecosystem is nitrogen-limited in this state, resulting

in an intermediate level of productivity and a maximum productivity response to nitrogen fertilization. This hypothesis is consistent with the ANPP data.

It is also worth noting that MODIS observes a different mosaic of land cover than the homogeneous grassland in which the plot-scale data is collected. The footprint of the MODIS data analyzed here is 3x3 pixels, or approximately 750x750 m, whereas the experimental area footprint is approximately 100x50 m. Therefore, it is very likely that the MODIS data incorporates information from other vegetation communities, nearby roads and developments, and areas that were affected by the 2007 drought but not by the 2007 fire. Therefore, the ANPP data is more applicable to the question posed here.

While the evidence from the literature may be inconclusive, the question of how 2008 productivity compares to the typical year is further illuminated by application of the ecosystem model. Figure 3-16 compares the calibration scenario above with a similar scenario under the assumption that the October 2007 fire removed the entire litter N pool. In the first scenario, $k_{min} = 0.21$ [gN m^{-2} d^{-1}], the previously calibrated potential mineralization rate. For the second scenario, $k_{min} = 0.42$ [gN m^{-2} d^{-1}] to accommodate the assumed fire-induced nitrogen loss. Both models predict 2008 ANPP well, but Scenario 2 is a much better predictor of the observed inter-annual variability in following years. The primary difference here is that predicted productivity increases in 2008 and 2009 when the fire removes nitrogen, whereas 2008 is predicted as the peak productivity year when no nitrogen is lost in the fire.

Surely this is not the entire story at Loma Ridge, but a simple example of the multiple controls on the inter-annual variability of productivity. Other controls may include the dynamics of litter accumulation and decomposition and interaction between drought, fire, and the soil organic matter pools that cycle at longer time-scales than surface litter. These issues have been addressed only recently in LSMs [*Arora and Boer*, 2005; *Yi et al.*, 2010]. Initial studies suggest that modeling these interactions may result in complex non-linear and even chaotic behavior [*Stone and Ezrati*, 1996]. Therefore, with such a limited observational record (a common occurrence), accurate modeling of Loma Ridge NPP will require some effort. Nevertheless, this comparison provides some further insight into the physical processes controlling NPP in this ecosystem.

In addition to the effect of fire, the large discrepancy between 2011 and 2012 is interesting

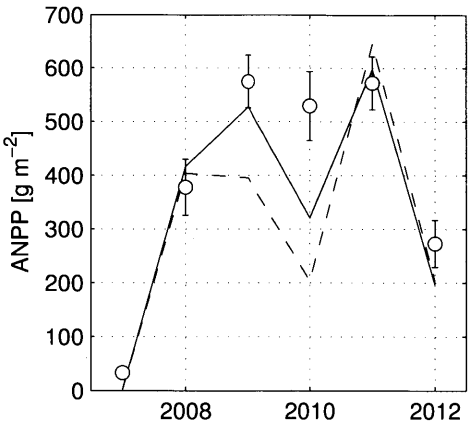

Figure 3-16: Comparison of predicted ANPP with observations (symbols) for different fire-effect assumptions. The solid line denotes the case where fire removes labile nitrogen from the soil surface and the dashed line denotes the case where soil nitrogen is not affected by fire.

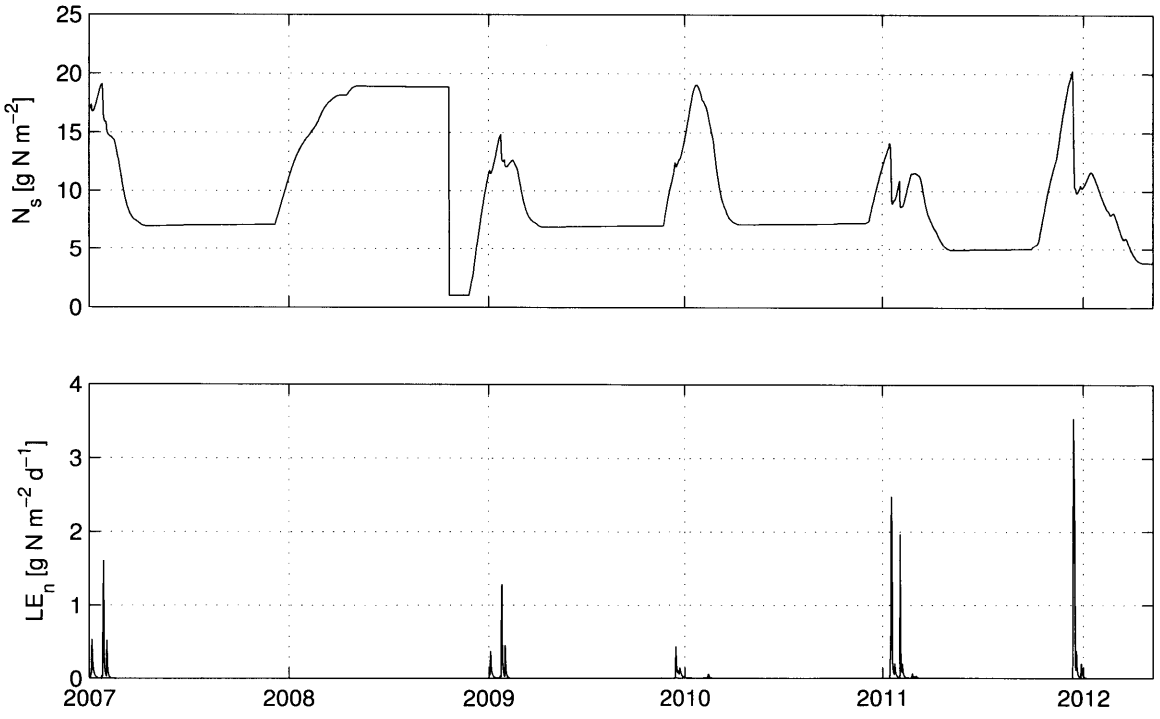

Figure 3-17: Modeled (a) soil nitrogen and (b) nitrogen leakage for the case where fire removes labile nitrogen from the soil surface.

to analyze from a hydrological perspective. Figure 3-17 shows the time history of predicted soil nitrogen and leakage losses. Note the large mass of nitrogen lost due to leakage during the anomalously wet 2011 growing season. In the next year, 2012, rainfall was average, but productivity was extremely low. The model suggests this resulted from a nitrogen deficit imposed by the previous years rainfall. This result also implies that 2012 is a poor candidate for evaluating the typical fertilization response for this ecosystem and it remains to be seen whether this response is truly transient.

Lastly, any of these factors may be coincident with inter-annual variability in rooting strategy, which is strongly tied to annual rainfall [*Schenk and Jackson*, 2002a; *Laio et al.*, 2006; *Collins and Bras*, 2007; *Sivandran*, 2011] and nitrogen availability [*Jobbagy and Jackson*, 2001]. The implications of this point will become more clear when root carbon allocation strategies are discussed in Chapter 4.

Comparing the average behavior of the model to the average observed behavior of the ecosystem provides further justification that 2008 was likely an intermediate productivity year associated with limiting water and nitrogen supplies. Figure 3-18 shows the sensitivity of NPP to rainfall and nitrogen deposition for the two calibration scenarios above. In aggregate, this model is consistent with the hypothesis that the negative effect of fire on nitrogen availability dominated the combined positive effects of fire and drought. Further, this model favors the most direct observation, plot-scale ANPP, over the indirectly obtained plot-scale and MODIS LAI observations. The parameterization demonstrated in Figure 3-18b, with $k_{min} = 0.42$ [g N m^{-2} d^{-1}] is thus chosen for further analysis.

Using this model, the mean behavior of the Loma Ridge annual grassland can be described. Under conditions of ambient soil fertility, ANPP is approximately 560 [g m^{-2}] in a typical year. ANPP saturates at this value at an annual water input volume of approximately 300 mm, which is quite similar to the long-term mean and median rainfall, 282 mm and 332 mm, respectively. This is considered the nitrogen-limited ANPP for this ecosystem. Interestingly, the nitrogen-limited ANPP is very closely associated with the mean rainfall condition, indicating potential large-scale organization of the carbon, water, and nitrogen cycles (for example, see *Schimel et al.* [1997]). Below this value, ANPP varies linearly with rainfall and is negligible below approximately 100 mm. In the fertilized plots, ANPP satu-

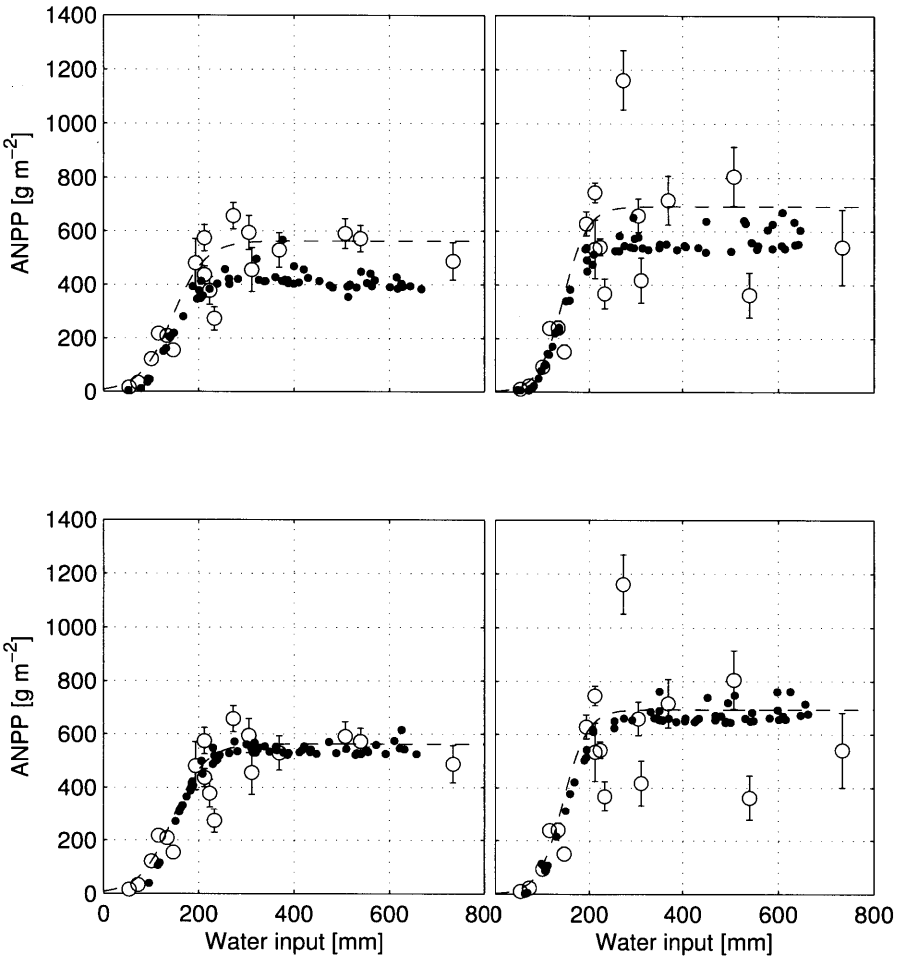

Figure 3-18: Sensitivity of ANPP to water input and nitrogen fertilization treatment (left: control N; right: fertilized N) for (a) $k_{min} = 0.21$ [g N m^{-2} d^{-1}] and (b) $k_{min} = 0.42$ [g N m^{-2} d^{-1}]. The open symbols denote observed ANPP, the dashed lines denote fitted logistic curves, and the closed symbols denote simulated values.

rates at approximately 690 [g m^{-2}] at a slightly lower water input of 230 mm. Again, ANPP below this value is strongly controlled by water input and the slope of this relationship is greater than in the control N plots. Note the substantial variability in the experimental data that is not captured by the model. As argued earlier, this variability is a consequence of the combined drought and fire preceding the experiment and the particular sequence of annual rainfall in the years following. Fire was not considered in the model and annual rainfall was treated as a random variable with no auto-correlation. Therefore, the model is not expected to reproduce the observed variability.

3.4 Conclusions

In this chapter, an ecosystem model is introduced that couples the water, carbon, and nitrogen cycles at the daily scale. The model builds on ecohydrology models by incorporating the nitrogen cycle and builds on ecology models by incorporating the water cycle. The model reproduces the seasonal dynamics of the Loma Ridge annual grass ecosystem and captures the sensitivity of ANPP to experimental water input and nitrogen fertilization treatments. This latter capability is important in that it allows one to judge the relative ecological success of competing ecological strategies. Strategies involved in the simultaneous acquisition of nitrogen and carbon for growth as constrained by the soil water conditions are now studied in Chapter 4.

Chapter 4

Plant resource use strategies and the hydrologic response to nitrogen fertilization

With a verified model of the coupled water, carbon, and nitrogen cycles, the analysis in *Chapter 2* can now be extended to study plant interactions with two soil resources, water and nitrogen. Because canopy conductance and rooting depth together govern rates of resource uptake and are jointly constrained by primary productivity, the root-leaf biomass allocation ratio, f_r, is assumed to be the primary control on the relative acquisition of above- and below-ground resources. The objective of the following chapter is therefore to study the role of f_r, and its response to changes in climate and nitrogen supply, on ecosystem processes. To do so, optimality hypotheses are assumed to provide the functional ecosystem response to changes in the resource environment constrained by the coupled model. This analysis provides a new interpretation of the Loma Ridge experiment and improved understanding of ecohydrological function under multi-dimensional environmental change.

4.1 Optimal resource use strategies

Plant resource use strategies play a central role in ecological and evolutionary dynamics and interact with the hydrologic and biogeochemical cycles. Most previous work on plant-resource (or biotic-abiotic ecosystem) interactions has been accomplished through two distinct lines of research – that concerned with water as the exclusive limiting resource [e.g. *Rodriguez-Iturbe et al.*, 2001a; *Zea-Cabrera et al.*, 2006; *Collins and Bras*, 2007; *Sivandran*, 2011] and another considering the balance of nitrogen and light as simultaneous limiting resources [e.g. *Reynolds and Pacala*, 1993; *Tilman*, 1994; *Vincent and Vincent*, 1996]. Some

more recent models have attempted to synthesize these results by allowing particular aspects of the plant strategy, for example biomass allocation, to vary simultaneously with light, nitrogen, and water availability [e.g. *Friedlingstein et al.*, 1999]. This latter study assumes functions to relate the resource use strategy (i.e. root, stem, and leaf carbon allocation) to resource availability (i.e. light, nitrogen, and water). The analysis below assumes the resource use strategy is that which optimizes plant function.

4.1.1 Optimality criteria

Throughout this chapter, three optimality criteria previously discussed in the literature will be compared to better understand their behavior and to determine which is most applicable for modeling this ecosystem. These are: (1) maximum stress-weighted transpiration; (2) maximum transpiration; and (3) maximum net primary productivity, or,

$$F_1 = \max_u \left[\overline{T}(1-\overline{\chi})\right] \tag{4.1}$$

$$F_2 = \max_u \left[\overline{T}\right] \tag{4.2}$$

$$F_3 = \max_u \left[\overline{NPP}\right] \tag{4.3}$$

where u represents the resource use strategy.

4.1.2 Ecosystem processes and the optimal water use strategy

First, consider the resource use strategy that optimizes plant function with respect to water availability only. This exercise is undertaken to determine whether the model described here successfully reproduces results obtained under other assumptions, namely vertical discretization of the soil column [*Collins and Bras*, 2007; *Sivandran*, 2011] and dynamic vertical root distributions [*Sivandran*, 2011]. Optimal water use strategies are investigated under two alternative conditions where the rooting depth is either (1) not constrained or (2) constrained by root carbon allocation. The first condition identifies the globally optimal root depth, equivalent to that computed by *Collins and Bras* [2007], whereas the second condition identifies the optimal rooting strategy accessible under the extant growth conditions, specific to

the annual grass species found at Loma ridge. The latter case is more similar to *Sivandran* [2011] in that productivity constrains root depth. However, in this study the constraint is imposed by an assumed constant specific root depth as compared to an upper limit on root carbon density [*Sivandran*, 2011]. Also, f_r is optimized here, whereas *Sivandran* [2011] assumes a function relating f_r to soil water content [*Ivanov et al.*, 2008a].

Assumptions specific to this scenario are as follows:

- A 30-year times-series of daily rainfall volumes is generated from the stochastic rainfall model (see Chapter 2). Rainfall is assumed to be concentrated in the wet season, November through March, and no rainfall occurs during the dry season. Mean annual rainfall is $\overline{P} = 332$ [mm].
- Potential evapotranspiration is given by the fitted sinusoidal curve, Equation 3.12.
- The nitrogen balance is turned off and a_{max} is calculated assuming $N_p = 2.5$ [g N m^{-2}], which reproduces the range of NPP values in Figure 3-18.

For the unconstrained case, the model predicts an optimal water use strategy $u^* = (k_v, z_r)^*$ that maximizes NPP and effectively balances transpiration and water stress (Figure 4-1). The max[NPP] rooting depth is approximately $z_r = 40$ cm and increases slightly as f_r increases. The max[NPP] transpiration efficiency varies between $k_v = 0.6$ and $k_v = 0.9$ and increases with f_r. The variability in k_v is indicative of the joint control of k_v and LAI on transpiration. When f_r is high, less carbon is allocated to the canopy, resulting in lower LAI, which is compensated by increased k_v. This is analogous to the trade-off computed in Figure 2-2.

The relationship between the optimal strategies and the water balance demonstrate the distinct ecohydrological functions of z_r and k_v (Figure 4-1). z_r is optimized toward an efficient use of the hydrologic cycle and k_v is optimized with respect to the trade-off between transpiration and water stress. For any given value of k_v, the ratio of productive, or "green," soil water losses to rainfall, f_{green}, is maximized at a root depth of approximately 65 cm, which coincides with the max[T] strategy. This suggests there exists an optimal z_r independent of k_v that maximizes the fraction of rainfall available to the ecosystem. While the max[T]

strategy is located at this z_r and maximum k_v, the max[NPP] and max[T(1-χ)] strategies are located at intermediate z_r and k_v values. NPP is therefore increased by a strategy characterized by an intermediate transpiration rate and hydrological efficiency. With respect to productivity, transpiration is thus large enough to limit non-productive, or "blue," water losses, but regulated to maintain soil water storage and delay the onset of water stress.

Note also that the max[T(1-χ)] strategy is similar to the max[NPP] strategy and, therefore, may be a good surrogate for fitness derived exclusively from the water balance. However, the small discrepancy indicates the formulation is not exact.

Although the analysis above identified an optimal $k_v - z_r$ strategy, it did not consider whether z_r^* could be reached given the specified f_r and growth parameters. With z_r linked to f_r through the carbon balance, Figure 4-2 shows how productivity and the water balance respond to variation in the resource use strategy $u = (k_v, f_r)$. This optimal strategy strongly favors canopy over root development, with 75% of the growth yield allocated above-ground, and again represents an intermediate transpiration efficiency.

Comparing Figures 4-1 and 4-2, the effect of the carbon cycle constraint on the optimal plant strategy becomes clear. First, note that the maximum root depth achievable by any strategy is approximately 70 cm. Therefore, any strategy in the unconstrained case with $z_r > 70$ cm is not feasible given the growth, respiration, and mortality parameters used here. This maximum root depth is not associated with the maximum NPP. Secondly, the constrained max[T] strategy results in a shallower z_r^* (i.e. 43 cm $<$ 65 cm). Both differences can be explained by the carbon cycle, which imposes finite canopy and root growth rates and strong competition between canopy and root growth. That is, increased ANPP comes at a cost to BNPP (and vice versa) and this cost, in terms of carbon, was not considered in the unconstrained case. Interestingly, the max[T] and max[NPP] z_r^* values are more similar in the constrained case, 43 and 37 cm respectively (versus 65 and 43 in the unconstrained case). While globally the constrained max[NPP] strategy does not maximize f_{green}, it does for the given value of k_v^*.

The water balance shown in Figure 4-2 provides some insight into why the low f_r strategy is successful. In this ecosystem, leakage is more sensitive to k_v than to f_r. That is, by increasing k_v, leakage is essentially minimized while increased root depth has less effect.

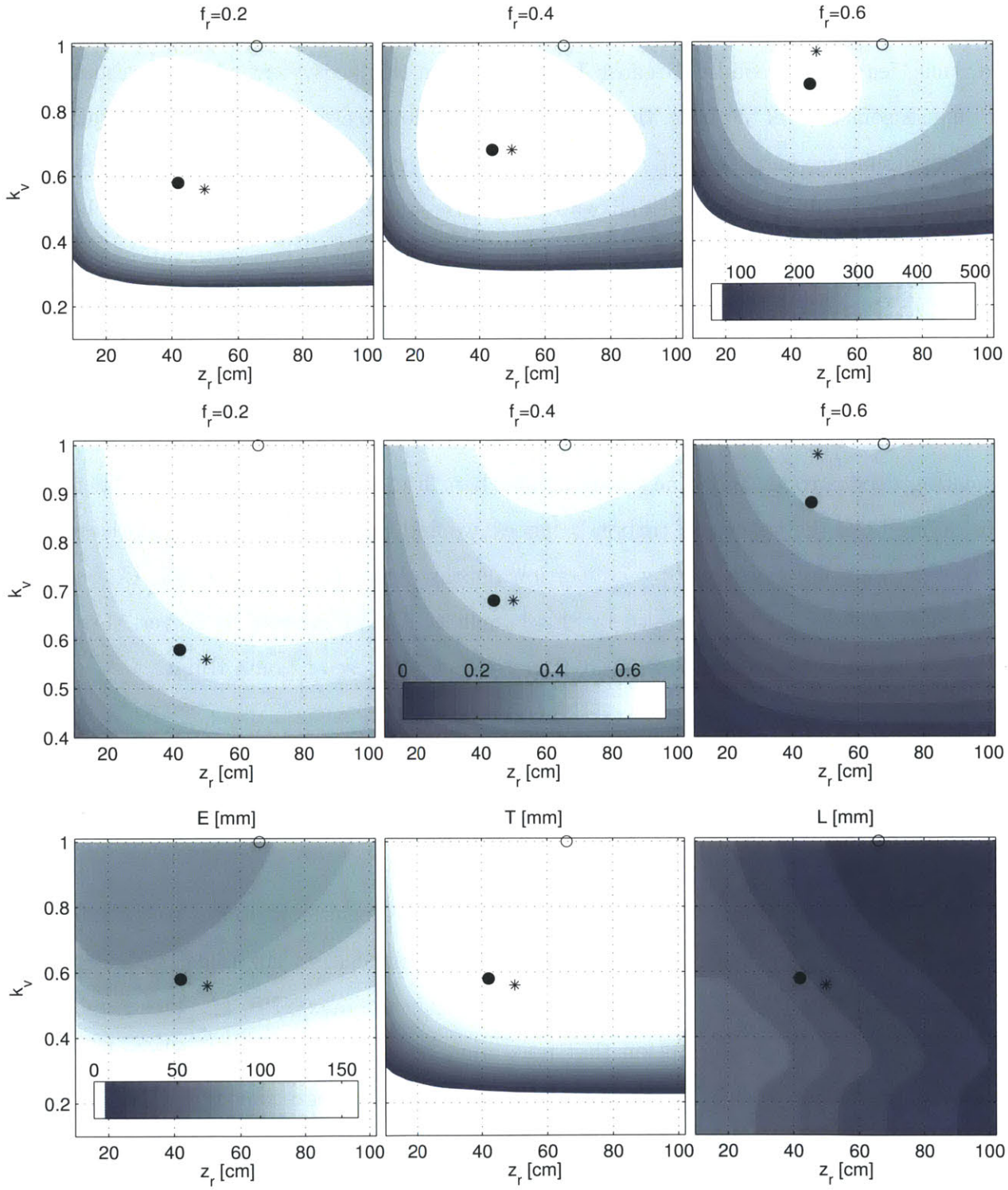

Figure 4-1: Sensitivity of productivity and the water balance to root depth and transpiration efficiency: (a) NPP [g m^{-2}]; (b) f_{green} [-]; and (c) annual water balance components E, T, and L [mm yr^{-1}]. In (c), $f_r = 0.2$. The optimal strategies are marked as follows: $T(1-\chi)$ $*$, T $\circ$, NPP $\bullet$.

Low rainfall and high evaporation rates minimize the duration of time spent above s_{fc} and, thus, leakage. Secondly, because PET is high in this ecosystem and the rainfall and growing seasons are out of phase, the ratio of transpiration to evaporation is strongly affected by canopy shading and, thus, f_r. When f_r is low, a dense canopy develops quickly and evaporation is limited. The optimal water use strategy is therefore the strategy that (a) builds the largest canopy in the shortest time possible to limit bare soil evaporation and (b) transpires at a rate high enough to limit leakage, but low enough to extend the growing season and delay the onset of water stress. The difference between the unconstrained and constrained max[T] z_r^* suggests that condition (a) outweighs the benefit of increased z_r in terms of water access. That is, the unconstrained z_r^* is deeper than the constrained z_r^*, indicating deeper roots aren't necessarily more beneficial than a larger canopy. Therefore, considering both the water and carbon balances, we find that shallow rooting depths in arid ecosystems may not be driven by infiltration depths alone [*Laio et al.*, 2006; *Collins and Bras*, 2007; *Schenk*, 2008], but also by this benefit of canopy growth. However, this effect may only be important for fully vegetated plots, such as those at Loma Ridge.

The difference between the max[T] and max[NPP] strategies contributes to the interpretation of the aforementioned studies. In the unconstrained case, the max[T] z_r^* is deeper than the max[NPP] z_r^* and the max[T] k_v^* is larger than the max[NPP] k_v^*. This result calls into question the broad assumption that maximum transpiration is a suitable indicator of maximum reproductive success. However, the max[NPP] strategy converges to the max[T] strategy as f_r increases. Therefore, it may be that max[T] is a reasonable assumption in arid climates where below-ground structures are larger relative to above-ground structures [*Schenk and Jackson*, 2002b]. In the constrained case, the max[T] and max[NPP] z_r^*'s are more similar, but the difference in k_v^* remains. Thus, a max[T] assumption may be adequate for predicting z_r when coupled with the carbon cost of building roots, but the resulting T, LAI, and k_v are expected to be less accurate at least at sub-annual time-scales.

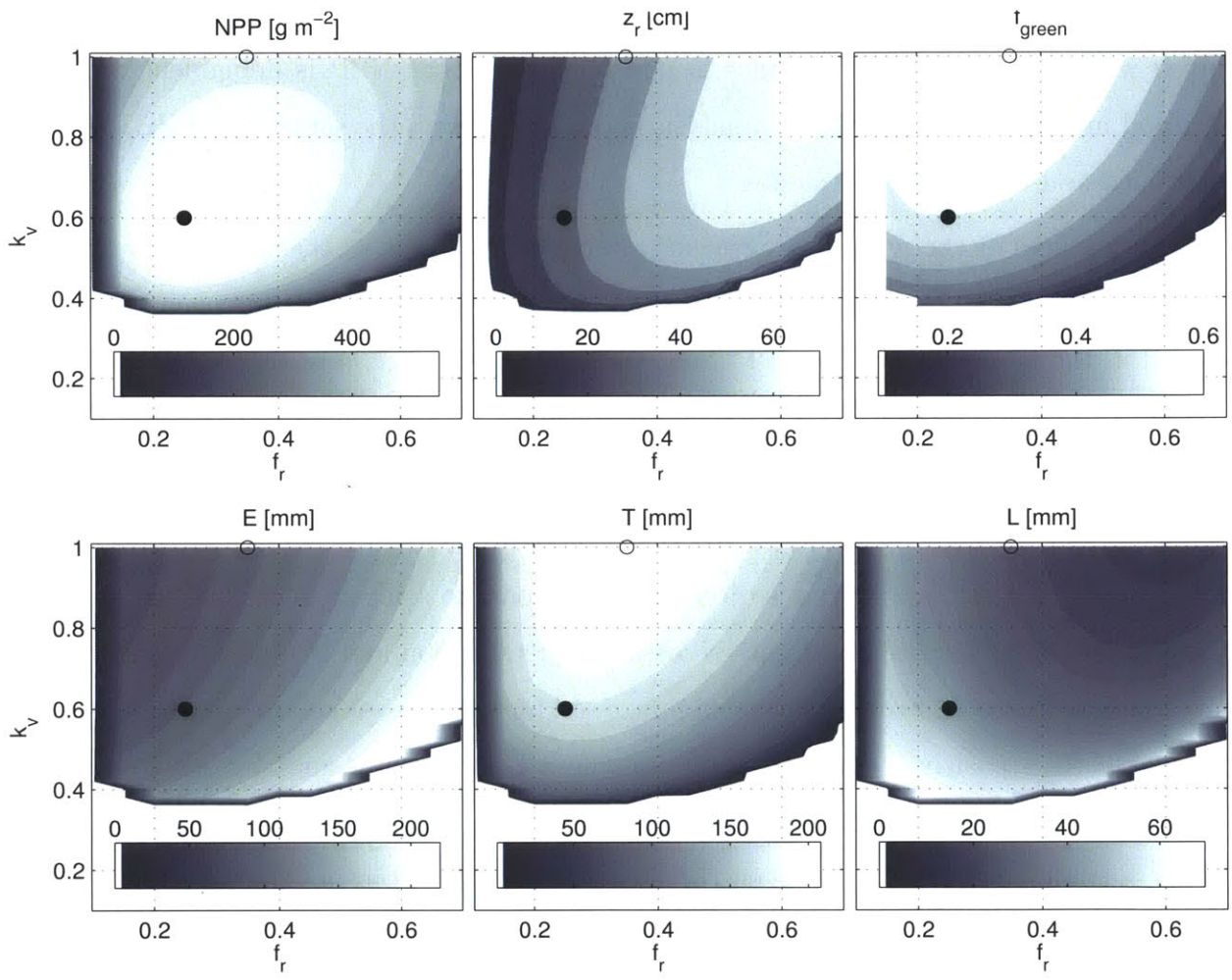

Figure 4-2: Sensitivity of productivity and the water balance to root allocation fraction and transpiration efficiency: (a) NPP [g m^{-2}]; z_r [cm]; and f_{green} [-]; and (b) annual water balance components E, T, and L [mm yr^{-1}]. The optimal strategies are marked as follows: $T(1-\chi)$ $*$, T $\circ$, NPP $\bullet$. The max[NPP] and max[T(1-χ)] strategies are equivalent.

4.1.3 Ecosystem processes and the optimal water-nitrogen use strategy

Extending the analysis of section 4.1.2, the second resource use strategy considered is that which optimizes plant function with respect to water and nitrogen availability. The fully coupled water-carbon-nitrogen balance is now solved, so that NPP is dependent on both water and nitrogen availability. The analysis is conducted with the same P and PET and in constrained and unconstrained modes.

Many features of the water-nitrogen use strategy are similar to the water use strategy. First, as expected, the max[T] strategy does not change when a dynamic nitrogen balance is included in the model. The max[NPP] and max[T(1-χ)] strategies are slightly deeper than in the water-only case, but show the same relationship to the max[T] strategy.

Figure 4-3 also demonstrates how each strategy is related to the coupled water and nitrogen balances. With respect to leakage, the water and nitrogen use strategies are equivalent. Because nitrogen loss via leaching is directly proportional to soil water loss via leakage, any strategy that limits leakage also limits N losses. Mineralization and N uptake, on the other hand, are maximized at strategies that minimize soil moisture losses and maximize soil moisture, due to their positive response to soil moisture. This indicates an interesting potential competition/mutualism dynamic between plant and microbes, modulated by soil moisture. That is, a trade-off may exist between the growth benefits of transpiration and the benefit of maintaining soil moisture to support microbial activity and mineralization, which also stimulates productivity. Note, however, that uptake decreases sharply at low k_v as transpiration decreases. Also, in wetter climates where soil moisture spends a large amount of time above field capacity, mineralization will decrease with increasing soil moisture, implying the opposite conclusion.

Although Figure 4-4 confirms several of the previous conclusions from the water-only analysis, the strategy can now be interpreted as one that simultaneously addresses the costs and benefits of water and nitrogen acquisition. Specifically, the intermediate value of k_v is not only beneficial for balancing transpiration and water stress, but also increases N availability and, thus, NPP. Therefore, the optimal water-nitrogen use strategy is the strategy that (a)

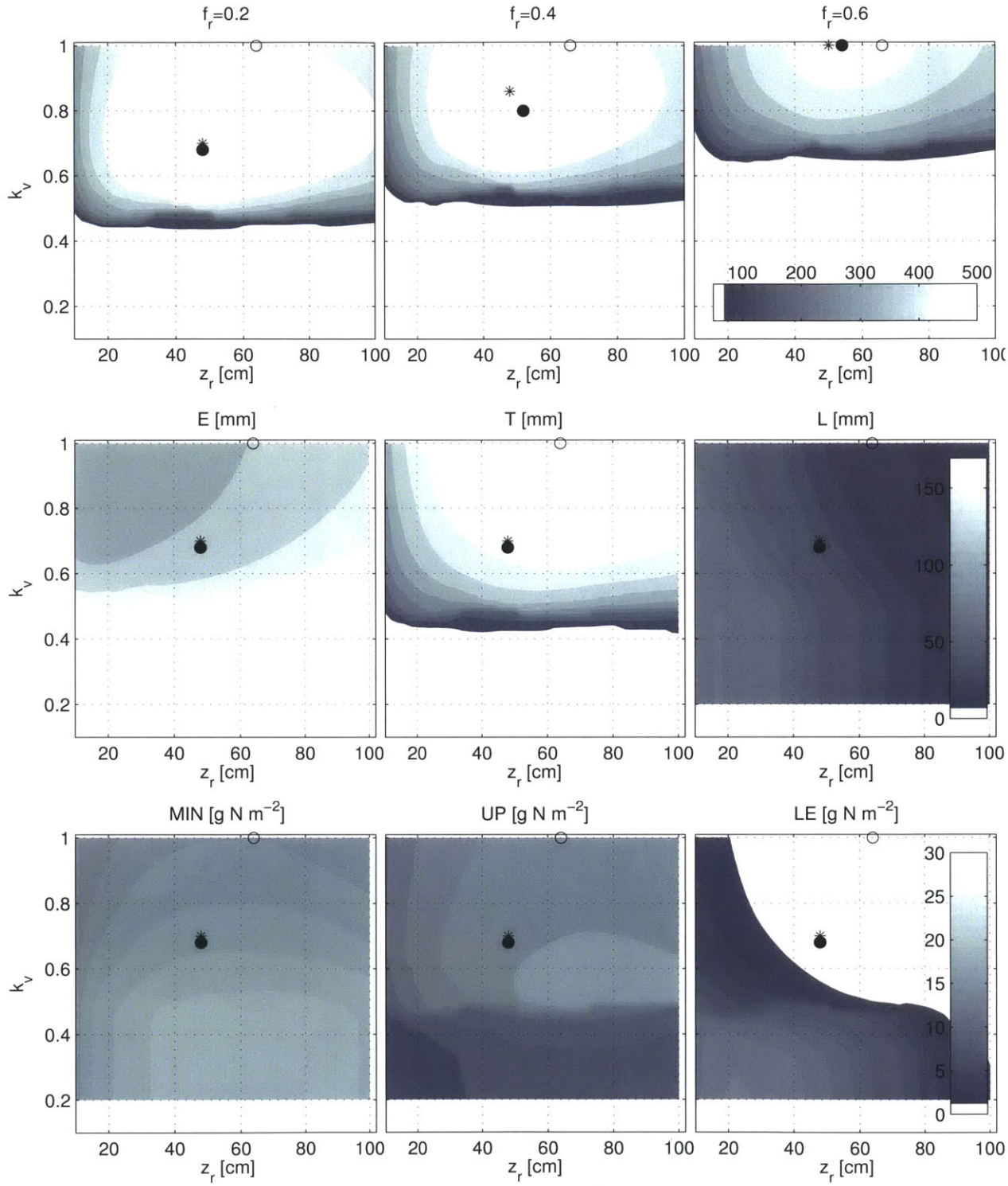

Figure 4-3: Sensitivity of the carbon, water, and nitrogen balances to root depth and transpiration efficiency: (a) NPP [g m^{-2}]; (b) annual water balance components [mm yr^{-1}]; and (c) annual nitrogen balance components [g N m^{-2} yr^{-1}]. In (b) and (c), $f_r = 0.2$. The optimal strategies are marked as follows: $T(1-\chi)$ $*$, T $\circ$, NPP $\bullet$.

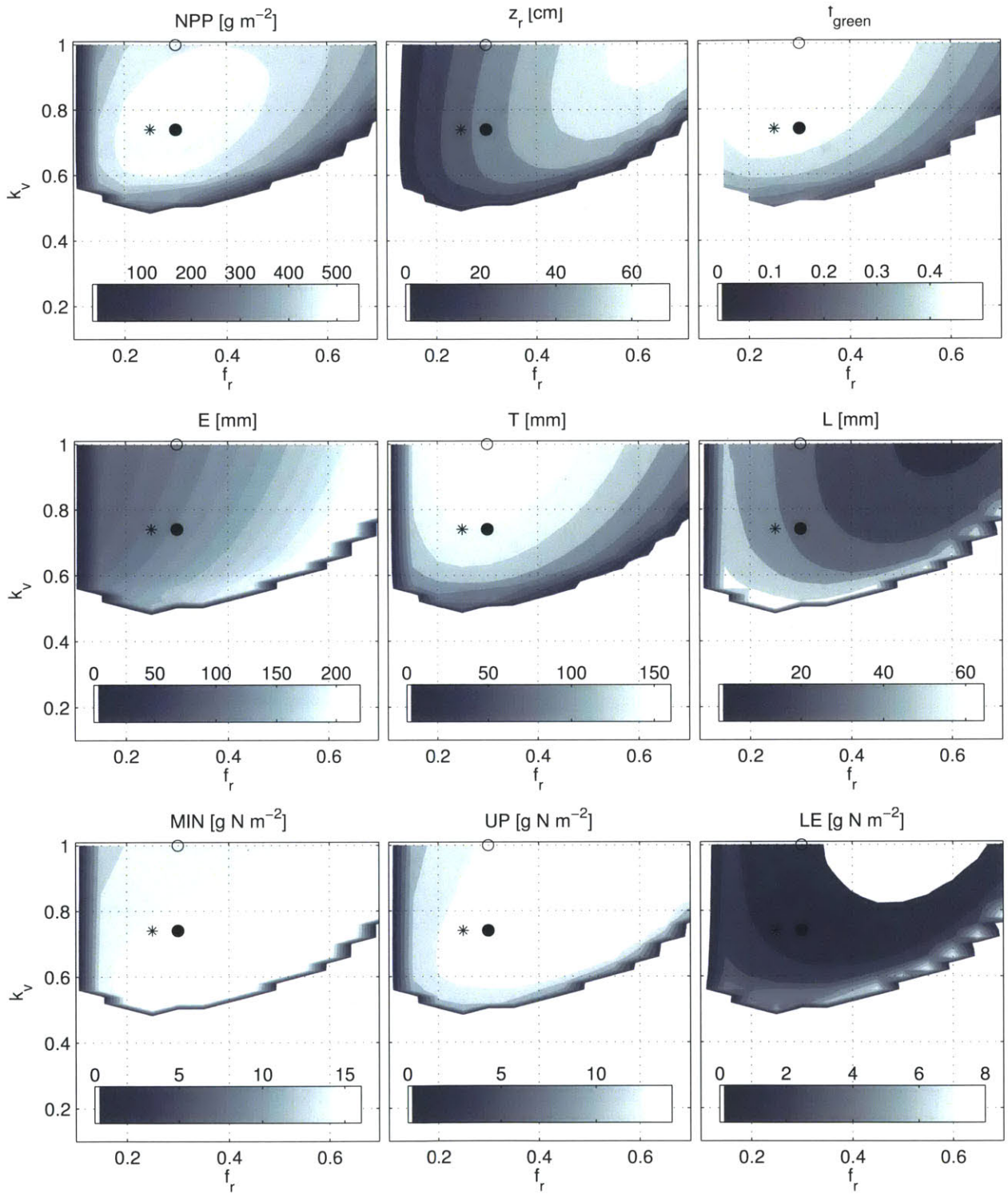

Figure 4-4: Sensitivity of the carbon, water, and nitrogen balances to root allocation fraction and transpiration efficiency: (a) NPP [g m^{-2}]; z_r [cm]; and f_{green} [-]; (b) annual water balance components [mm yr^{-1}]; and (c) annual nitrogen balance components [g N m^{-2} yr^{-1}]. The optimal strategies are marked as follows: $T(1-\chi)$ $*$, T $\circ$, NPP $\bullet$.

builds the largest canopy in the shortest time possible to limit bare soil evaporation and (b) transpires at a rate high enough to limit leakage, but low enough to maintain adequate moisture conditions for N production and uptake and to extend the growing season to delay the onset of water stress. The variability of this strategy with climate and soil fertility is addressed in the next section.

4.2 Resource use strategy sensitivity to environmental parameters

The optimal resource use strategies calculated with the above procedure are sensitive to the parameters that define the environment experienced by the vegetation. The resource environment that interacts with the resource use strategy is defined by climate (i.e. P and PET), soil fertility (k_{min}), and external N input (N_{dep}). This section demonstrates the model sensitivity to each of these parameters and identifies the climate and soil regimes under which either water or nitrogen can be considered the primary control on ecosystem rooting depth.

4.2.1 Hypothetical resource supply gradients

For this analysis, the model is forced with several combinations of water and nitrogen supply rates. Water availability is defined by the aridity index, $\phi = E_p/P$ [*Budyko*, 1986]. Several values of ϕ are generated by varying E_p and P independently according to the following ranges: $750 < E_p < 1300$ [mm yr^{-1}] and $160 < P < 1300$ [mm yr^{-1}], giving $0.5 < \phi < 8$. Time-series of E_p are generated by scaling the climatic mean at Loma Ridge (i.e. equation 3.13). Time-series of P are generated by scaling a single 30-year stochastic realization according to annual precipitation values sampled from a log-normal distribution with the assumed mean and the variance as calculated from the Loma Ridge record. Nitrogen availability is defined by k_{min} and N_{dep}, which are assumed to fall in the following ranges: $5 < k_{min} < 30$ [g N m^{-2}] and $4 < N_{dep} < 60$ [kg ha^{-1} yr^{-1}]. Therefore, the modeled ecosystem is subject to conditions of high and low water and nitrogen availability.

Similar to Section 4.1.3, this analysis is conducted in unconstrained and constrained modes. When the underlying environmental template is varied independently of the plant growth parameters, these assumptions take a specific meaning. In the unconstrained case,

the results below represent the optimal rooting depth for the given environment for any plant functional type. The constrained case, on the other hand, represents the rooting strategy of annual grasses as parameterized for Loma Ridge, if they were placed in the assumed environment. Because plant functional types vary predictably with climate and soil fertility [*Whittaker*, 1975; *Craine et al.*, 2002], and annual grasses are not competitive in every environment, the unconstrained case is likely to provide a better picture of how rooting depths vary with water and nitrogen availability across soil resource gradients. Results from the constrained case, on the other hand, may be interpreted as an indicator of changes that may be expected at Loma Ridge in response to environmental changes.

It is important to note that this analysis includes the seasonality characteristic of seasonally-dry ecosystems. Annual grasses and drought-deciduous shrub species, such as those found at Loma Ridge, are active during a distinct growing season that begins at the onset of winter rains and ends early in the summer as solar radiation, soil water deficit, and temperature increase [*Schoenherr*, 1995]. This characteristic is represented in the model via two mechanisms. First, the mortality term depends on water stress, therefore carbon losses increase during the dry, latter part of the year. Second, the growing season is artificially limited by a threshold of 170 days [*Istanbulluoglu et al.*, 2011], which accounts for the fact that temperatures exceed those favorable for growth during the summer, without explicitly modeling temperature. Therefore, the results and interpretation presented below are only applicable to plant functional types that are unable to grow during the summer.

4.2.2 Root depth and resource supply rates

Across a wide range of N_{dep} and k_{min} values, z_r^* exhibits a peak with respect to ϕ (Figure 4-5) and P (Figure 4-6). z_r^* increases with increasing aridity when $\phi < 3$ and decreases with increasing aridity when $\phi > 3$. The value of ϕ that maximizes z_r^* decreases as the total N supply increases, while the sensitivity of z_r^* to ϕ increases. When N supply is high, z_r^* increases with P for $P < 500$ [mm yr^{-1}] and decreases for $P > 500$ [mm yr^{-1}]. As N supply decreases, the value of P that maximizes z_r^* decreases. These model simulations suggest two general climatic regimes that govern variability in z_r^* – rooting depths increase with aridity in wet climates and decrease with aridity in dry climates. N supply does not influence the

existence of these regimes, but does influence the boundary between them and the range of z_r^*.

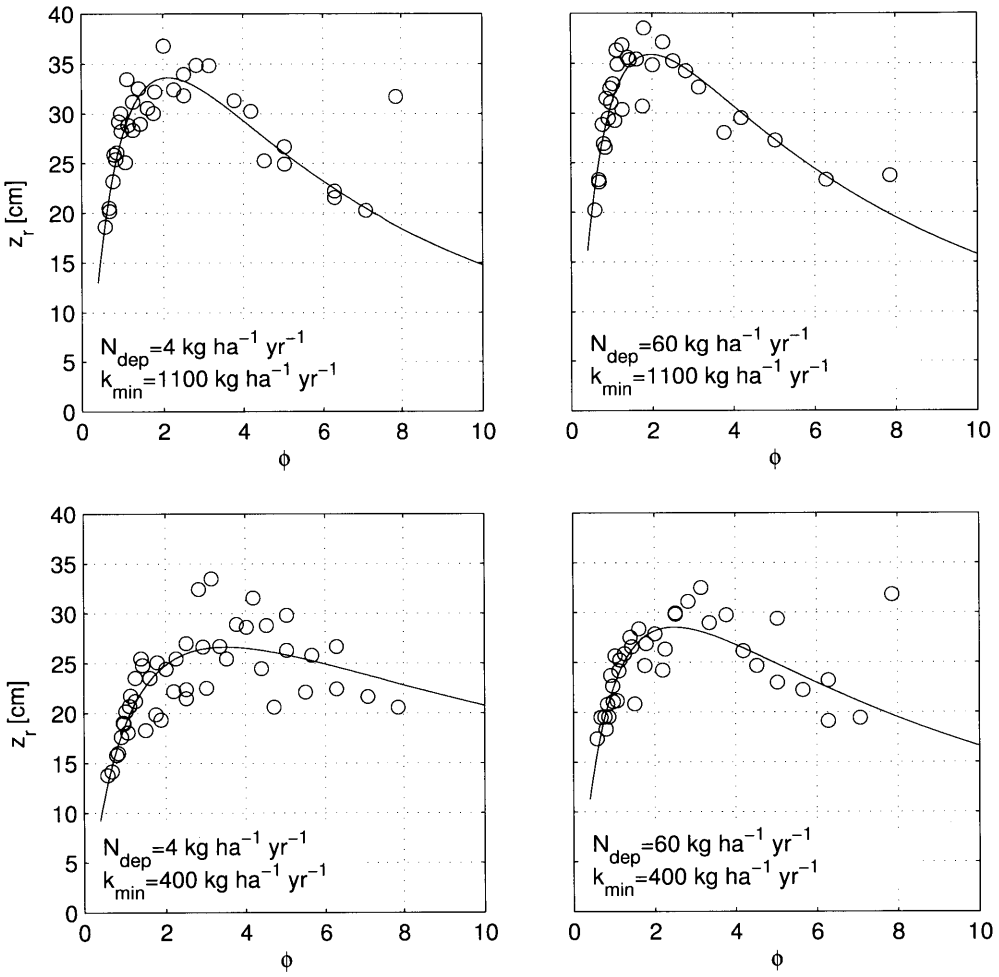

Figure 4-5: Sensitivity of the optimized root depth to environmental parameters ϕ, k_{min}, and N_{dep}. The open symbols correspond to several simulations where these three parameters were varied and the solid line denotes a lognormal function fit by minimized sum square error. The panels are arranged according to increasing N_{dep} (left to right) and k_{min} (bottom to top). $f_r = 0.2$ for all simulations.

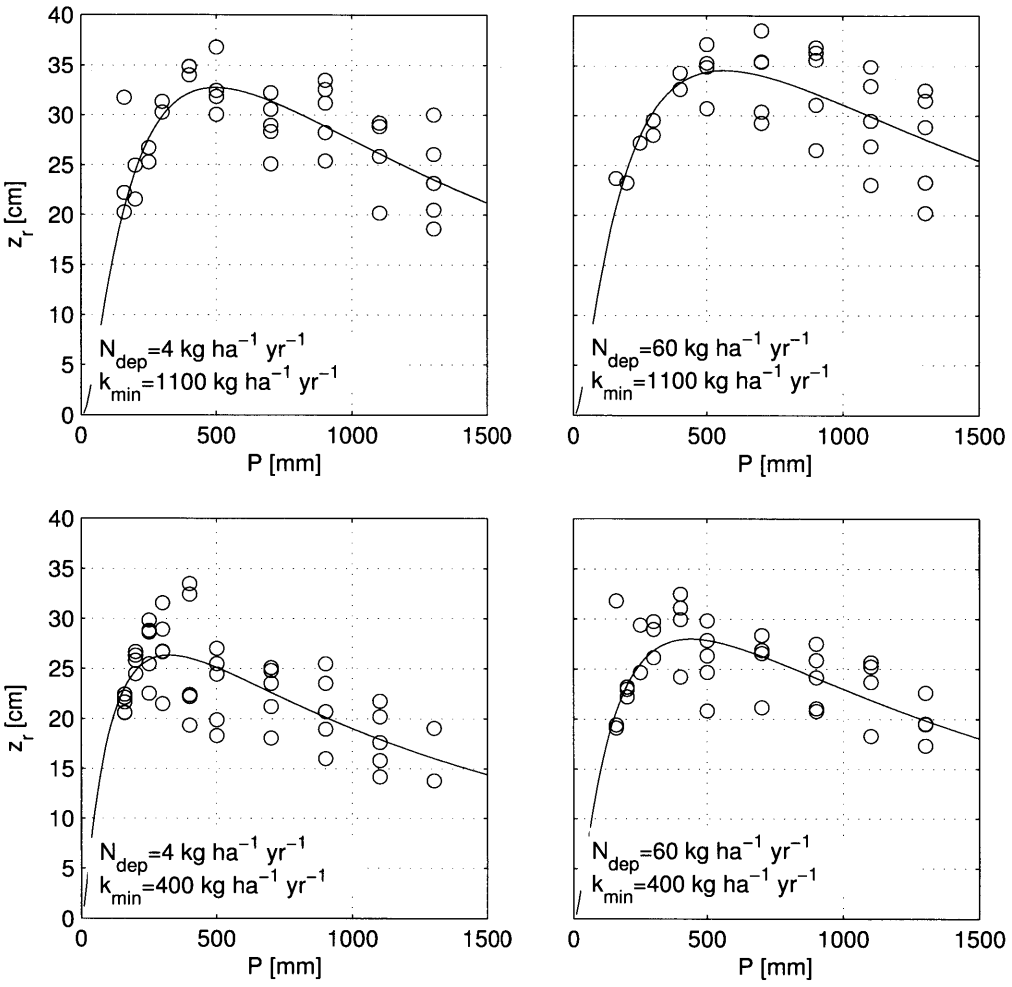

Figure 4-6: Sensitivity of the optimized root depth to environmental parameters P, k_{min}, and N_{dep}. The open symbols correspond to several simulations where these three parameters were varied and the solid line denotes a lognormal function fit by minimized sum square error. The panels are arranged according to increasing N_{dep} (left to right) and k_{min} (bottom to top). $f_r = 0.2$ for all simulations.

The two z_r^* regimes are associated with varying degrees of resource use efficiency. Efficient use of the water balance is represented by f_{green} and efficient use of the nitrogen balance is represented by the fraction of nitrogen supply (either through mineralization or deposition) captured by the vegetation, or $f_{up} = \frac{UP}{MIN+N_{dep}}$. In arid climates ($\phi = 5$, solid lines in Figure 4-7), there exists an intermediate z_r that maximizes f_{green} and a similar, but deeper z_r that maximizes f_{up}. In humid climates (dashed lines), however, f_{green} increases monotonically

with z_r, indicating the most hydrologically efficient strategy is the deepest strategy attainable by the ecosystem. While f_{green} exhibits a single maxima, f_{up} is maximized at both a shallow and a deep z_r. Therefore, in humid climates, either the most shallow or the most deep strategy represents efficient use of the nitrogen cycle at the expense of inefficient use of the water cycle. The peak z_r^* in Figures 4-5 and 4-6 may then indicate the climate at which the optimal strategy shifts between water control and nitrogen control. The existence of multiple optima in the $f_{up} - z_r$ curve also suggests that nitrogen availability is an important factor in the coexistence of shallow rooted annual grasses and deeper rooted perennial grasses and shrubs at Loma Ridge.

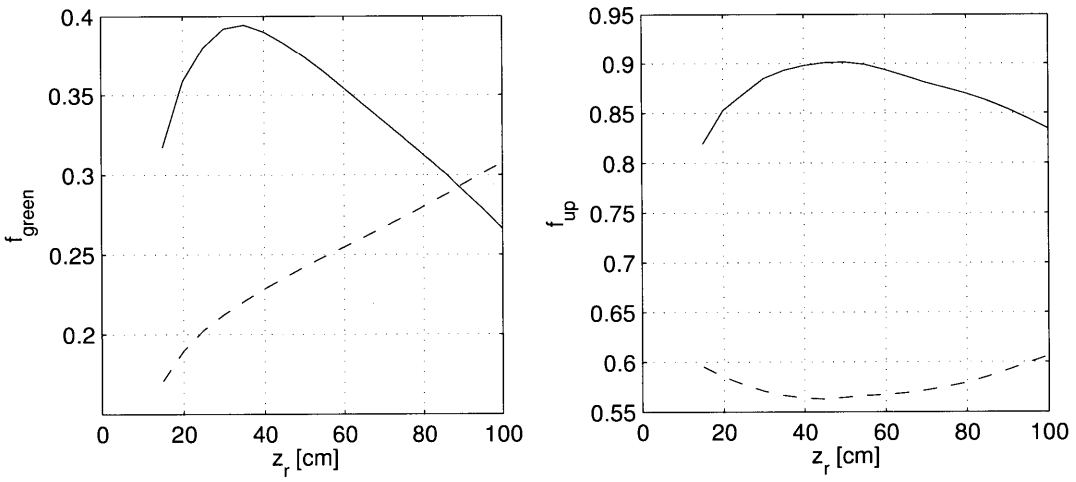

Figure 4-7: Sensitivity of resource use efficiencies to root depth: (a) green water and (b) nitrogen uptake fraction. The solid lines denote results for $\phi = 5$ and the dashed lines for $\phi = 1$.

The water and nitrogen balances subject to z_r^* are plotted in Figure 4-8. Increased humidity has little effect on E, but is associated with substantial increases in T, L, and R. Along the same gradient, NPP increases monotonically. Therefore, although a larger fraction of the water balance is partitioned to "blue" water, T and NPP still show a positive response to increased water availability. Nitrogen production and leakage losses also increase with humidity, while nitrogen uptake shows a single mode at an intermediate value of ϕ. Interestingly, when combined with Figure 4-5, it is found that z_r^* scales most directly with nitrogen uptake (Figure 4-9).

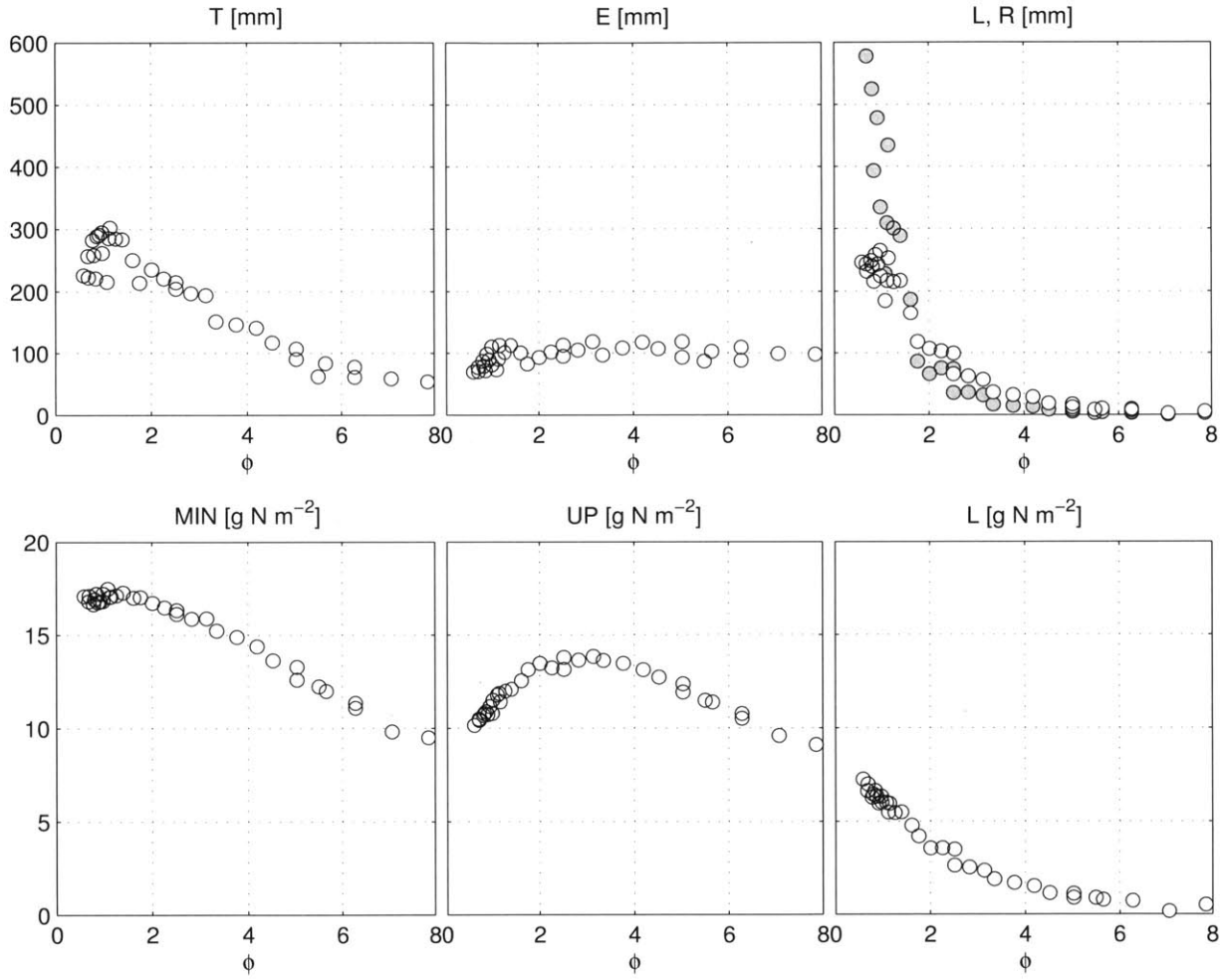

Figure 4-8: Sensitivity of ecosystem processes to aridity index: (a) water balance (E, T, L, and R) and (b) nitrogen balance (MIN, UP, L_n).

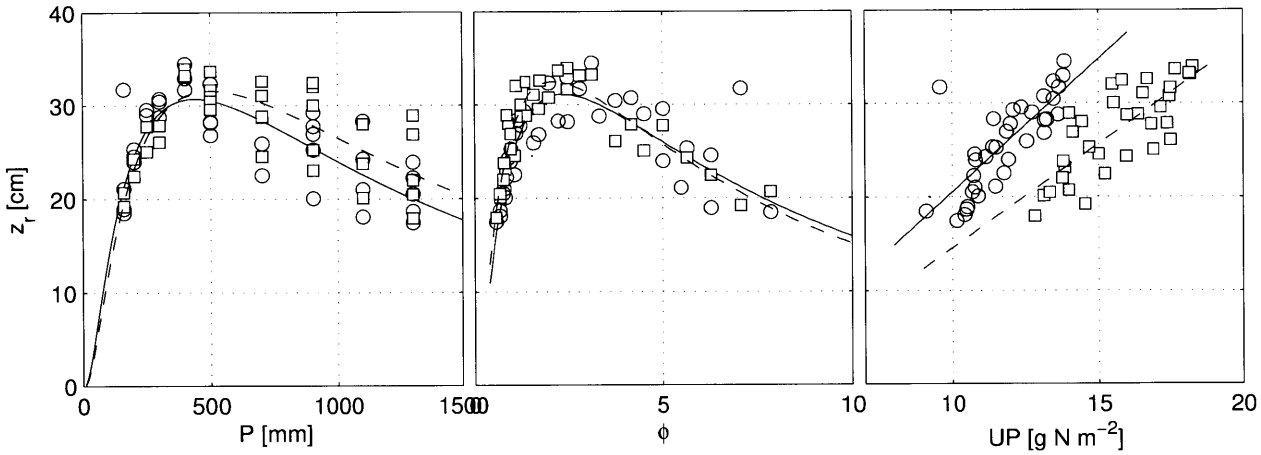

Figure 4-9: Scaling of z_r with varying measures of resource availability: (a) rainfall, (b) aridity index, and (c) nitrogen uptake. The circles and solid lines correspond to $N_{dep} = 4$ [kg ha^{-1} yr^{-1}] and the squares and dashed lines correspond to $N_{dep} = 60$ [kg ha^{-1} yr^{-1}]. $k_{min} = 0.1$ [g N m^{-2} d^{-1}].

The strong relationship between the max[NPP] z_r^* and UP is consistent with the physical and biochemical controls on nitrogen uptake. Nitrogen must first be mineralized, which requires a suitable soil moisture level for microbial activity. Then, mineralized nitrogen is either acquired through the transpiration stream, or via diffusion through soil pores to the root surface – both processes that depend on soil moisture. Indeed, the model formulation of uptake is,

$$UP = a\frac{T(s)}{snz_r}N_s + a\frac{Fs^d}{snz_r}N_s \tag{4.4}$$

This understanding of the basic uptake processes demonstrates how nitrogen uptake embeds information from both the water and nitrogen balances. This would support the idea that water-limited ecosystems are "water-limited" primarily due to the restrictions low soil moisture places on nitrogen availability [*Craine*, 2009].

4.2.3 Root biomass allocation and resource supply rates

When z_r is constrained by the carbon cycle and the resource use strategy is defined in terms of f_r, many of the above conclusions are confirmed and additional plant-resource patterns emerge. In the constrained case, the sensitivity of f_r^* to climate and fertility is much more evident than that for z_r^*. Across a wide range of ϕ values, f_r^* very clearly scales linearly with ϕ (Figure 4-10). The $f_r^* - \phi$ slope depends on the nitrogen supply rate. As N supply increases, either through increased k_{min} or increased N_{dep}, f_r^* and its slope with ϕ decrease. f_r^* also exhibits a very predictable relationship with P (Figure 4-11) that is less sensitive to N supply. This would seem to suggest a strong role of evaporation in the optimal strategy.

In the constrained case, the sensitivity of z_r^* to ϕ and P are similar to those for the unconstrained case. That is, a peak z_r^* is found to occur at an intermediate level of aridity and the sensitivity of z_r^* to climate is increased with increasing N supply. However, there is much more scatter in the constrained case than in the unconstrained case (Figures 4-12 and 4-13).

Finally, the variability of f_r^* and z_r^* with P confirms the synthetic study of *Schenk and Jackson* [2002b], who concluded from a dataset restricted to $P < 500$ [mm]: "... relative rooting depths tended to increase with aridity, although absolute rooting depths decreased with aridity." f_r^* decreases with P, but z_r^* increases with P. That is, the relative amount of carbon allocated below-ground is lower in wet climates as compared to dry climates, but the absolute rooting depth is greater (at least when $P < 750$ mm).

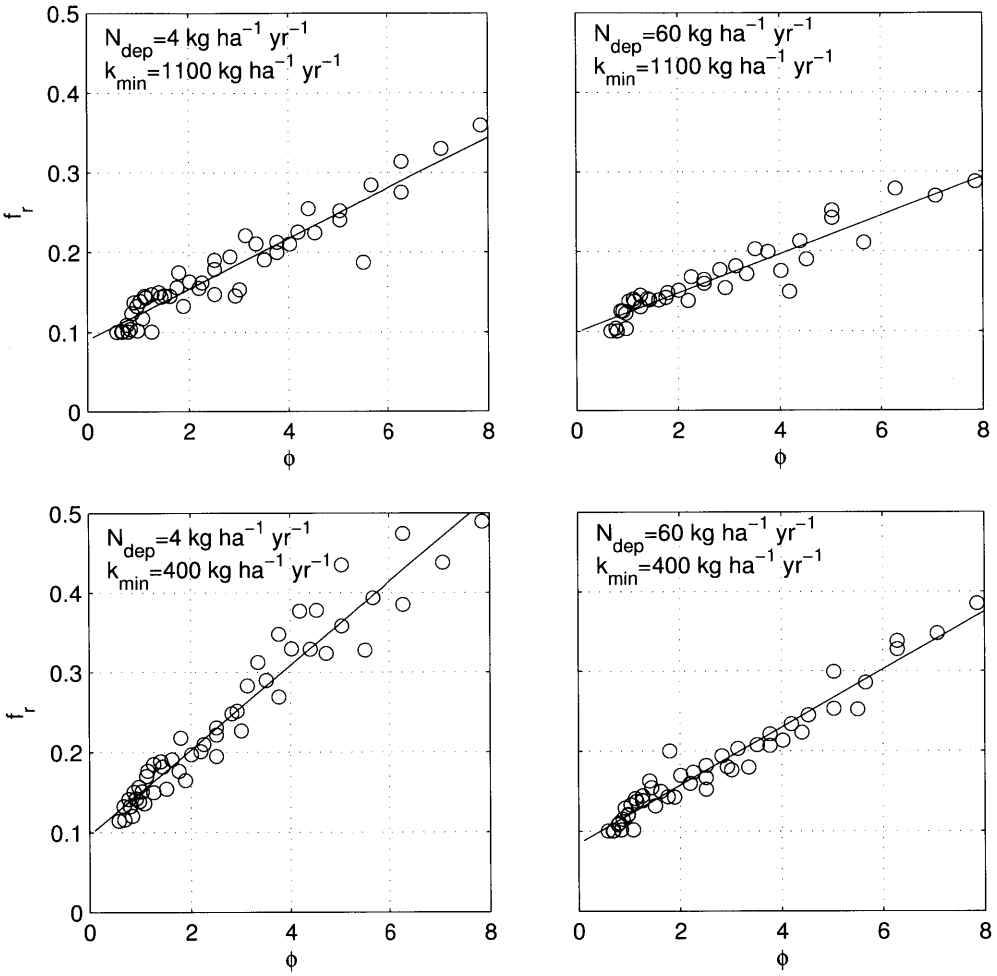

Figure 4-10: Sensitivity of the optimized root biomass allocation fraction to environmental parameters ϕ, k_{min}, and N_{dep}. The open symbols correspond to several simulations where these three parameters were varied and the solid lines denote a linear function fit by minimized sum square error. The panels are arranged according to increasing N_{dep} (left to right) and k_{min} (bottom to top).

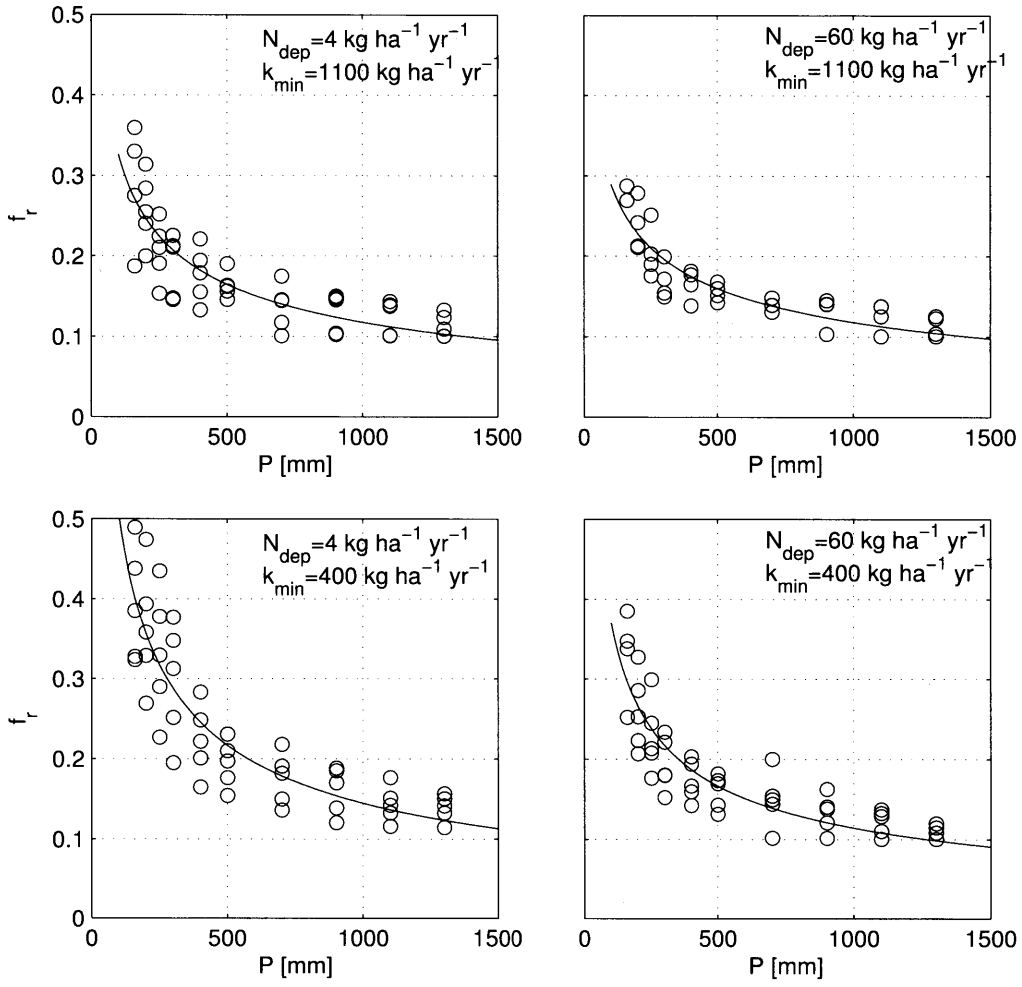

Figure 4-11: Sensitivity of the optimized root biomass allocation fraction to environmental parameters P, k_{min}, and N_{dep}. The open symbols correspond to several simulations where these three parameters were varied and the solid lines denote a log-normal function fit by minimized sum square error. The panels are arranged according to increasing N_{dep} (left to right) and k_{min} (bottom to top).

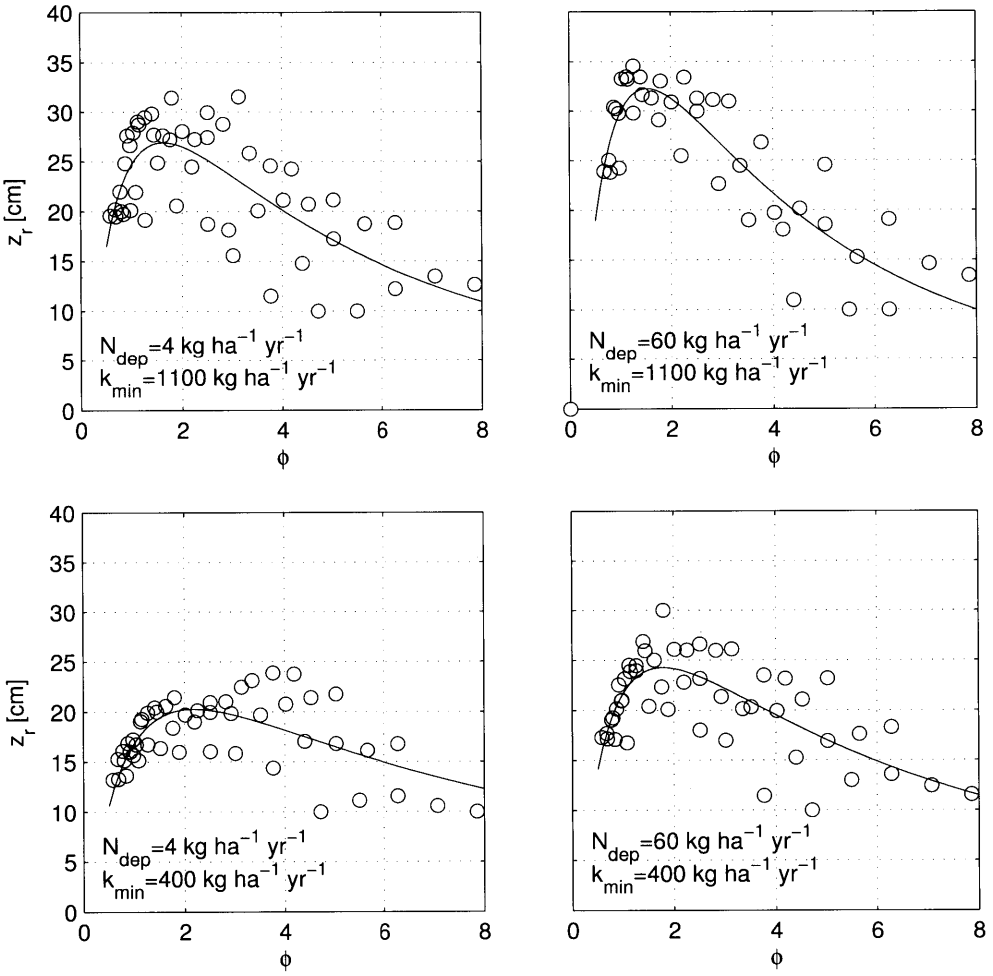

Figure 4-12: Sensitivity of the optimized root depth to environmental parameters ϕ, k_{min}, and N_{dep}. The open symbols correspond to several simulations where these three parameters were varied and the solid lines denote a log-normal function fit by minimized sum square error. The panels are arranged according to increasing N_{dep} (left to right) and k_{min} (bottom to top).

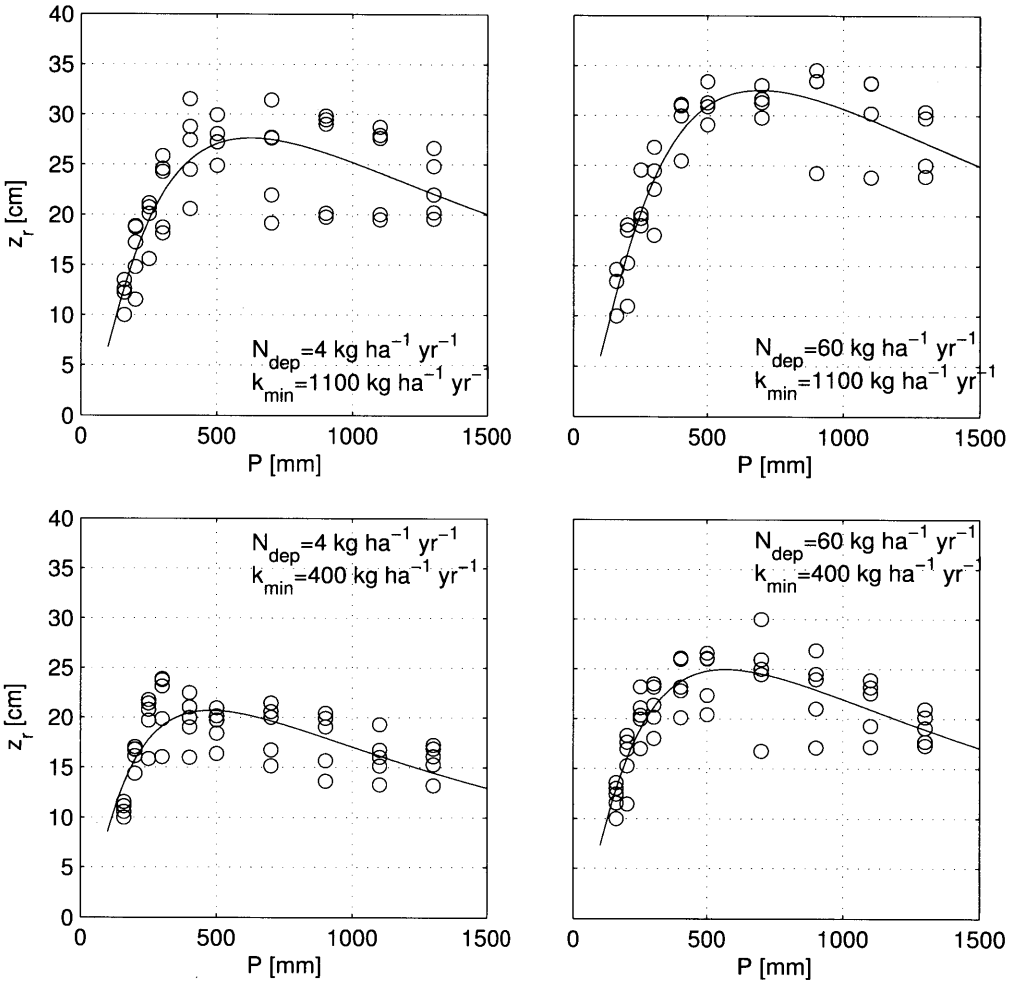

Figure 4-13: Sensitivity of the optimized root depth to environmental parameters P, k_{min}, and N_{dep}. The open symbols correspond to several simulations where these three parameters were varied and the solid lines denote a log-normal function fit by minimized sum square error. The panels are arranged according to increasing N_{dep} (left to right) and k_{min} (bottom to top).

4.2.4 Ecosystem processes in a multi-dimensional environment

Using the above data, ecosystem process rates can be estimated with respect to climate and soil fertility gradients. Figure 4-14 shows the range of f_r and z_r estimated for several values of ϕ, bounded by the highest and lowest total N supply simulated above. These N supply rates fall within the experimental N input gradient imposed at Loma Ridge and the uncertainty in k_{min} explored in Chapter 3. In the following three figures (4-15, 4-16, and 4-17), the differences in several ecosystem process rates between the high N supply and low N supply treatments are plotted. These are the water balance, the nitrogen balance, and NPP, respectively.

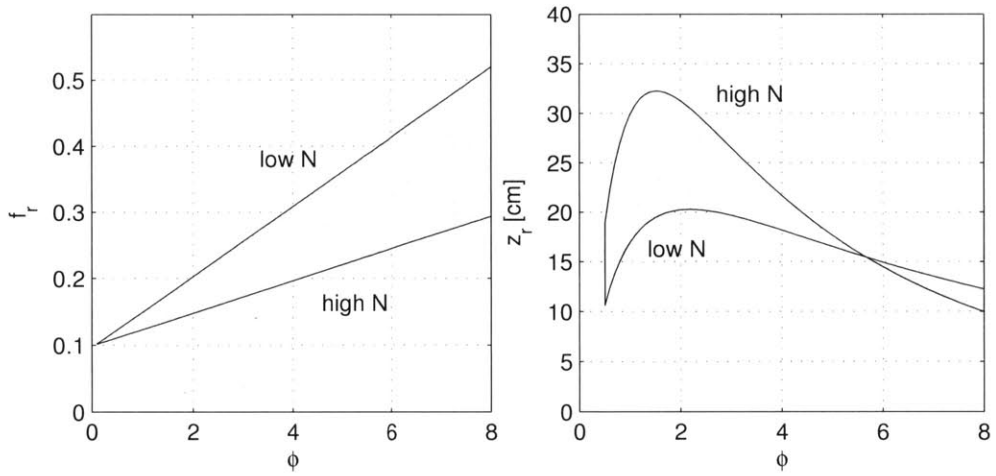

Figure 4-14: Sensitivity of the optimized resource use strategy to aridity index and nitrogen supply: (a) f_r and (b) z_r.

Estimated ET rates demonstrate two climatic regimes with respect to the hydrologic response to N fertilization (Figure 4-15). First, the N supply gradient generally decreases E and increases T and the magnitude of these changes decreases with aridity. The sum $E+T$, which is critical from a total water balance perspective, shows an interesting behavior. For arid ecosystems with $\phi > 4$, increased N supply does not change $E + T$; while for humid ecosystems with $\phi > 4$, $E+T$ increases with increasing N supply. The tight regulation of the water cycle in the arid regime indicates an organization around the efficient use of the most limiting resource which is not evident in the humid regime. $\phi = 3.7$ at Loma Ridge, which

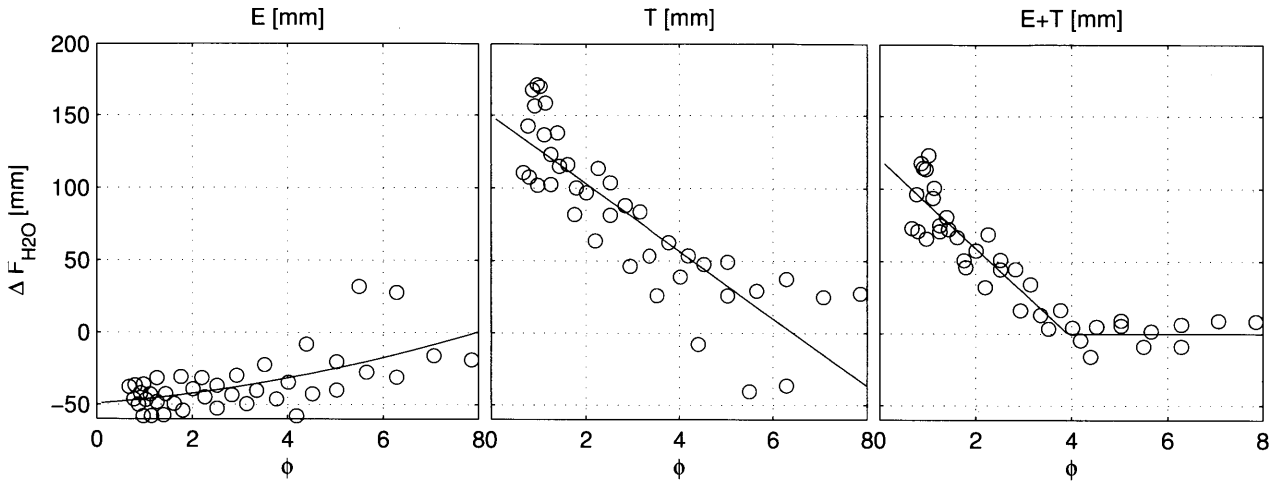

Figure 4-15: Sensitivity of the water balance to aridity index and nitrogen supply: (a) E, (b) T, and (c) $E + T$.

implies an approximate 30 mm decrease in E and 50 mm increase in T. That is, in terms of the climatic mean, the high N supply scenario produces a 6% increase in ET over the low N supply scenario. Therefore, the Loma Ridge mean annual water balance is relatively insensitive to N supply. As far as the model extrapolation is reliable, however, more humid ecosystems may be more sensitive to this level of increased N supply.

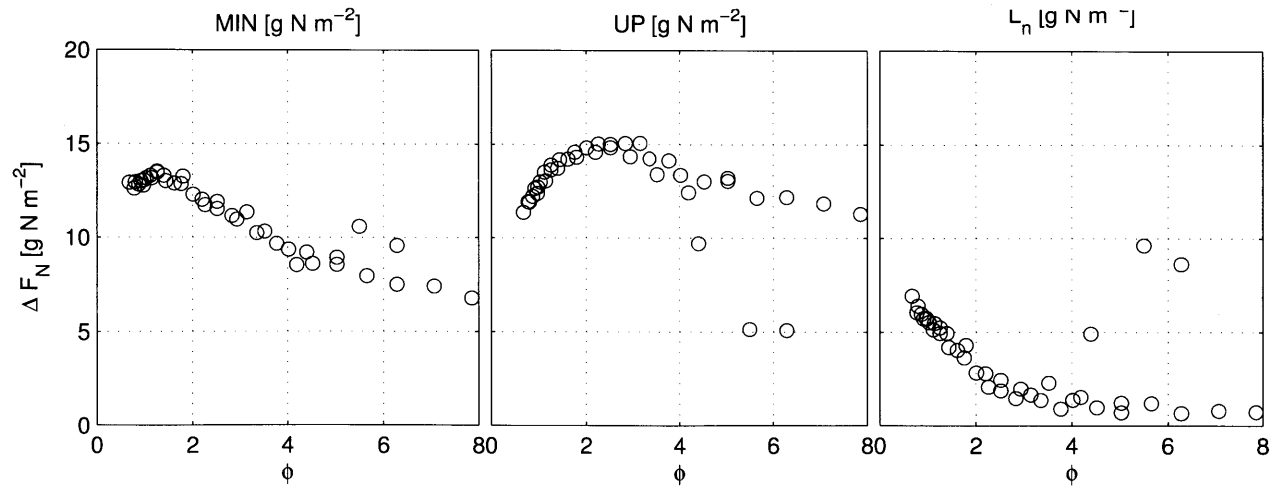

Figure 4-16: Sensitivity of the nitrogen balance to aridity index and nitrogen supply: (a) MIN, (b) UP, and (c) L_n.

Sensitivity of the nitrogen balance to increased N supply is consistent with the model assumptions and the results presented above (Figure 4-16). In general, all N fluxes increase with increased N supply. Because UP and L_n depend directly on the soil N concentration, this result is intuitive. The trend in MIN is likely related to changes in soil moisture mediated by changes in root depth. Shallow roots under humid conditions lead to elevated soil moisture levels, which stimulates MIN.

Because both nitrogen and water availability increase with decreasing aridity, NPP is shown to respond more positively to increased N supply in humid ecosystems (Figure 4-17). This result may also be related to the relative limitation of water and nitrogen to productivity at either end of the aridity gradient. When water is most limiting, the NPP response to N fertilization is restricted. However, when water is plentiful and N is most limiting, the vegetation can take full advantage of the added N.

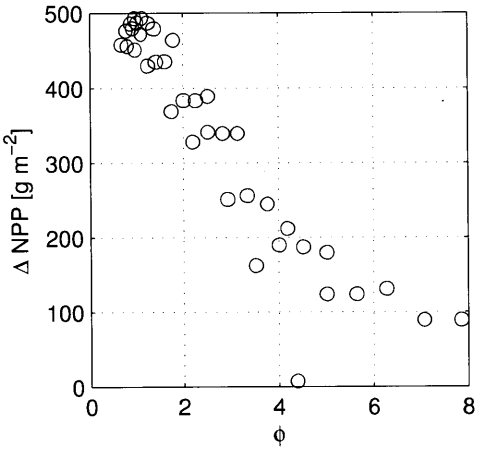

Figure 4-17: Sensitivity of NPP to aridity index and nitrogen supply.

4.3 Model-informed interpretation of the Loma Ridge experiment

The model and optimality hypotheses are now used to simulate the 2008 growing season at Loma Ridge to obtain a more detailed explanation for the soil moisture, LAI, and gas exchange observations presented in Chapter 2. Drawing on the results from Section 4.1.4, the following analysis treats the 2008 growing season as an isolated event, not influenced by conditions in previous years. Therefore, the environment is characterized by 2008 conditions, $\overline{P} = P_{2008}$ and $\sigma_P = 0$. This assumption is further justified by the large uncertainty in the initial condition of soil nitrogen, imposed by the fire and drought, and in the observed value of k_{min}, which may also have been influenced by the disturbance. As was noted in Chapter 3, it is recognized that previous years do influence the current year's dynamics; but it has proven difficult to include this explicitly in the model parameterization without additional observations.

Across the experimental nitrogen deposition gradient, the three optimality hypotheses result in different optimal resource use strategies, but similar variation in NPP (Figure 4-18). All hypotheses predict similar $k_v^* \sim 1$. However, the max[T(1-χ)] and max[NPP] hypotheses predicted decreasing f_r^*, whereas the max[T] strategy predicts f_r^* is not sensitive to N_{dep}. This result is consistent with Section 4.1.2 above. Because z_r depends on both f_r and NPP, the strategies predict different relationships between z_r^* and N_{dep}. max[T(1-χ)] predicts no change in z_r^*, max[T] predicts increasing z_r^*, and max[NPP] predicts decreasing z_r^*, all with increasing N_{dep}. All predicted z_r^* values fall between 19 and 26 cm.

The plant strategy optimization approach provides a more sophisticated interpretation of the Loma Ridge experiment. Comparing the predicted seasonal variability in soil moisture for control N and fertilized N conditions, the differences are well within the landscape variability observed in the experiment (Figure 4-19). This confirms the previous result that the water balance state, θ, is not sensitive to N fertilization in this ecosystem.

However, the predicted seasonal variability in water balance fluxes E and T call into question the original hypothesis that the observed consistency in θ resulted from a coordinated response of canopy structure and physiology to nitrogen fertilization that maintained a climate- and soil-controlled transpiration rate (Chapter 2). While T may have been equiv-

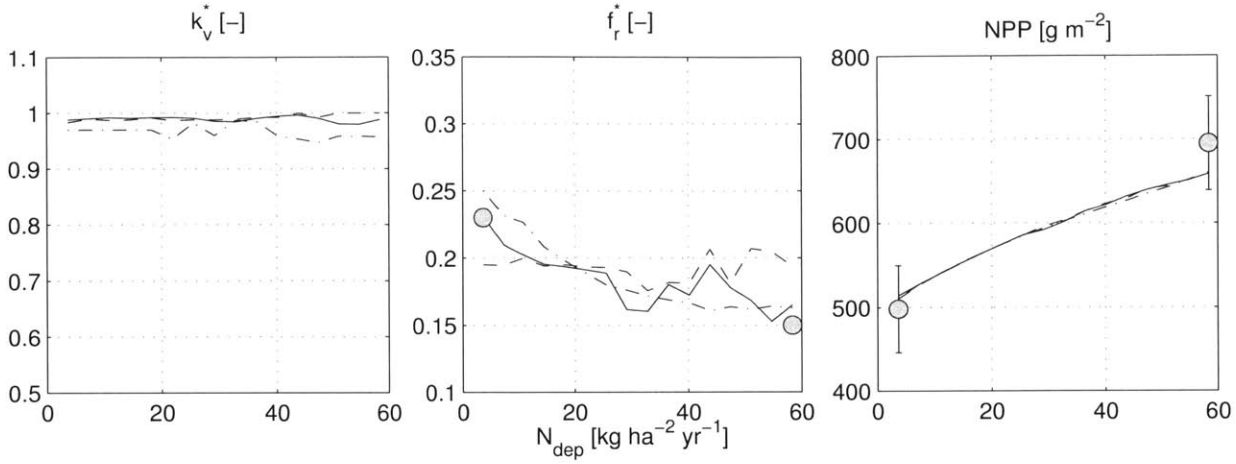

Figure 4-18: Comparison of observed and modeled ecosystem sensitivity to nitrogen deposition: (a) k_v^*; (b) f_r^*; and (c) NPP* [g m^{-2}]. The optimality assumptions are marked as follows: $T(1-\chi)$ (solid), T (dashed), NPP (dot dashed).

alent during March when the gas exchange measurements were made, this does not make any statement about T at other times of the year. This error in extrapolation is apparent in the early season predicted E and T. The model predicts N fertilization increases T and decreases E early in the season. Because these changes offset one another, the total water flux and soil moisture do not change. Late in the season, both control and fertilized plots are under similar levels of water stress and, thus, exhibit similar T, which is consistent with the observations.

Last, the modeling approach is used to estimate the sensitivity of the annual water balance for the 2008 growing season at Loma Ridge (Figure 4-21). At the annual scale, T increases from 98 [mm] to 118 [mm], while E decreases from 109 mm to 91 mm and L decreases from 15 mm to 13 mm. Therefore, over an approximate 10-fold increase in N input, T increases approximately 20% and this increase is almost entirely offset by decreased E. At the annual scale, $E+T$ is essentially constant across the experimental deposition gradient.

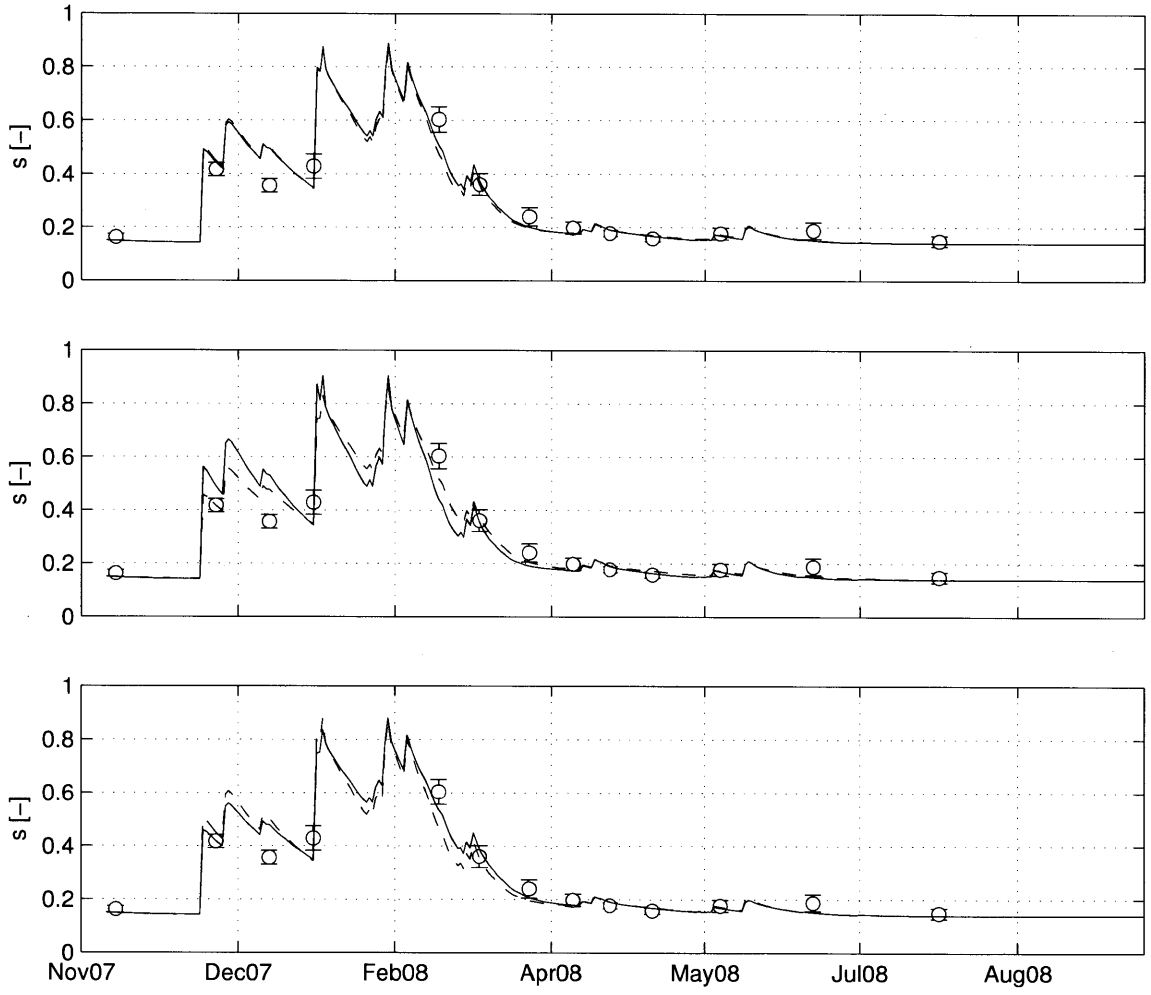

Figure 4-19: Comparison of observed and modeled soil moisture seasonality at Loma Ridge: (a) max[T(1-χ)]; (b) max[T]; and (c) max[NPP]. The solid lines denote ambient N conditions and the dashed lines denote fertilized N conditions.

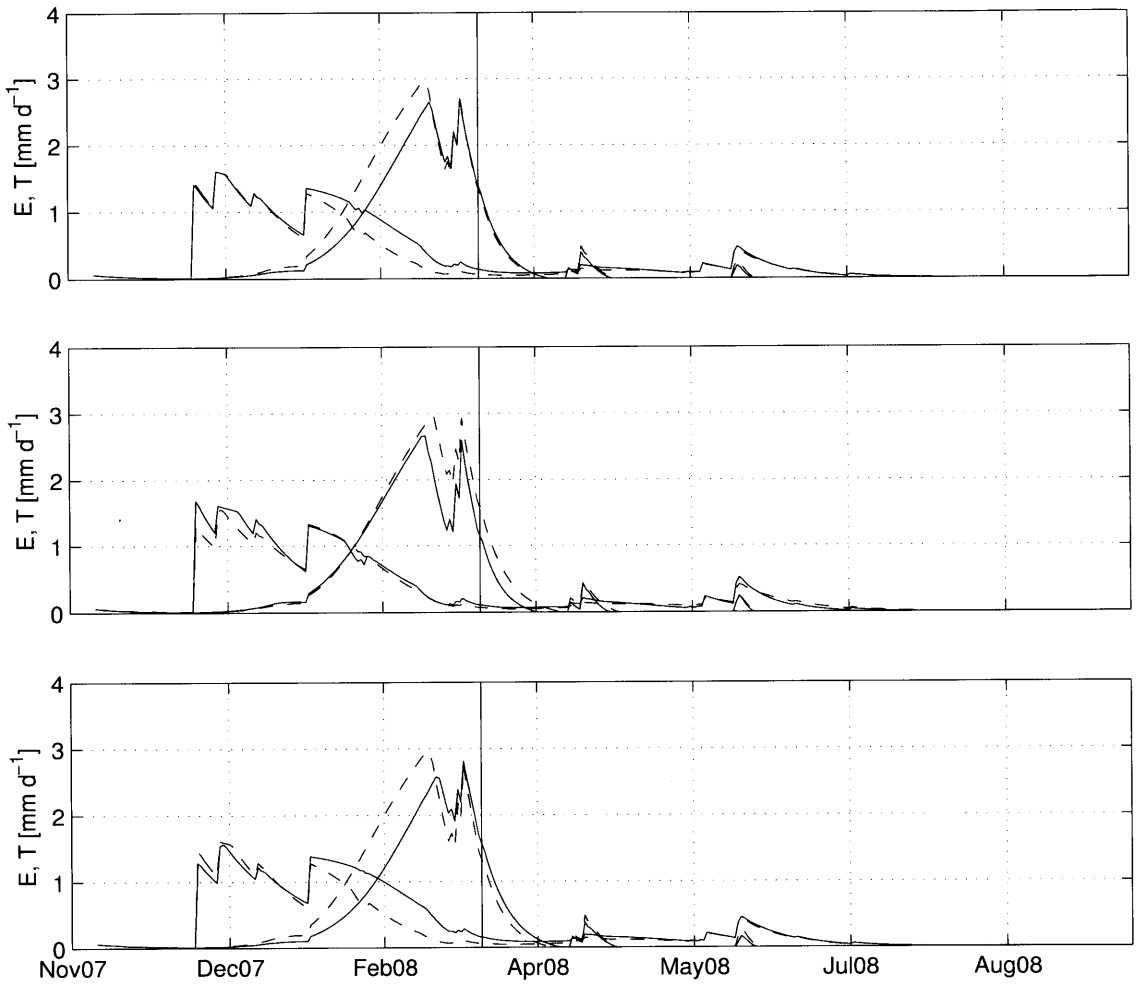

Figure 4-20: Comparison of observed and modeled water balance seasonality at Loma Ridge: (a) max[T(1-χ)]; (b) max[T]; and (c) max[NPP]. The solid lines denote ambient N conditions and the dashed lines denote fertilized N conditions. The vertical lines are drawn at 13 March, when the LAI and leaf gas exchange observations were collected.

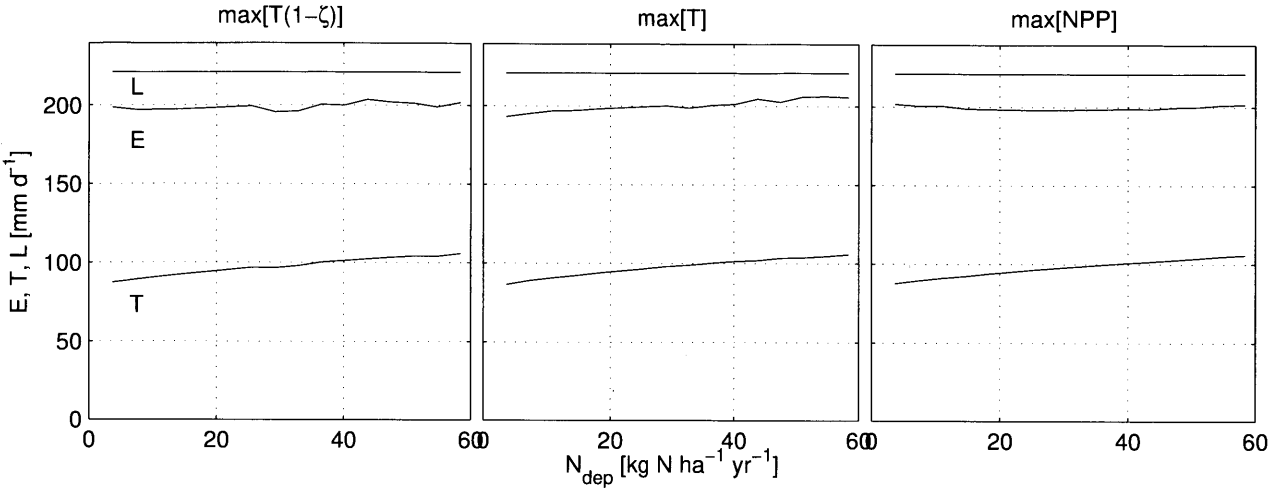

Figure 4-21: Sensitivity of the annual water balance to nitrogen deposition for conditions representative of the 2008 growing season at Loma Ridge.

4.4 Conclusions

In this chapter, an ecosystem model with coupled water, carbon, and nitrogen cycles was analyzed to estimate ecosystem responses to changes in environmental conditions controlling soil water and nitrogen availability. Several conclusions from this exercise expand our understanding of vegetation organization with their resource environments:

1. The addition of biomass allocation to the estimate of optimal rooting strategies suggests that shading achieved by canopy development is a potential driver of shallow rooting depths in arid climates.

2. The optimal root depth was shown to vary with the aridity index in two distinct climatic regimes – rooting depth increases with aridity in humid climates and decreases with aridity in arid climates. These regimes may result from a tendency toward efficient use of the most limiting resource. In arid climates, the optimal root depth is associated with a maximum hydrological efficiency, f_{green}, which also corresponds to a maximum nitrogen uptake efficiency, f_{up}. In humid climates, the optimal root depth is associated with a maximum f_{up}, but a minimum f_{green}.

3. The optimal root depth scales most directly with nitrogen uptake, a component of the model that integrates information from both ecosystem climate and fertility. The optimal biomass allocation ratio, on the other hand, scales most directly with the aridity index.

4. The optimal root biomass allocation ratio is closely related to both ϕ and P.

5. The ecosystem response to nitrogen fertilization was found to vary with aridity index in two distinct regimes. When $\phi > 4$ and water is limiting, the water balance is relatively insensitive to N supply, even though the carbon and nitrogen balances are. When $\phi < 4$, nitrogen fertilization causes increased ET, MIN, and NPP, responses which increase as ϕ decreases.

6. The model confirms the Loma Ridge observations – soil moisture is not sensitive to the N input treatment. In addition, the model predictions suggest that N fertilization increases transpiration at the expense of evaporation early in the growing season, although the total water flux remains the same.

Chapter 5

Conclusions and Future Research Prospectus

5.1 Research summary and conclusions

The primary objective of this thesis was to investigate the role of the nitrogen cycle in dryland ecohydrological systems. This objective was achieved through a synthesis of field observations and modeling. Specifically, the sensitivity of the water balance and net primary productivity to factorial water and nitrogen experimental treatments was studied for a seasonally-dry grassland. Inferences were made from estimation of the water balance using experimental observations and from application of a simple ecosystem model. The model was then extended to different climate and soil fertility conditions to study the relative controls of water and nitrogen on ecosystem processes. The results from this work offer a new perspective on the organization of dryland ecohydrological systems and illuminate several research areas where land surface studies can benefit from improved characterization of soil biogeochemical cycles.

Specific conclusions are summarized as follows:

1. When exposed to experimental water and nitrogen input gradients, water use characteristics of Loma Ridge grasses respond in a manner that is consistent with the hypothesized optimization of a theoretically derived trade-off between transpiration and water stress. NPP and LAI responded positively to nitrogen fertilization, but leaf gas exchange responded negatively. At least during the latter part of the 2008 growing season, these canopy responses offset one another, resulting in a canopy-scale transpiration rate consistent with the optimality hypothesis. The optimality hypothesis is also consistent with an increased root depth with increased water input.

2. A simple daily-scale ecosystem model coupling the water, carbon, and nitrogen cycles was developed from a physically-based sub-daily land surface model parameterization. The hydrologic controls on mineralization, uptake, and leaching were emphasized in the nitrogen cycle. The model was shown to provide an adequate description of the sensitivity of NPP to water and nitrogen supply in the Loma Ridge grassland. The model was also able to reproduce some of the observed inter-annual variability in productivity; however, there was substantial uncertainty in the initial soil nitrogen condition and the combined effect of the 2007 drought and fire.

3. The model was applied to estimate the ecohydrologic response to nitrogen fertilization observed during the 2008 growing season, under the assumption that the ecosystem responds to variability in water and nitrogen supply in a way that maximizes NPP. This assumption reproduced the observed decrease in root biomass allocation fraction, increase in NPP, and consistency in transpiration across the experimental nitrogen deposition gradient. The model also predicted a shift from evaporation to transpiration early in the season, resulting in an approximate 20% increase in transpiration in the fertilized plots, although total evapotranspiration did not change.

4. The model was subjected to hypothetical gradients of water and nitrogen supply, predicting two distinct resource use strategies for arid and humid climates. The optimized root depth decreased with aridity in arid ecosystems and increased with aridity in humid ecosystems. These strategies were shown to be associated with efficient use of the water cycle in arid climates and efficient use of the nitrogen cycle in humid climates. In all cases, root depth scaled most directly with nitrogen uptake, an ecosystem process that fully integrates both water and nitrogen availability.

5. The hydrologic response to nitrogen fertilization was shown to coincide with the two climatic regimes. In arid, water-limited ecosystems (i.e. $\phi > 4$), nitrogen fertilization has very little effect on total evapotranspiration. In humid, nitrogen-limited ecosystems (i.e. $\phi < 4$), however, nitrogen fertilization causes up to a 20% increase in total evapotranspiration. Loma Ridge climatology is located very near this transition and, thus, the water balance is relatively insensitive to nitrogen fertilization.

5.2 The importance of the nitrogen cycle in modeling ecohydrological systems

The land surface is a critical component in the dynamics of the Earth system and the ability to predict its behavior is essential to the understanding and management of global change. Land cover and its dynamics control rates of water vapor and CO_2 exchange between the land surface and the atmosphere as well as the transport of water, sediment, and their associated chemistry from the land surface to the subsurface and oceans. Each of these pathways plays a role in climate and ecosystems, on which we depend for food and water.

The land surface is best understood as a dynamic system composed of interacting physical, chemical, and biological processes. For example, at Loma Ridge, rates of CO_2 uptake by the land surface are observed to be related to water availability, nitrogen availability, and the interaction between the two. However complex these systems may be, from an engineering perspective, there still exists the question of how much of this complexity must be adequately described to effectively model and manage the system. Below, the results of this thesis are used to evaluate the necessity and practicality of incorporating a dynamic nitrogen cycle in Earth surface prediction and observation systems.

5.2.1 Water balance

Observation and modeling of the water cycle is needed at several scales to aid important societal functions. Estimates of soil moisture, evapotranspiration, runoff, and groundwater recharge have widespread application in weather prediction, disaster monitoring and prediction (e.g. hurricanes, floods, landslides), water resources planning for drinking water and agricultural applications, and monitoring global change indicators and assessing their risks. From the data presented in this thesis, a statement can be made with regards to the relationship between the nitrogen cycle and two of these properties – soil moisture and evapotranspiration.

For sufficiently arid ecosystems, which given the data presented here can be defined as either $\phi > 3$ or $P > 500$ mm, it would seem that detailed knowledge of the nitrogen cycle is not necessary for an accurate estimate of the water balance. This conclusion is apparent

from a comparison between the observed water balance sensitivity to nitrogen deposition and the typical accuracy of water balance observations. The accuracy of soil moisture and ET estimates depends on the method and the scale of application. For the sake of comparison, consider the scale of the Loma Ridge estimates, which varies between the plot and hillslope scales or 10^1-10^2 m. Soil moisture was measured at Loma Ridge by the TDR method, with typical measurement error on the order of 10% [*Walker et al.*, 2004] and an observed landscape variability of approximately 10-20% (Figure 2-12). ET was measured by the eddy covariance method, which can be associated with measurement errors up to 20% [*Goulden et al.*, 1996; *Wilson et al.*, 2002], and by combined g_s and LAI measurements, which may have greater uncertainty [*Breda*, 2003] (also see Figures 2-11 and 2-13). Other estimates of E and T have similar errors and the uncertainty across model predictions is at least this high [*Mahfouf et al.*, 1996; *Wang and Dickinson*, 2012]. The model predicted no change in the total ET with increasing N deposition and a maximum 20% increase in T at the upper limit of estimated N deposition rates in the region. Therefore, it is not likely that existing measurement technology would be capable of adequately attributing changes in ET or T to changes in nitrogen availability in these ecosystems. Much greater differences were predicted for humid ecosystems and, thus, it is anticipated that information on nutrient supply would be useful for modeling these systems. However, given the poor suitability of the model applied here to these ecosystems, this conclusion should be investigated further. Finally, it is unclear whether these conclusions would apply at scales larger than those observed and modeled here, such as those of global climate models and satellite observations (e.g. $\sim$1 km).

5.2.2 Carbon balance

Because the carbon balance is directly linked with the water balance through stomatal conductance and soil moisture, it is inherent to a comprehensive theory of land surface dynamics. Interest in the carbon balance is primarily organized around climate change and agricultural studies. From the climate change perspective, it is yet unknown how surface CO_2 fluxes will respond to the simultaneous rise in atmospheric CO_2 and changes in temperature and precipitation patterns [*Cox et al.*, 2000; *Friedlingstein et al.*, 2006] or whether these fluxes can be tuned through large-scale ecosystem management projects. Ecosystem CO_2

uptake is also directly related to agricultural efficiency and much research on the carbon cycle is therefore focused on food production [*Easterling et al.*, 2007]. Both applications require observations and models of photosynthesis and respiration.

While the Loma Ridge water balance was insensitive to nitrogen fertilization, the carbon balance, as measured by ANPP, responded positively. On average, ANPP was 23% greater in fertilized plots than in control plots. In addition to these observations, model predictions suggest the inter-annual variability in relative water and nitrogen availability may be a more important indicator of productivity than precipitation alone. Nitrogen losses during wet years may limit productivity in subsequent years. Also, drought and/or fire may cause changes in nitrogen availability that influence later productivity. Therefore, these results suggest that accurate knowledge of the nitrogen cycle is necessary for accurate estimates of the carbon balance. Further, because ANPP is tightly linked with T, it could also be argued that the nitrogen cycle is an important factor for this single component of the water balance, regardless of the impacts on the aggregate water balance. This last point highlights the need for better understanding of stomatal responses to environmental changes.

5.2.3 Surface processes

Landscape structure and sediment yield are important drivers of niche differentiation [e.g. *Ivanov et al.*, 2008b] and receiving water ecosystem health [e.g. *Scheffer et al.*, 1993]. The role of vegetative cover in landscape dynamics has long been known [*Hack and Goodlett*, 1960; *Costa*, 1975]. Recently, a model coupling vegetation and landscape dynamics demonstrated the ranges of landscape structure and sediment yield expected for surfaces with various assumptions of vegetation behavior [*Collins et al.*, 2004; *Istanbulluoglu and Bras*, 2005; *Collins and Bras*, 2008; 2010]. The signature of vegetation is clearly evident in these simulations, however, the time-scales of interaction between vegetation and surface dynamics have yet to be deduced. That is, is simply the long-term average vegetation cover sufficient information to model the range of observed landscape forms, or is the inter-annual variability in vegetation cover and its relation to climate and disturbance needed? If the latter case, then the results of the Loma Ridge experiment would support the inclusion of nitrogen cycle dynamics in these models.

5.3 Summary and future vision

The central assumption underlying many studies in ecohydrology, as well as the majority of land surface model parameterizations, is the exclusive water and energy limitation of transpiration and primary productivity. In other words, soil moisture and temperature are the land surface state assumed to be the primary controls on land-atmosphere carbon and water fluxes. This thesis attempted to join other recent studies in building upon this simple framework by investigating the impact of the nitrogen cycle on the ecohydrology of seasonally dry ecosystems. Insights gathered from this work provide a new perspective on the dynamics of "water-limited" ecosystems.

Considering the land surface as a coupled system, this analysis of the Loma Ridge experiment demonstrates the complexity needed to fully describe its dynamics. This thesis provides evidence that, while soil moisture may be sufficient for describing the water balance in arid ecosystems, it is not the only information needed to constrain the carbon balance. Further, in wetter ecosystems, which by some definitions would be considered "water-limited" (e.g. $\phi = 1$, [*Budyko*, 1986]), the model analyzed here suggests that the nitrogen balance, and its interaction with the water balance, is integral to the estimation of surface carbon *and* water fluxes. Therefore, although plant-water interactions may provide a first-order indicator of broad patterns of biogeography and niche differentiation (but, see *Everard et al.* [2010]), more detail seems to be necessary for accurate estimates of ecosystem process rates.

One theme reiterated throughout this study and others is the extreme complexity of ecosystems, which necessitates a constant struggle between further reduction of their underlying mechanics and the design of models that operate at practical scales. The optimality approach applied here is one example of the latter and other similar models show promise [*Shipley et al.*, 2006; *Dewar*, 2010; *Wang and Bras*, 2011; *Franklin et al.*, 2012]. Therefore, in addition to the research avenues suggested above that aim toward a more detailed physical basis for models, the continued search for organizing principles in ecosystems and their hydrologic behavior will be just as important.

Bibliography

Aerts, R., and F. Chapin (1999), The mineral nutrition of wild plants revisited: A re-evaluation of processes and patterns, *Advances in Ecological Research, 30*, 1–67.

Anten, N., F. Schieving, E. Medina, M. Werger, and P. Schuffelen (1995), Optimal leaf area indices in C_3 and C_4 mono- and dicotyledonous species at low and high nitrogen availability, *Physiologia Plantarium, 95*, 541–550.

Aranibar, J., L. Otter, S. Macko, C. Feral, H. Epstein, P. Dowty, F. Eckardt, H. Shugart, and R. Swap (2004), Nitrogen cycling in the soil-plant system along a precipitation gradient in the Kalahari sands, *Global Change Biology, 10*, 359–373.

Arora, V., and G. Boer (2005), Fire as an interactive component of dynamic vegetation models, *Journal of Geophysical Research, 110*.

Ball, J., I. Woodrow, and J. Berry (1987), A model predicting stomatal conductance and its contribution to the control of photosynthesis under different environmental conditions, in *Progress in Photosynthesis Research*, vol. IV, edited by J. Biggins, Martinus Nijhoff Publishers, Dordrecht, The Netherlands.

Barbour, M., T. Keeler-Wolf, and A. Schoenherr (2007), *Terrestrial vegetation of California*, 3rd ed., University of California Press, Berkeley, CA.

Barnosky, A., E. Hadly, J. Bascompte, E. Berlow, J. Brown, M. Fortelius, W. Getz, J. Harte, A. Hastings, P. Marquet, N. Martinez, A. Mooers, P. Roopnarine, G. Vermeij, J. Williams, R. Gillespie, J. Kitzes, C. Marshall, N. Matzke, D. Mindell, E. Revilla, and A. Smith (2012), Approaching a state shift in Earth's biosphere, *Nature, 486*, 52–58.

Barrett, J., R. McCulley, D. Lane, I. Burke, and W. Lauenroth (2002), Influence of climate variability on plant production and N-mineralization in Central US grasslands, *Journal of Vegetation Science, 13*, 383–394.

Basu, N., G. Destouni, J. Jawitz, S. Thompson, N. Loukinova, A. Darracq, S. Zanardo, M. Yaeger, M. Sivapalan, A. Rinaldo, and P. Rao (2010), Nutrient loads exported from managed catchments reveal emergent biogeochemical stationarity, *Geophysical Research Letters, 37*.

Bisht, G. (2010), Satellite-based estimates of net radiation and modeling the role of topography and vegetation on inter-annual hydro-climatology, Ph.D. thesis, Massachusetts Institute of Technology.

Biswas, A. (1970), *History of Hydrology*, North-Holland Publishing Company, Amsterdam, The Netherlands.

Bloor, J., and R. Bardgett (2012), Stability of above-ground and below-ground processes to extreme drought in model grassland ecosystems: interactions with plant species diversity and soil nitrogen availability, *Perspectives in Plant Ecology, Evolution and Systematics*, *14*(3), 193–204.

Bolker, B., S. Pacala, and W. Parton (1998), Linear analysis of soil decomposition: insights from the CENTURY model, *Ecological Applications*, *8*(2), 425–439.

Bolster, W. (2008), Putting the ocean in Atlantic history: Maritime communities and marine ecology in the Northwest Atlantic, 1500-1800, *American Historical Review*, *113*(1), 19–47.

Bonan, G. (2002), *Ecological Climatology: Concepts and Applications*, 1st ed., Cambridge University Press, Cambridge, UK.

Booth, M., J. Stark, and E. Rastetter (2005), Controls on nitrogen cycling in terrestrial ecosystems: a synthetic analysis of literature data, *Ecological Monographs*, *75*(2), 139–157.

Brady, N., and R. Weil (2004), *The Nature and Properties of Soils*, 13th ed., Prentice Hall, Upper Saddle River, NJ.

Bras, R. (1989), *Hydrology: An introduction to hydrologic science*, Addison-Wesley, Reading, MA.

Breda, N. (2003), Ground-based measurements of leaf area index: a review of methods, instruments and current controversies, *Journal of Experimental Botany*, *54*(392), 2403–2417.

Brookes, A. (1985), River channelization: traditional engineering methods, physical consequences and alternative practices, *Progress in Physical Geography*, *9*(1), 44–73.

Bucci, S., F. Scholz, G. Goldstein, F. Meinzer, A. Franco, P. Campanello, R. Villalobos-Vega, M. Bustamente, and F. Miralles-Wilhelm (2006), Nutrient availability constrains the hydraulic architecture and water relations of savannah trees, *Plant, Cell and Environment*, *29*, 2153–2167.

Buckley, T., K. Mott, and G. Farquhar (2003), A hydromechanical and biochemical model of stomatal conductance, *Plant, Cell and Environment*, *26*, 1767–1785.

Budyko, M. (1986), *The Evolution of the Biosphere*, Springer.

Burke, I., W. Lauenroth, and W. Parton (1997), Regional and temporal variation in net primary production and nitrogen mineralization in grasslands, *Ecology*, *78*(5), 1330–1340.

Carpenter, S., N. Caraco, D. Correll, R. Howarth, A. Sharpley, and V. Smith (1998), Non-point pollution of surface water with phosphorus and nitrogen, *Ecological Applications*, *8*(3), 559–568.

Caylor, K., T. Scanlon, and I. Rodriguez-Iturbe (2004), Feasible optimality of vegetation patterns in river basins, *Geophysical Research Letters*, *31*.

Caylor, K., S. Manfreda, and I. Rodriguez-Iturbe (2005), On the coupled geomorphological and ecohydrological organization of river basins, *Advances in Water Resources*, *28*, 69–86.

Caylor, K., T. Scanlon, and I. Rodriguez-Iturbe (2009), Ecohydrological optimization of pattern and processes in water-limited ecosystems: A tradeoff-based hypothesis, *Water Resources Research*, *45*.

Choudhury, B., and J. Monteith (1988), A four-layer model for the heat budget of homogeneous land surfaces, *Quarterly Journal of the Royal Meteorological Society*, *114*, 373–398.

Cohen, M., C. Henges-Jeck, and G. Castillo-Moreno (2001), Water balance for the Colorado River delta, *Journal of Arid Environments*, *49*, 35–48.

Collatz, G., J. Ball, C. Grivet, and J. Berry (1991), Physiological and environmental regulation of stomatal conductance, photosynthesis and transpiration: A model that includes a laminar boundary layer, *Agricultural and Forest Meteorology*, *54*, 107–136.

Collins, D. (2006), Geomorphology and ecohydrology of water-limited ecosystems: A modeling approach, Ph.D. thesis, Massachusetts Institute of Technology.

Collins, D., and R. Bras (2007), Plant rooting strategies in water-limited ecosystems, *Water Resources Research*, *43*.

Collins, D., and R. Bras (2008), Climatic control of sediment yield in dry lands following climate and land cover change, *Water Resources Research*, *44*.

Collins, D., and R. Bras (2010), Climatic and ecological controls of equilibrium drainage density, relief, and channel concavity in dry lands, *Water Resources Research*, *46*.

Collins, D., R. Bras, and G. Tucker (2004), Modeling the effects of vegetation-erosion coupling on landscape evolution, *Journal of Geophysical Research*, *109*.

Costa, J. (1975), Effects of agriculture on erosion and sedimentation in the piedmont province, Maryland, *Geological Society of America Bulletin*, *86*, 1281–1286.

Cowan, I., and G. Farquhar (1977), Stomatal function in relation to leaf metabolism and environment, *Symposia of the Society for Experimental Biology*, *31*, 471–505.

Cowling, S., and C. Field (2003), Environmental control of leaf area production: Implications for vegetation and land-surface modeling, *Global Biogeochemical Cycles*, *17*(1).

Cox, P., R. Betts, C. Jones, S. Spall, and I. Totterdell (2000), Acceleration of global warming due to carbon-cycle feedbacks in a coupled climate model, *Nature*, *408*, 184–187.

Craine, J. (2009), *Resource Strategies of Wild Plants*, Princeton University Press, Princeton, NJ.

Craine, J., D. Tilman, D. Wedin, P. Reich, M. Tjoelker, and J. Knops (2002), Functional traits, productivity, and effects on nitrogen cycling of 33 grassland species, *Functional Ecology, 16*, 563–574.

Daly, E., A. Porporato, and I. Rodriguez-Iturbe (2004a), Coupled dynamics of photosynthesis, transpiration, and soil water balance. Part I: Upscaling from hourly to daily level, *Journal of Hydrometeorology, 5*(3), 546–558.

Daly, E., A. Porporato, and I. Rodriguez-Iturbe (2004b), Coupled dynamics of photosynthesis, transpiration, and soil water balance. Part II: Stochastic analysis and ecohydrological significance, *Journal of Hydrometeorology, 5*, 559–566.

Dewar, R. (1996), The correlation between plant growth and intercepted radiation: An interpretation in terms of optimal plant nitrogen content, *Annals of Botany, 78*, 125–136.

Dewar, R. (2010), Maximum entropy production and plant optimization theories, *Philosophical Transactions of the Royal Society of London B, 365*, 1429–1435.

Dickinson, R., J. Berry, G. Bonan, G. Collatz, C. Field, I. Fung, M. Goulden, W. Hoffmann, R. Jackson, R. Myneni, P. Sellers, and M. Shaikh (2002), Nitrogen controls on climate model evapotranspiration, *Journal of Climate, 15*, 278–295.

Diggle, A. (1988), Rootmap: a model in 3-dimensional coordinates of the growth and structure of fibrous root systems, *Plant and Soil, 105*, 169–178.

D'Odorico, P., F. Laio, A. Porporato, and I. Rodriguez-Iturbe (2003), Hydrologic controls on soil carbon and nitrogen cycles. II. A case study, *Advances in Water Resources, 26*, 59–70.

Dunbabin, V., A. Diggle, and Z. Rengell (2002), Simulation of field data by a basic three-dimensional model of interactive root growth, *Plant and Soil, 239*, 39–54.

Dunne, T., and R. Black (1970), Partial area contributions to storm runoff in a small New England watershed, *Water Resources Research, 6*(5), 1296–1311.

Eagleson, P. (1978a), Climate, soil, and vegetation. 1. Introduction to water balance dynamics, *Water Resources Research, 14*(5), 705–712.

Eagleson, P. (1978b), Climate, soil, and vegetation. 2. The distribution of annual precipitation derived rom observed storm sequences, *Water Resources Research, 14*(5), 713–721.

Eagleson, P. (1978c), Climate, soil, and vegetation. 3. A simplified model of soil moisture movement in the liquid phase, *Water Resources Research, 14*(5), 722–730.

Eagleson, P. (1978d), Climate, soil, and vegetation. 4. The expected value of annual evapotranspiration, *Water Resources Research, 14*(5), 731–739.

Eagleson, P. (1978e), Climate, soil, and vegetation. 5. A derived distribution of storm surface runoff, *Water Resources Research, 14*(5), 741–748.

Eagleson, P. (1978f), Climate, soil, and vegetation. 6. Dynamics of the annual water balance, *Water Resources Research*, *14*(5), 749–764.

Eagleson, P. (1978g), Climate, soil, and vegetation. 7. A derived distribution of annual water yield, *Water Resources Research*, *14*(5), 765–776.

Eagleson, P. (1982), Ecological optimality in water-limited natural soil-vegetation systems. 1. Theory and hypothesis, *Water Resources Research*, *18*(2), 325–340.

Eagleson, P. (2002), *Ecohydrology: Darwinian expression of vegetation form and function*, Cambridge University Press, Cambridge, UK.

Eagleson, P., and R. Segarra (1985), Water-limited equilibrium of savanna vegetation systems, *Water Resources Research*, *21*(10), 1483–1493.

Eagleson, P., and T. Tellers (1982), Ecological optimality in water-limited natural soil-vegetation systems. 2. Tests and applications, *Water Resources Research*, *18*(2), 341–354.

Easterling, W., P. Aggarwal, P. Batima, K. Brander, L. Erda, S. Howden, A. Kirilenko, J. Morton, J.-F. Soussana, J. Schmidhuber, and F. Tubiello (2007), Food, fibre, and forest products, in *Climate Change 2007: Impacts, Adaptation and Vulnerability. Contribution of Working Group II to the Fourth Assessment Report of the Intergovernmental Panel on Climate Change*, edited by M. Parry, O. Canziani, J. Palutikof, P. van der Linden, and C. Hanson, Cambridge University Press.

Ehrenfeld, J., B. Ravit, and K. Elgersma (2005), Feedback in the plant-soil system, *Annual Review of Ecology and Systematics*, *30*, 75–115.

EIA (2006), International energy outlook 2006, *Tech. Rep. DOE/EIA-0484(2006)*, U.S. Department of Energy, Energy Information Administration.

Eltahir, E. (1998), A soil moisture-rainfall feedback mechanism. 1. Theory and observations, *Water Resources Research*, *34*(4), 765–776.

Emanuel, R., P. D'Odorico, and H. Epstein (2007), Evidence of optimal water use by vegetation across a range of North American ecosystems, *Geophysical Research Letters*, *34*.

Evans, J. (1989), Photosynthesis and nitrogen relationships in leaves of C_3 plants, *Oecologia*, *78*(1), 9–19.

Everard, K., E. Seabloom, W. Harpole, and C. de Mazancourt (2010), Plant water use affects competition for nitrogen: why drought favors invasive species in California, *The American Naturalist*, *175*(1).

Ewers, B., R. Oren, and J. Sperry (2000), Influence of nutrient versus water supply on hydraulic architecture and water balance in Pinus taeda, *Plant, Cell and Environment*, *23*, 1055–1066.

Falkowski, P., and C. Davis (2004), Natural proportions, *Nature*, *431*(7005), 131.

Federer, C. (1979), A soil-plant-atmosphere model for transpiration and availability of soil water, *Water Resources Research*, *15*(3), 555–562.

Federer, C. (1982), Transpirational supply and demand: plant, soil, and atmospheric effects evaluated by simulation, *Water Resources Research*, *18*(2), 355–362.

Feng, X., G. Vico, and A. Porporato (2012), On the effects of seasonality on soil water balance and plant grwoth, *Water Resources Research*, *48*.

Fenn, M., R. Haeuber, G. Tonnesen, J. Baron, S. Grossman-Clarke, D. Hope, D. Jaffe, S. Copeland, L. Geiser, H. Rueth, and J. Sickman (2003), Nitrogen emissions, deposition, and monitoring in the western united states, *Bioscience*, *53*(4), 391–403.

Fernandez-Illescas, C., and I. Rodriguez-Iturbe (2004), The impact of interannual rainfall variability on the spatial and temporal patterns of vegetation in a water-limited ecosystem, *Advances in Water Resources*, *27*.

Fernandez-Illescas, C., A. Porporato, F. Laio, and I. Rodriguez-Iturbe (2001), The ecohydrological role of soil texture in a water-limited ecosystem, *Water Resources Research*, *37*(12), 2863–2872.

Field, C., and H. Mooney (1986), The photosynthesis-nitrogen relationship in wild plants, in *On the economy of plant form and function*, edited by T. Givnish, Cambridge University Press, Cambridge, UK.

Field, C., M. Behrenfeld, J. Randerson, and P. Falkowski (1998), Primary production of the biosphere: Integrating terrestrial and oceanic components, *Science*, *281*(5374), 237–240.

Folke, C., S. Carpenter, B. Walker, M. Scheffer, T. Elmqvist, L. Gunderson, and C. Holling (2004), Regime shifts, resilience, and biodiversity in ecosystem management, *Annual Review of Ecology, Evolution, and Systematics*, *35*, 557–581.

Forster, P., V. Ramaswamy, P. Artaxo, T. Bernstsen, R. Betts, D. Fahey, J. Haywood, J. Lean, D. Lowe, G. Myhre, J. Nganga, R. Prinn, G. Raga, M. Schulz, and R. V. Dorland (2007), Changes in atmospheric constituents and in radiative forcing, in *Climate Change 2007: The Physical Science Basis. Contribution of Working Group I to the Fourth Assessment Report of the Intergovernmental Panel on Climate Change*, Cambridge University Press, Cambridge, UK.

Franklin, O., J. Johansson, R. Dewar, U. Dieckmann, R. McMurtrie, A. Brannstrom, and R. Dybzinski (2012), Modeling carbon allocation in trees: a search for principles, *Tree Physiology*.

Fredeen, A., J. Gamon, and C. Field (1991), Responses of photosynthesis and carbohydrate partitioning to limitations in nitrogen and water availability in field grown sunflower, *Plant, Cell and Environment*, *14*, 963–970.

Friedlingstein, P., G. Joel, C. Field, and I. Fung (1999), Toward an allocation scheme for global terrestrial carbon models, *Global Change Biology*, *5*, 755–770.

Friedlingstein, P., P. Cox, R. Betts, L. Bopp, W. von Bloh, V. Brovkin, P. Cadule, S. Doney, M. Eby, I. Fung, G. Bala, J. John, C. Jones, F. Joos, T. Kato, M. Kawamiya, W. Knorr, K. Lindsay, H. Matthews, T. Raddatz, P. Rayner, C. Reick, E. Roeckner, K.-G. Schnitzler, R. Schnur, K. Strassmann, A. Weaver, C. Yoshikawa, and N. Zeng (2006), Climate-carbon cycle feedback analysis: results from the C4MIP model intercomparison, *Journal of Climate*, *19*, 3337–3353.

Galloway, J., and E. Cowling (2002), Reactive nitrogen and the world: 200 years of change, *Ambio*, *31*(2), 64–71.

Gardner, L. (1990), The role of rock weathering in the phosphorus budget of terrestrial watersheds, *Biogeochemistry*, *11*, 97–110.

Gottschalk, L. (1945), Effects of soil erosion on navigation in upper Chesapeake Bay, *The Geographical Review*, *35*, 219–238.

Goulden, M., J. Munger, S.-M. Fan, B. Daube, and S. Wofsy (1996), Measurements of carbon sequestration by long-term eddy covariance: Methods and a critical evaluation of accuracy, *Global Change Biology*, *2*, 169–182.

Gruber, N., and J. Galloway (2008), An earth-system perspective of the global nitrogen cycle, *Nature*, *451*, 293–296.

Guidry, M., and F. Mackenzie (2000), Apatite weathering and the Phanerozoic phosphorus cycle, *Geology*, *28*, 631–634.

Gutschick, V. (1978), Energy and nitrogen fixation, *Bioscience*, *28*(9), 571–575.

Hack, J., and J. Goodlett (1960), Geomorphology and forest ecology of a mountain region in the Central Appalachians, *United States Geological Survey Professional Paper 347*, U.S. Geological Survey.

Harden, J., J. Neff, D. Sandberg, M. Turetsky, R. Ottmar, G. Gleixner, T. Fries, and K. Manies (2004), Chemistry of burning the forest floor during the FROSTFIRE experimental burn, interior alaska, 1999, *Global Biogeochemical Cycles*, *18*.

Harpole, W., D. Potts, and K. Suding (2007), Ecosystem responses to water and nitrogen amendment in a California grassland, *Global Change Biology*, *13*, 2341–2348.

Hastings, A. (1997), *Population Biology: Concepts and Models*, Springer-Verlag, New York, NY.

Hatton, T., G. Salvucci, and H. Wu (1997), Eagleson's optimality theory of an ecohydrological equilibrium: quo vadis?, *Functional Ecology*, *11*, 665–674.

Hedin, L. (2004), Global organization of terrestrial plant-nutrient interactions, *Proceedings of the National Academy of Sciences of the United States of America*, *101*(30), 10,849–10,850.

Hickler, T., I. Prentice, B. Smith, M. Sykes, and S. Zaehle (2006), Implementing plant hydraulic architecture within the LPJ dynamic global vegetation model, *Global Ecology and Biogeography*, *15*, 567–577.

Hildebrandt, A., M. A. Aufi, M. Amerjeed, M. Shammas, and E. Eltahir (2007), Ecohydrology of a seasonal cloud forest in Dhofar: 1. Field experiment, *Water Resources Research*, *43*.

Holmes, T., and K. Rice (1996), Patterns of growth and soil-water utilization in some exotic annuals and native perennial bunchgrasses of California, *Annals of Botany*, *78*(2), 233–243, doi:10.1006/anbo.1996.0117.

Hooke, R. (2000), On the history of humans as geomorphic agents, *Geology*, *28*(9), 843–846.

Hooper, D., and L. Johnson (1999), Nitrogen limitation in dryland ecosystems: responses to geographical and temporal variation in precipitation, *Biogeochemistry*, *46*, 247–293.

Horton, R. (1933), The role of infiltration in the hydrologic cycle, *Transactions of the American Geophysical Union*.

Hunt, E., J. Weber, and D. Gates (1985a), Effects of nitrate application on Amaranthus powellii Wats.: II. Stomatal response to vapor pressure difference is consistent with optimization of stomatal conductance, *Plant Physiology*, *79*, 614–618.

Hunt, E., J. W, and D. Gates (1985b), Effects of nitrate application on Amaranthus powellii Wats.: I. Changes in photosynthesis, growth rates, and leaf area, *Plant Physiology*, *79*, 609–613.

Hunt, E., J. Weber, and D. Gates (1985c), Effects of nitrate application on Amaranthus powellii Wats.: III. Optimal allocation of leaf nitrogen for photosynthesis and stomatal conductance, *Plant Physiology*, *79*, 619–624.

Hwang, T., L. Band, and T. Hales (2009), Ecosystem processes at the watershed scale: extending optimality theory from plot to catchment, *Water Resources Research*, *45*.

Islam, S., D. Entekhabi, R. Bras, and I. Rodriguez-Iturbe (1990), Parameter estimation and sensitivity analysis for the modified Bartlett-Lewis rectangular pulses model of rainfall, *Journal of Geophysical Research*, *95*(D3), 2093–2100.

Istanbulluoglu, E., and R. Bras (2005), Vegetation-modulated landscape evolution: effects of vegetation on landscape processes, drainage density, and topography, *Journal of Geophysical Research*, *110*.

Istanbulluoglu, E., T. Wang, and D. Wedin (2011), Evaluation of ecohydrologic model parsimony at local and regional scales in a semiarid grassland ecosystem, *Ecohydrology*, *5*(1), 121–142.

Ivanov, V. (2006), Effects of dynamic vegetation and topography on hydrological processes in semi-arid areas, Ph.D. thesis, Massachusetts Institute of Technology.

Ivanov, V., R. Bras, and E. Vivoni (2008a), Vegetation-hydrology dynamics in complex terrain of semiarid areas: 1. A mechanistic approach to modeling dynamic feedbacks, *Water Resources Research*, *44*.

Ivanov, V., R. Bras, and E. Vivoni (2008b), Vegetation-hydrology dynamics in complex terrain of semiarid areas: 2. Energy-water controls of vegetation spatiotemporal dynamics and topographic niches of favorability, *Water Resources Research*, *44*.

Jarvis, P. (1976), The interpretation of the variations in leaf water potential and stomatal conductance found in canopies in the field, *Philosophical Transactions of the Royal Society of London B*, *273*, 593–610.

Jenny, H. (1994), *Factors of Soil Formation: A system of quantitative pedology*, Dover, New York, NY.

Jobbagy, E., and R. Jackson (2001), The distribution of soil nutrients with depth: global patterns and the imprint of plants, *Biogeochemistry*, *53*, 51–77.

Katul, G., R. Leuning, and R. Oren (2003), Relationship between plant hydraulic and biochemical properties derived from a steady-state coupled water and carbon transport model, *Plant, Cell and Environment*, *26*(3), 339–350.

Keeley, J., and C. Fotheringham (2001), Historic fire regime in southern California shrublands, *Conservation Biology*, *15*(6), 1536–1548.

Kerkhoff, A., S. Martens, and B. Milne (2004), An ecological evaluation of Eagleson's optimality hypotheses, *Functional Ecology*, *18*, 404–413.

Kern, J. (1994), Spatial patterns of soil organic carbon in the contiguous united states, *Soil Sci. Soc. Am. J.*, *58*(2), 439–455.

Kleidon, A. (2004), Optimized stomatal conductance of vegetated land surfaces and its effects on simulated productivity and climate, *Geophysical Research Letters*, *31*.

Kleidon, A. (2012), How does the Earth system generate and maintain thermodynamic disequilibrium and what does it imply for the future of the planet?, *Philosophical Transactions of the Royal Society of London A*, *370*, 1012–1040.

Knapp, A., J. Briggs, D. Hartnett, and S. Collins (1998), *Grassland Dynamics: Long-term Ecological Research in Tallgrass Prairie*, Oxford University Press, New York, NY.

Knight, T. (1806), On the direction of the radicle and germen during the vegetation of seeds, *Philosophical Transactions of the Royal Society of London*, *96*, 99–108.

Kochendorfer, J., and J. Ramirez (2010), Modeling the monthly mean soil-water balance with a statistical-dynamical ecohydrology model as coupled to a two-component canopy model, *Hydrology and Earth System Sciences*, *14*, 2099–2120.

Konikow, L. (2011), Contribution of global groundwater depletion since 1900 to sea-level rise, *Geophysical Research Letters*, *38*.

Kopp, G., and J. Lean (2011), A new, lower value of total solar irradiance: Evidence and climate significance, *Geophysical Research Letters*, *38*.

Kramer, P., and J. Boyer (1995), *Water relations of plants and soils*, Academic Press, San Diego, CA.

Krinner, G., N. Viovy, N. de Noblet-Ducoudre, J. Ogee, J. Polcher, P. Friedlingstein, P. Ciais, S. Sitch, and I. Prentice (2005), A dynamic global vegetation model for studies of the coupled atmosphere-biosphere system, *Global Biogeochemical Cycles*, *19*.

Laio, F., A. Porporato, L. Ridolfi, and I. Rodriguez-Iturbe (2001a), Plants in water-controlled ecosystems: active role in hydrologic processes and response to water stress II. Probabilistic soil moisture dynamics, *Advances in Water Resources*, *24*(7).

Laio, F., A. Porporato, C. Fernandez-Illescas, and I. Rodriguez-Iturbe (2001b), Plants in water-controlled ecosystems: active role in hydrologic processes and response to water stress IV. Discussion of real cases, *Advances in Water Resources*, *24*, 745–762.

Laio, F., P. D'Odorico, and L. Ridolfi (2006), An analytical model to relate the vertical root distribution to climate and soil properties, *Geophysical Research Letters*, *33*.

Lambers, H., F. Chapin, and T. Pons (2008), *Plant Physiological Ecology*, 2nd ed., Springer Science, New York, NY.

Leuning, R. (1995), A critical appraisal of a combined stomatal-photosynthesis model for C_3 plants, *Plant, Cell and Environment*, *18*, 339–357.

Liou, K. (2002), *An Introduction to Atmospheric Radiation*, Academic Press, San Diego, CA.

Mackay, D. (2001), Evaluation of hydrologic equilibrium in a mountainous watershed: incorporating forest canopy spatial adjustment to soil biogeochemical processes, *Advances in Water Resources*, *24*, 1211–1227.

Madigan, M., J. Martinko, and J. Parker (2002), *Brock Biology of Microorganisms*, 10th ed., Prentice Hall, Upper Saddle River, NJ.

Mahfouf, J.-F., C. Ciret, A. Ducharne, P. Irannejad, J. Noilhan, Y. Shao, P. Thornton, Y. Xue, and Z.-L. Yang (1996), Analysis of transpiration results from the rice and pilps workshop, *Global and planetary change*, *13*, 73–88.

Manzoni, S., and A. Porporato (2007), A theoretical analysis of nonlinearities and feedbacks in soil carbon and nitrogen cycles, *Soil biology and biochemistry*, *39*, 1542–1556.

Manzoni, S., A. Porporato, P. D'Odorico, F. Laio, and I. Rodriguez-Iturbe (2004), Soil nutrient cycles as a nonlinear dynamical system, *Nonlinear Processes in Geophysics*, *11*, 589–598.

McCulley, R., I. Burke, and W. Lauenroth (2009), Conservation of nitrogen increases with precipitation across a major grassland gradient in the central great plains of North America, *Oecologia*, *159*, 571–581.

Micklin, P. (2007), The Aral Sea disaster, *Annual Review of Earth and Planetary Sciences*, *35*, 47–72.

Minnich, R. (1983), Fire mosaics in southern California and northern Baja California, *Science*, *219*, 1287–1294.

Monsi, M., and T. Saeki (2005), On the factor light in plant communities and its importance for matter production, *Annals of Botany*, *95*(3), 549–567.

Mooney, H., C. Field, and S. Gulmon (1981), Photosynthesis capacity in relation to leaf position in desert versus old-field annuals, *Oecologia*, *50*, 109–112.

Nealson, K., and P. Conrad (1999), Life: past, present and future, *Philosophical Transactions of the Royal Society of London B*, *354*, 1923–1939.

Niu, G., Z. Yang, K. Mitchell, F. Chen, M. Ek, M. Barlage, A. Kumar, K. Manning, D. Niyogi, E. Rosero, M. Tewari, and Y. Xia (2011), The community Noah land surface model with multiparameterization options (Noah-MP): 1. Model description and evaluation with local-scale measurements, *Journal of Geophysical Research*, *116*.

Nobel, P. (2009), *Physicochemical and Environmental Plant Physiology*, 4th ed., Elsevier, Oxford, UK.

Nordbotten, J., I. Rodriguez-Iturbe, and M. Celia (2007), Stochastic coupling of rainfall and biomass dynamics, *Water Resources Research*, *43*.

Noy-Meir, I. (1973), Desert ecosystems: environment and producers, *Annual Review of Ecology and Systematics*, *4*, 25–51.

Oleson, K., D. Lawrence, G. Bonan, M. Flanner, E. Kluzek, P. Lawrence, S.Levis, S. Swenson, and P. Thornton (2010), Technical description of version 4.0 of the Community Land Model (CLM), *Tech. Rep. 478*, National Center for Atmospheric Research, Boulder, CO.

Osterman, L., R. Poore, P. Swarzenski, D. Senn, and S. DiMarco (2009), The 20th-century development and expansion of Louisiana shelf hypoxia, Gulf of Mexico, *Geo-Marine Letters*, *29*(6), 405–414.

Polley, H., H. Johnson, C. Tischler, and H. Torbert (1999), Links between transpiration and plant nitrogen: variation with atmopsheric CO_2 concentration and nitrogen availability, *International Journal of Plant Sciences*, *160*(3), 435–542.

Poorter, H., C. Remkes, and H. Lambers (1990), Carbon and nitrogen economy of 24 wild species differing in relative growth rate, *Plant Physiology*, *94*, 621–627.

Poorter, H., K. Niklas, P. Reich, J. Oleskyn, P. Poot, and L. Mommer (2012), Biomass allocation to leaves, stems and roots: meta-analyses of interspecific variation and environmental control, *New Phytologist, 193*, 30–50.

Porporato, A., F. Laio, L. Ridolfi, and I. Rodriguez-Iturbe (2001), Plants in water-controlled ecosystems: active role in hydrologic processes and response to water stress III. Vegetation water stress, *Advances in Water Resources, 24*, 725–744.

Porporato, A., F. Laio, L. Ridolfi, K. Caylor, and I. Rodriguez-Iturbe (2003a), Soil moisture and plant stress dynamics along the Kalahari precipitation gradient, *Journal of Geophysical Research, 108*.

Porporato, A., P. D'Odorico, F. Laio, and I. Rodriguez-Iturbe (2003b), Hydrologic controls on soil carbon and nitrogen cycles. I. Modeling scheme, *Advances in Water Resources, 26*, 45–58.

Porporato, A., E. Daly, and I. Rodriguez-Iturbe (2004), Soil water balance and ecosystem response to climate change, *The American Naturalist, 164*(5), 625–632.

Postel, S., G. Daily, and P. Ehrlich (1996), Human appropriation of renewable fresh water, *Science, 271*(5250), 785–788.

Potts, D., K. Suding, G. Winston, A. Rocha, and M. Goulden (2012), Ecological effects of experimental drought and prescribed fire in a southern California coastal grassland, *Journal of Arid Environments*.

Radin, J. (1981), Water relations of cotton plants under nitrogen deficiency: IV. Leaf senescence during drought and its relation to stomatal closure, *Physiologia Plantarium, 51*, 145–149.

Radin, J., and L. Parker (1979), Water relations of cotton plants under nitrogen deficiency: II. Environmental interactions on stomata, *Plant Physiology, 64*, 499–501.

Ramirez, C., and E. Worrell (2006), Feeding fossil fuels to the soil an analysis of energy embedded and technological learning in the fertilizer industry, *Resources, Conservation, and Recycling, 46*, 75–93.

Rawls, W., D. Brakensiek, and K. Saxton (1982), Estimation of soil water properties, *Transactions of the American Society of Agricultural Engineers, 25*(5), 1316–1320, 1328.

Redfield, A. (1958), The biological control of chemical factors in the environment, *American Scientist, 46*(3), 205–221.

Restrepo-Posada, P., and P. Eagleson (1982), Identification of independent rainstorms, *Journal of Hydrology, 55*, 303–319.

Reynolds, H., and S. Pacala (1993), An analytical treatment of root-to-shoot ratio and plant competition for soil nutrient and light, *The American Naturalist, 141*(1), 51–70.

Reynolds, J., D. Smith, E. Lambin, B. T. II, M. Mortimore, S. Batterbury, T. Downing, H. Dowlatabadi, R. Fernandez, J. Herrick, E. Huber-Sannwald, H. Jiang, R. Leemans, T. Lynam, F. Maestre, M. Ayarza, and B. Walker (2007), Global desertification: building a science for dryland development, *Science*, *316*, 847–851.

Richards, M., and E. Trinkaus (2009), Isotopic evidence for the diets of european neanderthals and early modern humans, *Proceedings of the National Academy of Sciences*, *106*(38), 16,034–16,039.

Rietkerk, M., F. van den bosch, and J. van de Koppel (1997), Site-specific properties and irreversible vegetation changes in semi-arid grazing systems, *Oikos*, *80*(2), 241–252.

Riveros-Iregui, D., and B. McGlynn (2009), Landscape structure control on soil CO_2 efflux variability in complex terrain: scaling from point observations to watershed scale fluxes, *Journal of Geophysical Research*, *114*.

Riveros-Iregui, D., B. McGlynn, L. Marshall, D. Welsch, R. Emanuel, and H. Epstein (2011), A watershed-scale assessment of a process soil CO_2 production and efflux model, *Water Resources Research*, *47*.

Riveros-Iregui, D., B. McGlynn, R. Emanuel, and H. Epstein (2012), Complex terrain leads to bidirectional responses of soil respiration to inter-annual water availability, *Global Change Biology*, *18*, 749–756.

Rodriguez-Iturbe, I., and A. Porporato (2004), *Ecohydrology of Water-Controlled Ecosystems: Soil moisture and plant dynamics*, Cambridge University Press, Cambridge, UK.

Rodriguez-Iturbe, I., D. Entekhabi, and R. Bras (1991), Nonlinear dynamics of soil moisture at climate scales 1. stochastic analysis, *Water Resources Research*, *27*(8), 1899–1906.

Rodriguez-Iturbe, I., A. Porporato, L. Ridolfi, V. Isham, and D. Cox (1999a), Probabilistic modelling of water balance at a point: the role of climate, soil and vegetation, *Proceedings of the Royal Society of London A*, *455*, 3789–3805.

Rodriguez-Iturbe, I., P. D'Odorico, A. Porporato, and L. Ridolfi (1999b), Tree-grass coexistence in savannas: the role of spatial dynamics and climate fluctuations, *Geophysical Research Letters*, *26*(2), 247–250.

Rodriguez-Iturbe, I., A. Porporato, F. Laio, and L. Ridolfi (2001a), Plants in water-controlled ecosystems: active role in hydrologic processes and response to water stress I. Scope and general outline, *Advances in Water Resources*, *24*(7), 695–705.

Rodriguez-Iturbe, I., A. Porporato, F. Laio, and L. Ridolfi (2001b), Intensive or extensive use of soil moisture: plant strategies to cope with stochastic water availability, *Geophysical Research Letters*, *28*(23), 4495–4497.

Sage, R., and R. Pearcy (1987), The nitrogen use efficiency of C_3 and C_4 plants: II. Leaf nitrogen effects on the gas exchange characteristics of Chenopodium album (L.) and Amaranthus retroflexus (L.), *Plant Physiology*, *84*, 959–963.

Sala, O., W. Parton, L. Joyce, and W. Lauenroth (1988), Primary production of the central grassland region of the united states, *Ecology*, *69*(1), 40–45.

Salvucci, G., and P. Eagleson (1992), A test of ecological optimality for semiarid vegetation, *Technical Report 335*, Massachusetts Institute of Technology.

Scanlon, T., and J. Albertson (2003), Inferred controls on tree/grass competition in a savanna ecosystem: Combining 16-year normalized difference vegetation index data with a dynamic soil moisture model, *Water Resources Research*, *39*(8).

Scheffer, M., S. Hosper, M. Meijer, B. Moss, and E. Jeppesen (1993), Alternative equilibria in shallow lakes, *Trends in Ecology and Evolution*, *8*(8), 275–279.

Schenk, H. (2008), The shallowest possible water extraction profile: A null model for global root distributions, *Vadose Zone Journal*, *7*(3), 1119–1124.

Schenk, H., and R. Jackson (2002a), The global biogeography of roots, *Ecological Monographs*, *72*(3), 311–328.

Schenk, H., and R. Jackson (2002b), Rooting depths, lateral root spreads and belowground/above-ground allometries of plant in water-limited ecosystems, *The Journal of Ecology*, *90*(3), 480–494.

Schimel, D., B. B, E. Holland, R. McKeown, D. Ojima, T. Painter, W. Parton, and A. Townsend (1994), Climatic, edaphic, and biotic controls over storage and turnover of carbon in soils, *Global Biogeochemical Cycles*, *8*(3), 279–293.

Schimel, D., B. Braswell, R. McKeown, D. Ojima, W. Parton, and W. Pulliam (1996), Climate and nitrogen controls on the geography and timescales of terrestrial biogeochemical cycling, *Global Biogeochemical Cycles*, *10*(4), 677–692.

Schimel, D., B. Braswell, and W. Parton (1997), Equilibration of the terrestrial water, nitrogen, and carbon cycles, *Proceedings of the National Academy of Sciences*, *94*(16), 8280–8283.

Schimel, J., and J. Bennett (2004), Nitrogen mineralization: challenges of a changing paradigm, *Ecology*, *85*(3), 591–602.

Schlesinger, W., J. Reynolds, G. Cunningham, L. Huenneke, W. Jarrell, R. Virginia, and W. Whitford (1990), Biological feedbacks in global desertification, *Science*, *247*(4946), 1043–1048.

Schoenherr, A. (1995), *A Natural History of California*, University of California Press, Berkeley, CA.

Schymanski, S., M. Sivapalan, M. Roderick, L. Hutley, and J. Beringer (2009), An optimality-based model of the dynamic feedbacks between natural vegetation and the water balance, *Water Resources Research*, *45*.

Seastedt, T., and A. Knapp (1993), Consequences of nonequilibrium resource availability across multiple time scales: the transient maxima hypothesis, *The American Naturalist*, *141*(4), 621–633.

Sellers, P., R. Dickinson, D. Randall, A. Betts, F. Hall, J. Berry, G. Collatz, A. Denning, H. Mooney, C. Nobre, N. Sato, C. Field, and A. Henderson-Sellers (1997), Modeling the exchanges of energy, water, and carbon between continents and the atmosphere, *Science*, *275*, 502–509.

Shaw, M., E. Zavaleta, N. Chiariello, E. Cleland, H. Mooney, and C. Field (2002), Grassland responses to global environmental changes suppressed by elevated CO_2, *Science*, *298*, 1987–1990.

Shipley, B., and D. Meziane (2002), The balanced-growth hypothesis and the allometry of leaf and root biomass allocation, *Functional Ecology*, *16*, 326–331.

Shipley, B., D. Vile, and E. Garnier (2006), From plant traits to plant communities: a statistical mechanistic approach to biodiversity, *Science*, *314*, 812–814.

Sitch, S., B. Smith, I. Prentice, A. Arneth, A. Bondeau, W. Cramer, J. Kaplan, S. Levis, W. Lucht, M. Sykes, K. Thonicke, and S. Venevsky (2003), Evaluation of ecosystem dynamics, plant geography and terrestrial carbon cycling in the LPJ dynamic global vegetation model, *Global Change Biology*, *9*, 161–185.

Sivandran, G. (2011), The role of rooting strategies on the ecohydrology of semi-arid regions, Ph.D. thesis, Massachusetts Institute of Technology.

Sokolov, A., D. Kicklighter, J. Melillo, B. Felzer, C. Schlosser, and T. Cronin (2008), Consequences of considering carbon-nitrogen interactions on the feedbacks between climate and the terrestrial carbon cycle, *Journal of Climate*, *21*, 3776–3796.

Sperry, J., F. Adler, G. Campbell, and J. Comstock (1998), Limitation of plant water use by rhizosphere and xylem conductance: results from a model, *Plant, Cell and Environment*, *21*, 347–359.

Stone, L., and S. Ezrati (1996), Chaos, cycles and spatiotemporal dynamics in plant ecology, *Journal of Ecology*, *84*, 279–291.

Tague, C., and L. Band (2004), Rhessys: Regional hydro-ecologic simulation system-an object-oriented approach to spatially distributed modeling of carbon, water, and nutrient cycling, *Earth Interactions*, *8*, 1–42.

Tardieu, F., T. Lafarge, and T. Simmoneau (1996), Stomatal control by fed or endogenous xylem ABA in sunflower: interpretation of correlations between leaf water potential and stomatal conductance in anisohydric species, *Plant, Cell and Environment*, *19*(75-84).

Tilman, D. (1990), Constraints and tradeoffs: toward a predictive theory of competition and succession, *Oikos*, *58*, 3–15.

Tilman, D. (1994), Competition and biodiversity in spatially structured habitats, *Ecology*, *75*(1), 2–16.

Tilman, D., J. Fargione, B. Wolff, C. D'Antonio, A. Dobson, R. Howarth, D. Schindler, W. Schlesinger, D. Simberloff, and D. Swackhamer (2001), Forecasting agriculturally driven global environmental change, *Science*, *292*, 281–284.

Trenberth, K. E., J. T. Fasullo, and J. Kiehl (2009), Earth's Global Energy Budget, *Bulletin of the American Meteorological Society*, *90*(3), 311–323.

van Wijk, M., and I. Rodriguez-Iturbe (2002), Tree-grass competition in space and time: Insights from a simple cellular automata model based on ecohydrological dynamics, *Water Resources Research*, *38*(9).

Vincent, T., and T. Vincent (1996), Using the ESS maximum principle to explore root-shoot allocation, competition and coexistence, *Journal of Theoretical Biology*, *180*, 111–120.

Vitousek, P. (1982), Nutrient Cycling and Nutrient Use Efficiency, *American Naturalist*, *119*(4), 553–572.

Vitousek, P., and R. Howarth (1991), Nitrogen limitation on land and in the sea: how can it occur?, *Biogeochemistry*, *13*, 87–115.

Vitousek, P., P. Ehrlich, A. Ehrlich, and P. Matson (1986), Human appropriation of the products of photosynthesis, *Bioscience*, *36*(6), 368–373.

Vorosmarty, C., and D. Sahagian (2000), Anthropogenic disturbance of the terrestrial water cycle, *Bioscience*, *50*(9), 753–765.

Wackernagel, M., N. Schulz, D. Deumling, A. C. Linares, M. Jenkins, V. Kapos, C. Monfreda, J. Loh, N. Myers, R. Norgaard, and J. Randers (2002), Tracking the ecological overshoot of the human economy, *Proceedings of the National Academy of Sciences*, *99*(14), 9266–9271.

Walker, J., G. Willgoose, and J. Kalma (2004), In situ measurement of soil moisture: a comparison of techniques, *Journal of Hydrology*, *293*, 85–89.

Walker, T., and J. Syers (1976), Fate of phosphorus during pedogenesis, *Geoderma*, *15*(1), 1–19.

Wang, J., and R. Bras (2011), A model of evapotranspiration based on the theory of maximum entropy production, *Water Resources Research*, *47*.

Wang, K., and R. Dickinson (2012), A review of global terrestrial evapotranspiration: observation, modeling, climatology, and climatic variability, *Reviews of Geophysics*, *50*.

Wedin, D., and D. Tilman (1990), Species effects on nitrogen cycling: a test with perennial grasses, *Oecologia*, *84*(4), 433–441.

White, R., S. Murray, and M. Rohweder (2000), Pilot analysis of global ecosystems: Grassland ecosystems, *Tech. rep.*, World Resources Institute, Washington, DC.

White, R., D. Tunstall, and N. Henninger (2002), An ecosystem approach to drylands: building support for new development policies, *Tech. rep.*, World Resources Institute, Washington, DC.

Whittaker, R. (1975), *Communities and Ecosystems*, MacMillan Publishing Co., New York, NY.

Wilbanks, T., P. R. Lankao, M. Bao, F. Berkhout, S. Cairncross, J.-P. Ceron, M. Kapshe, R. Muir-Wood, and R. Zapata-Marti (2007), Industry, settlement and society, in *Climate Change 2007: Impacts, Adaptation and Vulnerability. Contribution of Working Group II to the Fourth Assessment Report of the Intergovernmental Panel on Climate Change*, edited by M. Parry, O. Canziani, J. Palutikof, P. van der Linden, and C. Hanson, Cambridge University Press, Cambridge, UK.

Wilkinson, S., and W. Davies (2002), ABA-based chemical signalling: the co-ordination of responses to stress in plants, *Plant, Cell and Environment*, *25*(2), 195–210.

Williams, C., and J. Albertson (2004), Soil moisture controls on canopy-scale water and carbon fluxes in an African savanna, *Water Resources Research*, *40*.

Williams, M., B. Law, P. Anthoni, and M. Unsworth (2001), Use of a simulation model and ecosystem flux data to examine carbon-water interactions in Ponderosa pine, *Tree Physiology*, *21*, 287–298.

Wilson, K., A. Goldstein, E. Falge, M. Aubinet, D. Baldocchi, P. Berbigier, C. Bernhofer, R. Ceulemans, H. Dolman, C. Field, A. Grelle, A. Ibrom, B. Law, A. Kowalski, T. Meyers, J. Moncrieff, R. Monson, W. Oechel, J. Tenhunen, R. Valentini, and S. Verma (2002), Energy balance closure at FLUXNET sites, *Agricultural and Forest Meteorology*, *113*, 223–243.

Wright, I., P. Reich, and M. Westoby (2003), Least-cost input mixtures of water and nitrogen for photosynthesis, *The American Naturalist*, *161*(1), 98–111.

Wright, I., P. Reich, M. Westoby, D. Ackerly, Z. Baruch, F. Bongers, J. Cavender-Bares, T. Chapin, J. Cornelissen, M. Diemer, J. Flexas, E. Garnier, P. Groom, J. Gulias, K. Hikosaka, B. Lamont, T. Lee, W. Lee, C. Lusk, J. Midgley, M.-L. Navas, U. Niinemets, J. Oleskyn, N. Osada, H. Poorter, P. Poot, L. Prior, V. Pyankov, C. Roumet, S. Thomas, M. Tjoelker, E. Veneklaas, and R. Villar (2004), The worldwide leaf economics spectrum, *Nature*, *428*, 821–827.

Yi, S., A. McGuire, E. Kasischke, J. Harden, K. Manies, M. Mack, and M. Turetsky (2010), A dynamic organic soil biogeochemical model for simulating the effects of wildfire on soil environmental conditions and carbon dynamics of black spruce forests, *Journal of Geophysical Research*, *115*.

Zaehle, S., and A. Friend (2010), Carbon and nitrogen cycle dynamics in the O-CN land surface model: 1. Model description, site-scale evaluation, and sensitivity to parameter estimates, *Global Biogeochemical Cycles*, *24*.

Zavaleta, E., M. Shaw, N. Chiariello, B. Thomas, E. Cleland, C. Field, and H. Mooney (2003), Grassland responses to three years of elevated temperature, CO_2, precipitation, and N deposition, *Ecological Monographs*, *73*(4), 585–604.

Zea-Cabrera, E., Y. Iwasa, S. Levin, and I. Rodriguez-Iturbe (2006), Tragedy of the commons in plant water use, *Water Resources Research*, *42*.

Zheng, X., and E. Eltahir (1998), A soil moisture-rainfall feedback mechanism 2. Numerical experiments, *Water Resources Research*, *34*(4), 777–786.